PB80-169626

Transverse Microcracking in Celion 6000/PMR-15 Graphite-Polyimide

Virginia Polytechnic Inst. and State Univ.
Blacksburg

Prepared for

National Aeronautics and Space Administration
Hampton, VA

Dec 79

PB81-169626

COLLEGE OF ENGINEERING

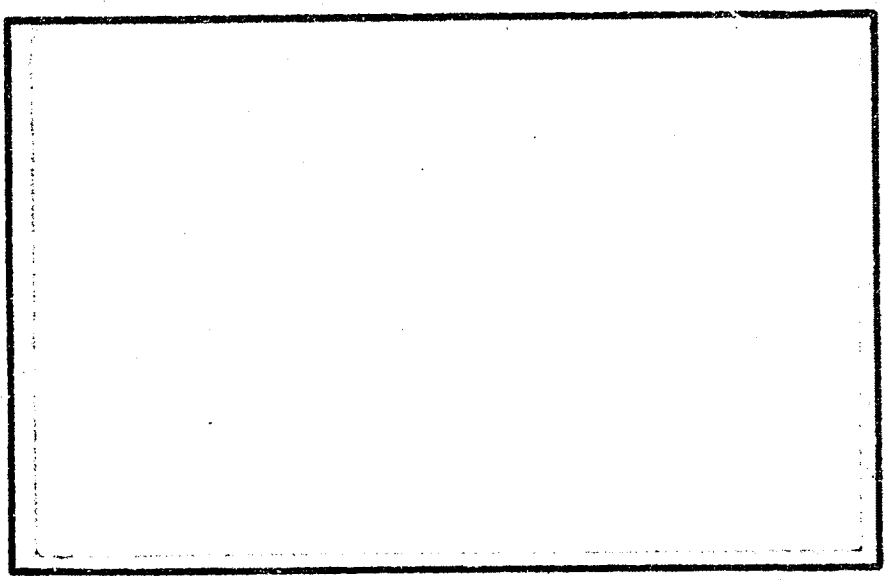

VIRGINIA POLYTECHNIC INSTITUTE AND STATE UNIVERSITY

BLACKSBURG, VIRGINIA

College of Engineering
Virginia Polytechnic Institute and State University
Blacksburg, VA. 24061

VPI-E-79-35 December, 1979

TRANSVERSE MICROCRACKING IN CELION 6000/PMR-15 GRAPHITE-POLYIMIDE

J. Steven Mills[1]
Carl T. Herakovich[2]
John G. Davis, Jr.[3]

Department of Engineering Science and Mechanics

Interim Report 17
The NASA-Virginia Tech Composites Program

NASA Grant NGR 47-004-129 and NASA Cooperative Agreement NCCI-15

Prepared for: Materials Application Branch
National Aeronautics & Space Administration
Langley Research Center
Hampton, VA. 23665

[1]Graduate Student - Virginia Tech (presently at McDonnell-Douglas)
[2]Professor of Engineering Science and Mechanics - Virginia Tech
[3]Materials Engineer - NASA Langley Research Center

SECURITY CLASSIFICATION OF THIS PAGE *(When Data Entered)*

REPORT DOCUMENTATION PAGE		READ INSTRUCTIONS BEFORE COMPLETING FORM
1. REPORT NUMBER VPI-E-79-35	2. GOVT ACCESSION NO.	3. RECIPIENT'S CATALOG NUMBER
4. TITLE *(and Subtitle)* TRANSVERSE MICROCRACKING IN CELION 6000/PMR-15 GRPAHITE-POLYIMIDE		5. TYPE OF REPORT & PERIOD COVERED
		6. PERFORMING ORG. REPORT NUMBER VPI-E-79-35
7. AUTHOR(s) J. Steven Mills, Carl T. Herakovich and John G. Davis, Jr.		8. CONTRACT OR GRANT NUMBER(s) NASA 47-004-129 and NASA CA NCCI-15
9. PERFORMING ORGANIZATION NAME AND ADDRESS Virginia Polytechnic Institute and State Univ. Engineering Science & Mechanics Blacksburg, VA. 24061		10. PROGRAM ELEMENT, PROJECT, TASK AREA & WORK UNIT NUMBERS
11. CONTROLLING OFFICE NAME AND ADDRESS National Aeronautics & Space Administration Langley Research Center Hampton, VA. 23665		12. REPORT DATE December, 1979 13. NUMBER OF PAGES
14. MONITORING AGENCY NAME & ADDRESS*(if different from Controlling Office)* Virginia Polytechnic Institute and State Univ. Engineering Science & Mechanics Blacksburg, VA. 24061		15. SECURITY CLASS. *(of this report)* unclassified 15a. DECLASSIFICATION/DOWNGRADING SCHEDULE

16. DISTRIBUTION STATEMENT *(of this Report)*
Approved for public release, distribution unlimited.

17. DISTRIBUTION STATEMENT *(of the abstract entered in Block 20, if different from Report)*
Approved for public release, distribution unlimited.

18. SUPPLEMENTARY NOTES

19. KEY WORDS *(Continue on reverse side if necessary and identify by block number)*
Graphite-Polyimide, transverse microcracking, thermal stress, tensile stress, cryogenic, x-ray, stress-free temperature, replicating

20. ABSTRACT *(Continue on reverse side if necessary and identify by block number)*
see page ii

DD FORM 1 JAN 73 1473 EDITION OF 1 NOV 65 IS OBSOLETE

SECURITY CLASSIFICATION OF THIS PAGE *(When Data Entered)*

ABSTRACT

The effects of room temperature tensile loading and five thermal loadings, in the range -320°F (-196°C) to 625°F (330°C), upon the development of transverse microcracks (TVM) in Celion 6000/PMR-15 graphite-polyimide laminates were investigated. Microcracks were observed using a replicating technique, microscopy and x-ray. The mechanical or thermal load at which microcracking initiates and the ply residual stresses were predicted using laminate analysis with stress- and temperature-dependent material properties. TVM density as a function of tensile load was predicted using the multiple cracking theory proposed by Garrett, Parvizi and Bailey.

It has been shown that TVM density and the load to initiate microcracking are functions of the type of loading and the laminate configuration. Generally, cross-ply laminates exhibit higher TVM density after thermal loading than do quasi-isotropic laminates, but the converse is true for tensile loading. Cross-ply laminates attain a saturation TVM density prior to failure, but the TVM density of quasi-isotropic laminates continues to increase until failure. Edge effects have a significant influence on the development of TVM, and TVM present at the free edge of a laminate extend across the entire width of the laminate. All laminates considered in this investigation were free of cracks after curing.

ACKNOWLEDGEMENTS

This research was supported by the NASA-Virginia Tech Composites Program (NASA Grant NGR 47-004-129 and NASA Cooperative Agreement NCCI-15). Mr. Mills completed seven months in residence at Langley Research Center during the course of the study. The support of numerous Langley engineers and technical staff is greatfully acknowledged as is the fine typing of Ms. Frances Carter of Virginia Tech. Mr. Mills also wishes to thank Dr. Les Cohen, Ms. Lisa Giorgi and Dr. Jerry C. Peck of McDonnell-Douglas Astronautics Company - West for their assitance and support.

TABLE OF CONTENTS

LIST OF TABLES

LIST OF FIGURES

Chapter 1

INTRODUCTION

The orthotropic nature of fiber reinforced materials requires that, for most applications, the material be laminated using several fiber orientations. Lamina properties such as modulus, coefficient of thermal expansion and strength vary with direction. The resulting mismatch in properties between layers with different orientations causes internal thermal stresses when ever the laminate is exposed to a temperature other than the stress free temperature. These laminate stresses are superposed on the thermal stresses which are present at the micro level due to the mismatch in properties between fiber and matrix. The thermal stresses due to these combined effects can have a significant influence on the initiation of failure in laminated composites. A transverse microcrack (TVM) is a form of ply failure. It is characterized by a crack in the matrix which runs parallel to the fibers. Figure 1 shows transverse microcracks in a cross-plied HTS1/PMR-15 graphite-polyimide laminate after cure.

The plane containing a TVM is generally perpendicular to the midplane of the ply and parallel to the fibers. The crack spacing is quite regular and depends upon a number of factors. Transverse microcracks have been attributed to static, creep and fatigue as well as thermal loading. The cross-plied laminates are generally considered to be most prone to thermal microcracking. The polyimide, polyquinoxaline and polysulfone resins are particularly susceptible to thermal microcracking because of their high cure temperatures and the

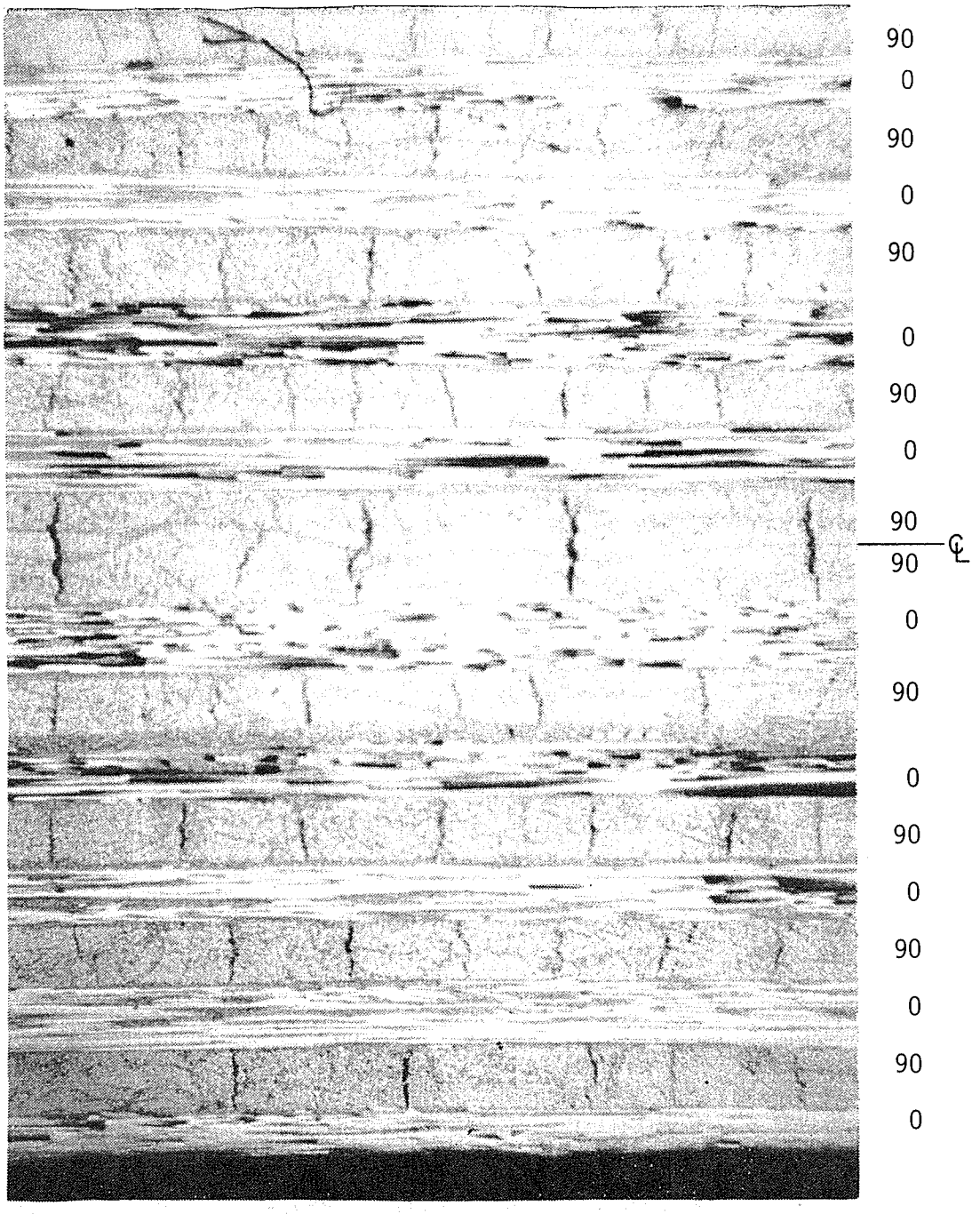

Fig. 1. Microphotograph of $[(0/90)_5]_s$ HTS1/PMR-15 Laminate After Cure

resulting high residual stresses associated with the large temperature change during cool-down to room temperature. Since significant TVM densities can be attained during fabrication, concern has arisen as to the effect of such localized damage on the mechanical properties and environmental stability of laminates.

The purpose of this study was to investigate the influence of temperature extremes and applied strain on the development of transverse microcracks in selected graphite-polyimide laminates. Specimens were subjected to five thermal exposures and tensile stress. Microscopic inspection and x-ray were used to detect TVM. Linear and nonlinear laminate analyses with temperature dependent material properties were used to predict the internal stresses due to mechanical and thermal loads. A multiple cracking theory based upon the shear lag method was used to predict TVM densities as a function of applied stress.

Celion 6000/PMR-15 graphite/polyimide composite was selected for use in this study because of its potential utilization for advanced space transportation systems.

Chapter 2

LITERATURE REVIEW

The existence of transverse microcracks in fiber-reinforced composites is well documented in the literature. The first publication reporting the observation of microcracks apparently was that of ref. [1], in 1967. Several representative papers in areas related to transverse microcracks are briefly reviewed in this chapter. Also a short history of the development of the PMR-15 polyimide resin used in this study is included.

2.1 Characteristics of Transverse Microcracks

The description of a TVM in Chapter 1 is similar to that given in refs. [2-6] which reported the observation of cracks along laminate edges. Molcho and Ishai [7] reported that the microcracks exist only very near the edge of laminates; however, they did not document their method of observation. According to ref. [1], the transverse microcracks have never been observed in unidirectional laminates. Spain [3] found that the TVM density in a laminate tends to increase as the acute angle between plies increases.

There is disagreement as to whether a TVM initiates at and borders high fiber density regions, or exists primarily within the high fiber density regions. McGarry and Willner [4] used microphotographs to show that glass fiber composites under cyclic loading exhibit microcracks primarily in the high fiber density regions. Lee and McGarry [8], and Spain [3] obtained similar results for graphite fiber

composites under thermal loading. However, Doner and Novak's [2] micromechanics model and photomicrographs indicate that the microcracks prefer the boundary between the high fiber density regions and resin rich regions.

Five methods which have been used for microcrack detection are: (1) transmission and reflective optical microscopy; (2) laminate stiffness loss or mechanical hysteresis; (3) weight gain of samples immersed in water; (4) x-ray; (5) edge replica. Transmission optical microscopy is very useful with glass fibers and translucent matrices [4], but the method is inadequate for graphite fiber composites since the material is opaque. The reflecting optical microscope is useful for any material and was the predominate method used by previous investigators [2-10]. The stiffness of a laminate has been reported to decrease during the development of microcracks in some laminate configurations and materials [4,7,9]. The weight gain of samples immersed in water yields the volumetric density of the transverse microcracks [4]; this method has been used only infrequently. X-ray [7] and edge replicas [9,11,12] are promising new techniques.

2.2 Factors Affecting Transverse Microcracks

A paper summarizing a very extensive experimental program on the effects of numerous variables on TVM densities was published by Spain [3]. He found that higher microcrack densities were associated with the following contributing factors:

1. increased resin shrinkage during cure

2. higher resin coefficient of thermal expansion
3. larger temperature drop from cure to ambient temperature
4. greater irregularity of fiber cross-section
5. greater fiber twist (no twist with "wild" strands produce lowest TVM densities).

The TVM densities due to thermal loading were also found to be higher for resin systems having lower tensile ultimate strain and shear strength.

TVM densities for Skybond 703 polyimide resin were found to be higher after cure when the prepreg volatile content and length of post-cure were increased [8]. The increased length of postcure causes a void metamorphosis from interconnected voids to translaminar micro-cracks. Variation of the cure breathing technique and bleeder cloth composition was also investigated in ref. [8], but the TVM density was found to be unaffected. Quackenbush and Doner [10] noted that for Thornel 50/Epon 828 and 1031, and Thornel 50/NARMCO1004 composites decreasing the fiber volume fraction increased the TVM density after cure. The application of pressure throughout the cure cycle, including cooldown, was found to prevent microcracking.

2.3 Microcracking and Material Behavior

Doner and Novak [2] tested cross-plied laminates made from Thornel 50 graphite fibers and FM150, ERLA4617, and 828/DMP-10 epoxy resins. They reported that transverse microcracks do not significantly

reduce composite strength or stiffness. Transverse microcracks induced by cyclic loading are reported by McGarry and Willner [4], and Reifsnider and Masters [9] to cause a 10 percent elastic modulus reduction in cross-plied and quasi-isotropic laminates. McGarry and Willner used glass fibers as reinforcement whereas Reifsnider and Masters used graphite fibers. Molcho and Ishai [7] report that the load-deflection curve of their (5208/T300) graphite/epoxy composites was moderately affected by transverse microcracks. Their tests were conducted on 28 ply laminates having twenty-0° plies and four-±45° plies arranged in various stacking configurations. They achieved a one-time, like new load-deflection curve by caulking the microcracks with additional resin and curing a second time. Quackenbush and Doner [8], among others [2,4,7], suggested that the primary effect of the microcracks is the accelerated degradation of material properties by the environment, especially moisture.

2.4 Residual Strains

TVM due to thermal loading is believed by most previous investigators of transverse microcracks to be the result of the residual strains exceeding the transverse ultimate strain of a ply. Daniel, Liber and Chamis [13] developed a technique for measuring residual strains in a laminate. High temperature strain gages were embedded in laminates prior to cure and used to monitor the residual strains during and after cure. Results obtained with this method for several material systems are reported by Daniel and Liber in refs.

[14-17]. The residual strains in the graphite/polyimide (Modmor I/WRD 9371) composite of ref. [16] were found to exceed the transverse ultimate strain in all plies of $[0_2/\pm45]_s$ and $[0_2/90_2]_s$ laminates.

2.5 Analytical Methods

The predominant analytical method reported in the literature for calculating the residual stresses in a laminate is linear elastic laminate analysis. Daniel and Liber [17] used linear laminate analysis in combination with their results from the embedded strain gages of refs. [13-17]. Chamis [18] concluded that residual stresses predicted by linear laminate analysis are reasonably accurate for numerous laminate configurations and material properties.

Linear laminate analysis with temperature independent material properties can impose an important limitation on the accuracy of this method for high temperature composites. The matrix dominated mechanical properties can be very temperature dependent and exhibit appreciable nonlinearity [19-22]. Improved material representation in laminate analysis has been achieved by several investigators. The methods used have been incremental solution, incremental solution with higher order terms [23], and a method using secant moduli and solving the simultaneous equations resulting from the equilibrium of the individual lamina [19]. Another method for predicting the residual stresses is an incremental finite element analysis which is capable of modeling the material properties as functions of temperature and strain [24,25].

The multiple cracking theory developed by Garrett and Bailey [26], and improved by Parvizi and Bailey [27] has been used to predict the average TVM spacing in a laminate as a function of applied stress. The method is based upon force equilibrium of a portion of a laminate with one crack present. Reifsnider [11] developed a theory similar to the multiple cracking theory which predicts the saturation TVM density of a laminate.

2.6 PMR Polyimide Resins

PMR polyimides were developed by Serafini and his colleagues [28,29] in 1972 while attempting to obtain an improved ablative resin. Additional chemistry and high temperature stability studies were conducted by Serafini and Delvigs [22]. These studies concluded that the most attractive form of the PMR polyimides was PMR-15. PMR-15 is obtained by the polymerization of the monomer reactants NE, MDA, and BTDE to achieve a formula molecular weight of 1500. PMR-15 demonstrates good stability of mechanical properties at 600°F (315°C) for 125-500 hours and for a more extended time at 550°F (290°C). The applicability of a HTS1/PMR-15 graphite fiber composite was successfully demonstrated by the construction and testing of complex molded turbine blades as reported in ref. [30,31]. Shuart and Herakovich [20] have presented longitudinal and transverse elastic moduli and Poisson's ratio in both tension and compression loading for PMR-15 reinforced with HTS1 graphite fiber. Celion 6000 graphite fiber/PMR-15 composite material is currently being investigated by NASA for

application to advanced space transportation systems. A complete set of room temperature mechanical properties for the neat (without fibers) resin were reported by Cavano [32], Cavano and Winters [31], and Hansen and Chamis [33].

Chapter 3

EXPERIMENTAL PROGRAM

3.1 Material Specifications

All specimens, except those used to determine stress-free temperature, were cut from six panels. Each panel was fabricated using Celion 6000/PMR-15 prepreg tape and vacuum bag curing in an autoclave. The cure cycle used is shown in Fig. 2. The material was not post-cured in order to avoid the possibility of causing additional micro-cracks due to the thermal loading. The glass transition temperature was measured by the slope-intercept method and found to be greater than 675°F (358°C). Generally, the glass transition temperature only needs to be above the highest expected exposure temperature to insure good mechanical properties. The fiber volume fraction was determined to be 57 percent using the random point method discussed in ref. [34]. Fabrication of specimens for determination of the stress-free temperature is discussed in Section 3.7.

Six laminate configurations were investigated: $[0_2/90_2]_s$, $[0/90/0/90/0/90]_s$, $[0_3/90_3]_s$, $[45/-45/0/90]_s$, $[0/45/90/-45]_s$, and $[0/60/0/-60]_s$. The three different cross-ply laminates were chosen to determine the effect of layer thickness and stacking sequence on TVM. The quasi-isotropic laminates with fibers at 0°, ±45°, and 90° were selected to study the influence of the stacking sequence on TVM density. The $[0/60/0/-60]_s$ laminate was selected as an alternate laminate.

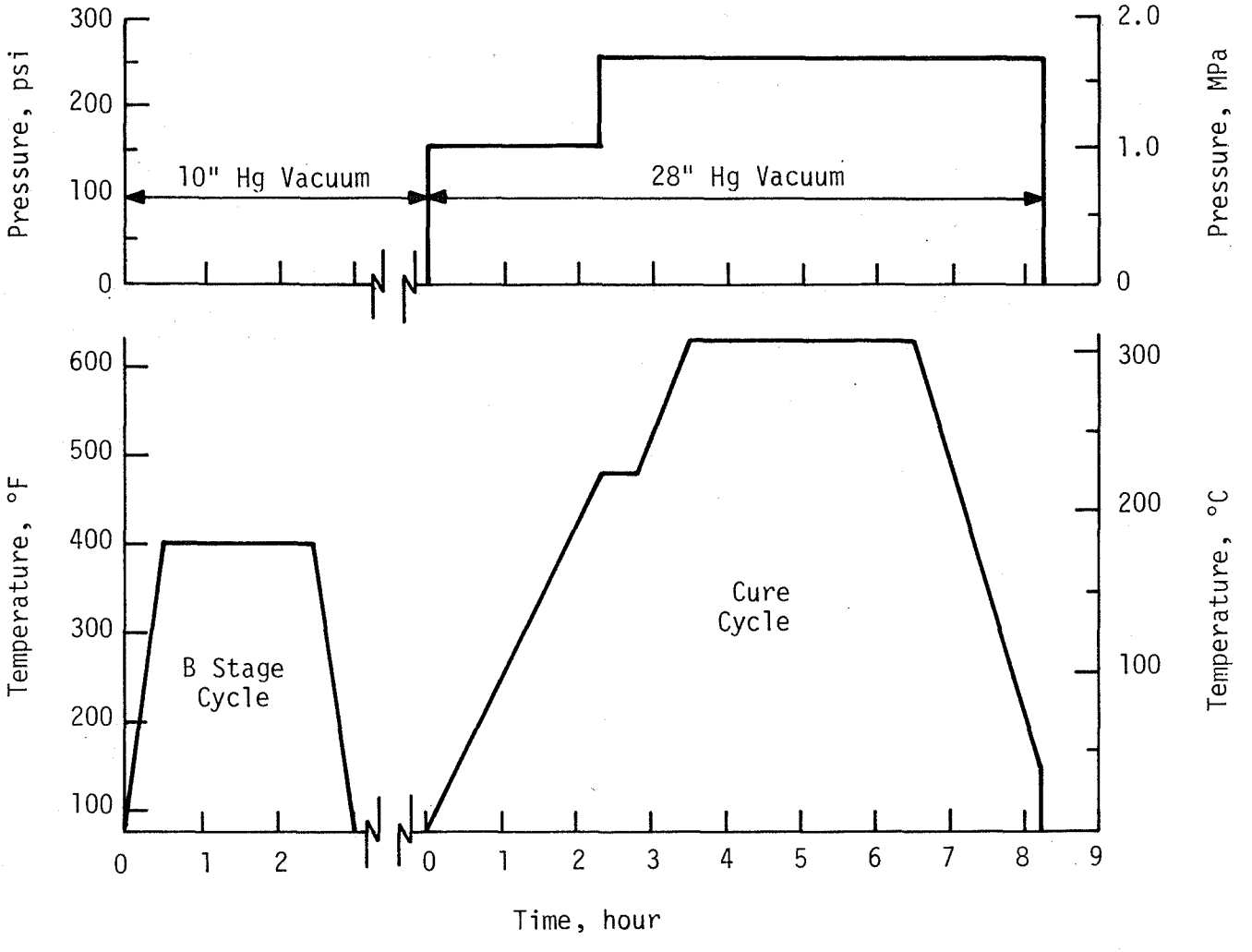

Fig. 2. Cure Cycle for Celion 6000/PMR-15 Graphite-Polyimide.

3.2 Metallographic Studies

Microscopic observation of TVM was greatly enhanced by polishing the surface using standard metallographic polishing techniques. This involves mounting the specimens in polyester mounts and polishing it with progressively finer abrasives. A final abrasive size between 5 micron and 0.3 micron normally produced good results.

A magnification of 50X or greater was generally necessary to discern details of a TVM. Two methods were employed to illuminate the specimens for microscopic work. In the first method, the light rays were directed nearly tangent to the specimen surface. Tangential lighting is primarily useful for exaggerating surface relief, especially near a TVM. This is necessary whenever a large TVM has become partially filled during polishing, rendering the microcrack nearly indistinguishable from resin rich regions.

The second method of illuminating the surface had the incident light perpendicular to the surface. Typically a metallographic microscope is equipped to function in this manner. Standard microscopes are capable of this type of lighting if a beam splitter is used to direct light from an external source through the objective lens onto the specimen. The perpendicular light is especially useful since excellent detail, bright lighting, and high magnification is possible; however surface relief is not easily observed.

Because of the difficulty in obtaining satisfactory photographs in the limited light from tangent illumination, photomicrographs using this method will not be presented in this work. However, the

method was useful in locating TVM. The perpendicular lighting was used predominantly in this study because of the aforementioned reasons.

3.3 X-Ray

The extent of TVM in from the laminate edge was found by x-raying specimens. The contrast between the TVM and surrounding material was enhanced by immersing the specimens in a liquid penetrant overnight before x-raying. The penetrant used was TBE(tetra-bromo-ethane). The penetrant was nearly opaque to x-rays and thereby yielded the desired high contrast between the TVM and adjacent material. The results of the x-ray study are discussed in section 4.1.

3.4 Replicating Technique

The replicating technique is a method for producing a copy of a surface. It has been in common usage in scanning electron microscopy and was first applied to composites by Stalnaker and Stinchcomb [12]. The replicating material used in this study was 0.08 mm thick acetyl cellulose film which possesses the characteristic of softening while in contact with acetone. This technique was used on the tensile specimens to determine the variation of TVM density with applied stress.

Before a satisfactory replica could be taken, the edge of the specimen had to be polished in a manner similar to that used for the metallographic studies. By using a final abrasive size of 5.0 micron instead of 0.3 micron, graphite fibers remained visible in the replica.

Care was taken to keep the polished surface flat since a rounded surface produced a poor replica. A replica was taken by placing a strip of acetyl cellulose (3/4 in. by 5 in. (2 cm. by 12 cm) is a convenient size) over the polished surface while it was in a vertical position. A few drops of acetone were applied to the upper portion of the inside surface of the cellulose film allowing capillary action and gravity to cause the acetone to flow between the film and specimen. After the acetone had softened the film, pressure was applied to the film by sliding the thumb down the length of the strip. This left an impression of the polished surface on the film. After the acetone was allowed to dry, the film was carefully peeled off.

Trapped air bubbles tended to be a problem, especially since they collected around microcracks. If the surface was cleaned with a soft cloth and acetone prior to taking the replica, the number of air bubbles was reduced. It was also found that better replicas were obtained if the film was not placed completely flat on the surface while applying the acetone. This improved the wetting of the film and polished surface by the acetone, and improved the resolution of the replica.

3.5 Thermal Loading Tests

Five of the six symmetric laminates in this investigation were free of transverse microcracking after cooldown from cure. The exception was the $[0_3/90_3]_s$ laminate. The $[0_3/90_3]_s$ laminate exhibited only a few TVM (2-3 per inch/1-2 per cm) in the outer plies on one side of the laminate. These cracks are believed to be the result of

inadvertent bending during specimen preparation. Since the TVM densities after cure were zero or very low, the densities reported after tensile testing are considered to be due entirely to that test.

The thermal loading tests were conducted using a heat-up rate of approximately 15°F/min (8°C/min), unless stated otherwise. The specimen geometry used for these tests was a 1 inch by 1 inch (2.54 cm by 2.54 cm) square. One specimen of each laminate configuration was subjected to one of five types of thermal loading. The Type 1 thermal loading was the cool-down from cure. The other four thermal loadings started from room temperature after the specimens had been cured. The loadings consisted of: Type 2 - a liquid nitrogen quench; Type 3 - heating to 625°F (330°C) followed by an ice water quench; Type 4 - a slow heating to 625°F (330°C) followed by a slow cooling to -320°F (-196°C); and Type 5 - heating to 625°F (330°C) followed by a liquid nitrogen quench (-320°F/-196°C). The Type 2 liquid nitrogen quench loading consisted of quickly immersing the specimens into boiling liquid nitrogen (-320°F/-196°C) for 15 minutes. The specimens were then returned to room temperature air. In the Type 3 625°F (330°C) to ice water quench loading, the specimens were heated at the standard rate to 625°F (330°C) and held there for one hour. The specimens were then quickly immersed into ice water for 15 minutes.

For both types of 625°F (330°C) to -320°F (-196°C) thermal loadings (Types 4 and 5) the specimens were held at 625°F (330°C) for one hour and then at -320°F (-196°C) for another hour. The

difference between thermal loadings was the rate of heating and cooling of the specimens. The Type 4 slow heating/slow cooling, 625°F to liquid nitrogen thermal loading, involved heating the specimens to 625°F (330°C) at approximately 5°F/min and cooling at 15°F/min to 20°F/min (8°C/min to 11°C/min) to -320°F (-196°C). The specimens were then re-heated to room temperature at approximately 5°F/min (3°C/min). In the Type 5 625°F to liquid nitrogen quench, the specimens were heated at the standard rate and cooled rapidly by immersing the specimens into boiling liquid nitrogen (-320°F/-196°C). The specimens were then re-exposed to room temperature air after the quench.

The specimens were heated in a Blue M circulating air oven which had an automatic thermostat to control the oven temperature. The specimens experienced only a ±5°F (±3°C) cyclic thermal loading, even though the oven air temperature had a fluctuation of about ±10°F (±6°C). The temperature variation of the specimens was moderated by placing the specimens between two 0.125 in (0.318 cm) thick aluminum sheets. The temperature of the specimens was determined by using two k-type thermocouples.

3.6 Tensile Tests

Tensile tests were conducted on the three laminate configurations, $[0_2/90_2]_s$, $[45/-45/0/90]_s$ and $[0/45/90/-45]_s$. Each specimen was loaded incrementally to increasing higher levels and a replica was taken after each load increment. These tests had a three-fold purpose, to determine: (1) the applied strain necessary to initiate TVM; (2) the TVM density

as a function of applied stress; (3) the correlation between microcracking and laminate mechanical properties such as elastic modulus and Poisson's ratio.

All specimens were 1 inch by 12 inches (2.54 cm by 30.5 cm) and approximately 0.05 inch (0.127 cm) thick (8 plies). Each specimen had 1 inch (2.54 cm) square tabs bonded to each end and longitudinal-transverse strain-gages attached to each side. Tensile load was applied at a constant head rate of 0.02 inch/minute (8.48 μm/sec). All test data were recorded using an automatic multi-channel data acquisition system. Data were acquired every two seconds.

3.6.1 Initiation of Microcracking

The applied strain necessary to initiate microcracks was found by taking replicas of the specimens at several low stress levels up to a maximum stress which was 40 percent of the experimentally determined ultimate stress. Replicas were not taken at higher stress levels for this particular group of specimens so that stress-strain data could be obtained from specimens which had not been subjected to extensive creep or cyclic loading.

3.6.2 TVM Densitites and Mechanical Properties

Tests were conducted to study the correlation between TVM density, applied stress and mechanical properties. Replicas of the specimens under load were taken at several stress levels below 50 percent of the predicted ultimate stress. For higher stress levels, the applied stress was reduced to 20 KSI (140 MPa) after each load step before taking a replica. Stress was then reapplied by

manual control to the previous maximum stress level. Then the 0.02 inch/minute (8.48 μm/sec) head rate was used to load to the next desired stress level. This process was repeated until the specimen failed.

3.7 Stress-Free Temperature Determination

The stress-free temperature of a laminate is defined as the temperature at which a laminate is free from residual stresses. These residual stresses are a result of the mismatch in coefficient of thermal expansion between fiber and matrix, and layers of different fiber orientation. The stress-free temperature corresponds to the temperature at which an unsymmetric laminate has zero curvature. This temperature can therefore be determined by studying the curvature of an unsymmetric laminate as a function of temperature.

An unsymmetric $[0_3/90_3]$ laminate was chosen to determine the stress-free temperature. Two panels, 6 inch by 8 inch (15 cm by 45 cm), were cured using the same cure cycle as described in Section 3.1. The glass transition temperature of both panels was measured to be 625°F (330°C). The two panels were made from different batches of prepreg tape. (Both panels could not be made from the same batch of material as were the symmetric panels because the supply had been exhausted.) Different batches of material have been known to result in laminates having slightly different characteristics for matrix dominated behavior. Panels from two different batches of prepreg tape were tested to obtain an indication of the possible variation in stress-free temperature of different batches of typical PMR-15 laminates. Each panel was cut into four 1 inch by 18 inch (2.54 cm

by 45.7 cm) specimens using a diamond saw. The curved specimens are shown in Fig. 3.

The unsymmetric specimens were clamped at one end to a 4 inch by 24 inch (10 cm by 60 cm) flat steel plate. The clamp was applied 5 inches (12 cm) from one end of the specimen as shown in Fig. 4. The assembly was then placed in an Instron model A74 2 oven which was capable of maintaining any desired temperature between room temperature and 640°F (340°C) within ±2°F (±1°C). The specimen was observed through a window in the oven as the temperature was increased at 5°F/min (3°C/min). As the curvature of a specimen approached zero, the rate of temperature increase was slowed to 1°F/min (1/2°C/min). The specimen was considered flat when a point 6 inches (15 cm) from the free end was visually determined to touch the steel plate.

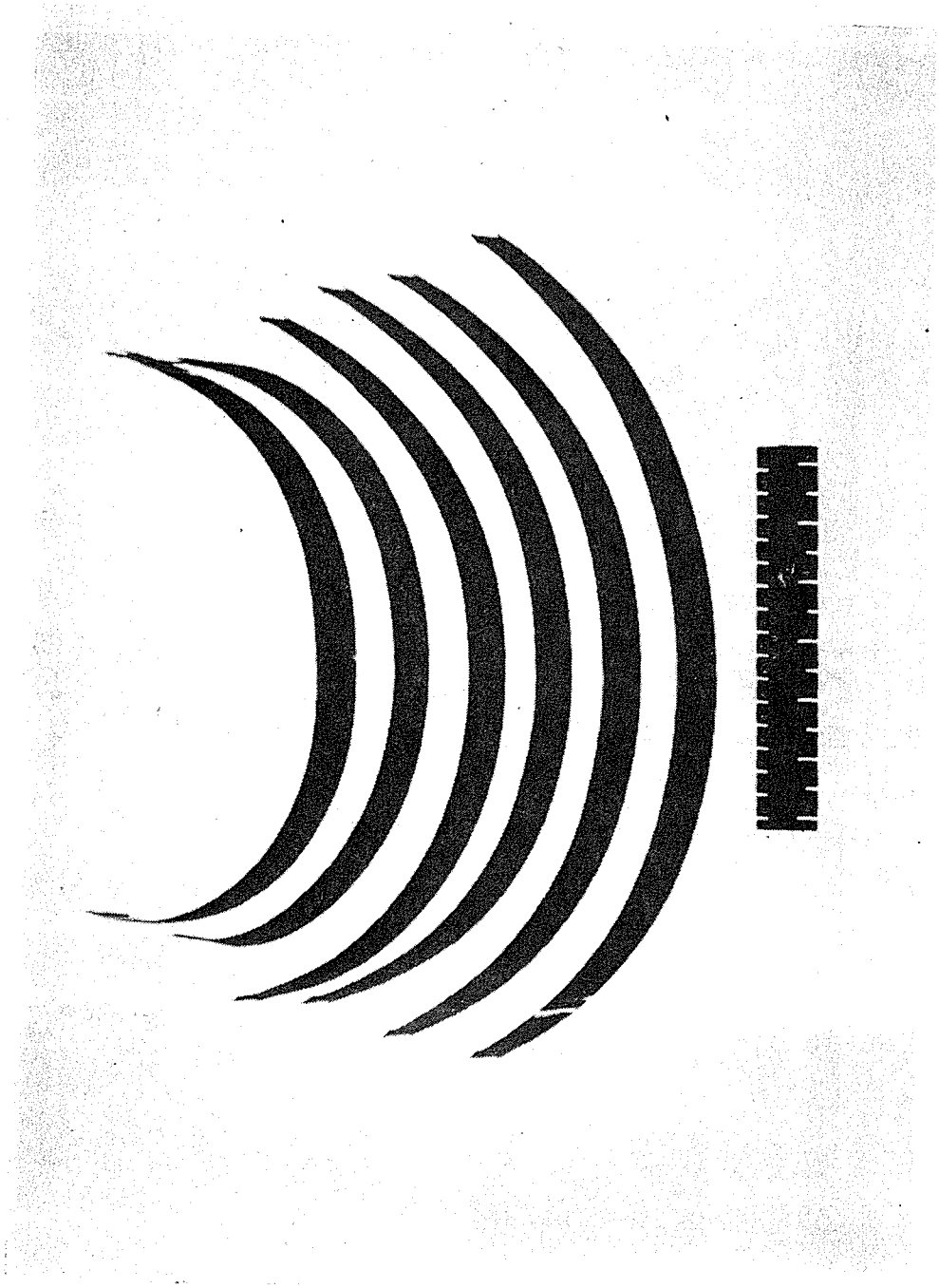

Fig. 3. Unsymmetric Laminates After Cure.

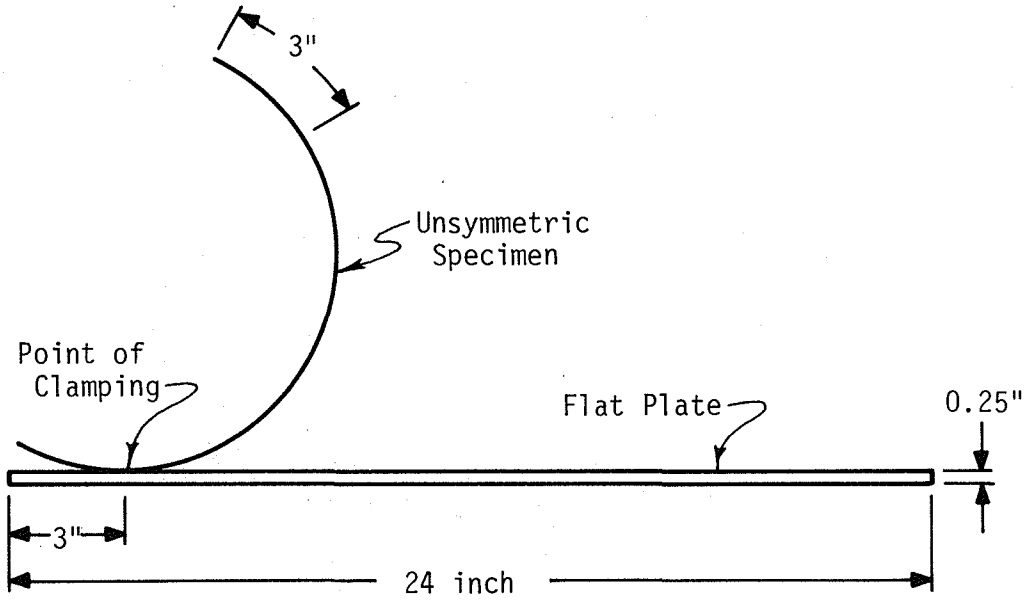

Fig. 4. Specimen and Fixture for Stress-Free Temperature Determination

Chapter 4

EXPERIMENTAL RESULTS

4.1 Characteristics of Transverse Microcracks

4.1.1 Viewing Direction

The viewing direction (illustrated in Fig. 5) is the acute angle between the 0° laminate direction and the normal to the surface observed. When a 0° ply is observed from the 0° viewing direction, the fiber cross sections are observed (Fig. 6a). When the viewing direction is varied, the plies in which TVM are visible changes as shown in Figs. 6a-c. Of course, changing the viewing direction only affects the observed TVM density not the actual TVM density. These differences are due to the fact that the microcracks in a ply are not visible when the fiber direction is perpendicular to the viewing direction. Figure 6c shows a $[0_3/90_3]_s$ specimen viewed from the 45° direction. This figure demonstrates that microcracks are visible in both layers when viewed from the 45° viewing direction. Thus, microcracks in the ±45° plies of quasi-isotropic laminates should be visible from the 0° and 90° viewing direction.

The specimens subjected to thermal loading Types 1 through 4 were observed from the 0° viewing direction only. The Type 5 thermally loaded specimens were observed from both the 0° and 90° viewing directions. A 90° viewing direction was used for all specimens loaded in tension.

4.1.2 Resin-Rich Regions

Transverse microcracks have been found to form after a critical

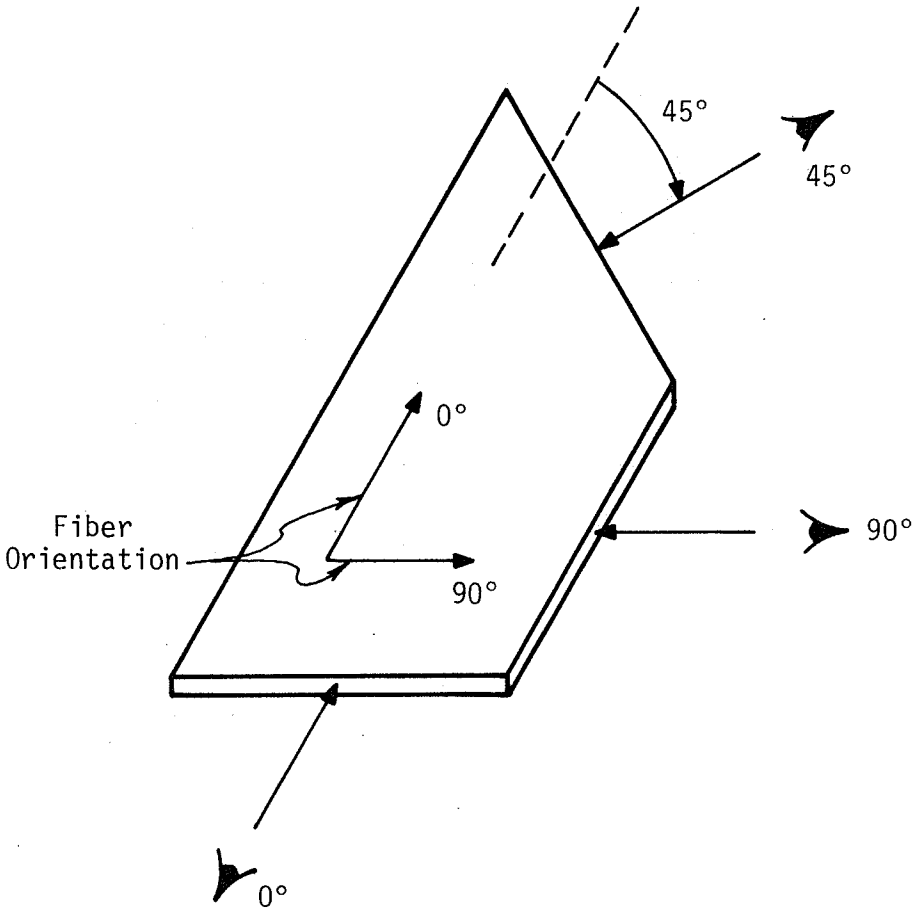

Fig. 5. Illustration of Viewing Directions.

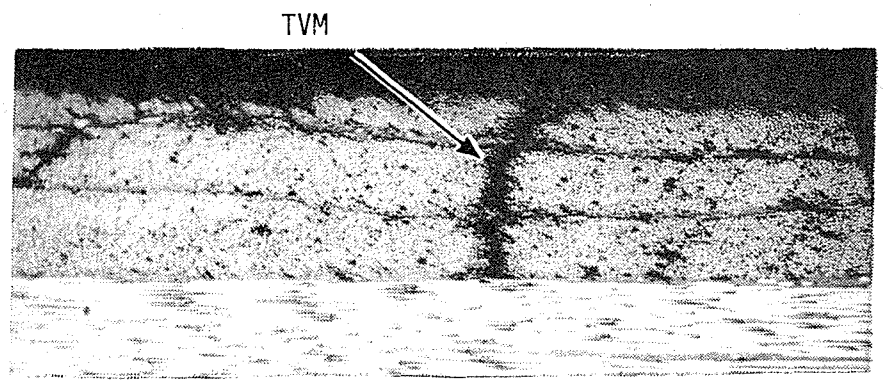

a) 0° Viewing Direction

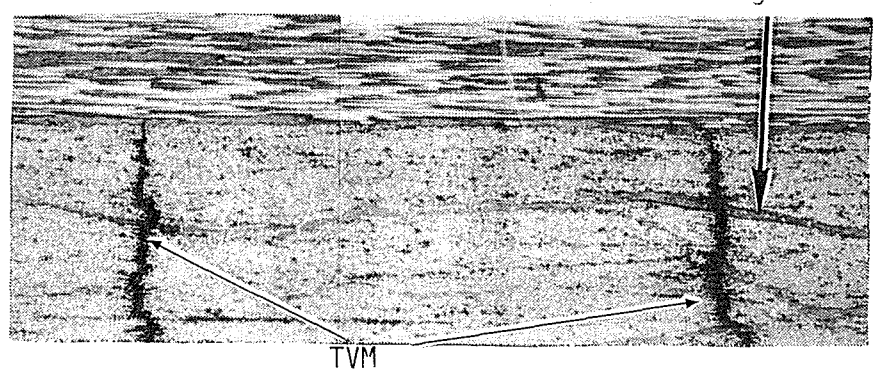

b) 90° Viewing Direction

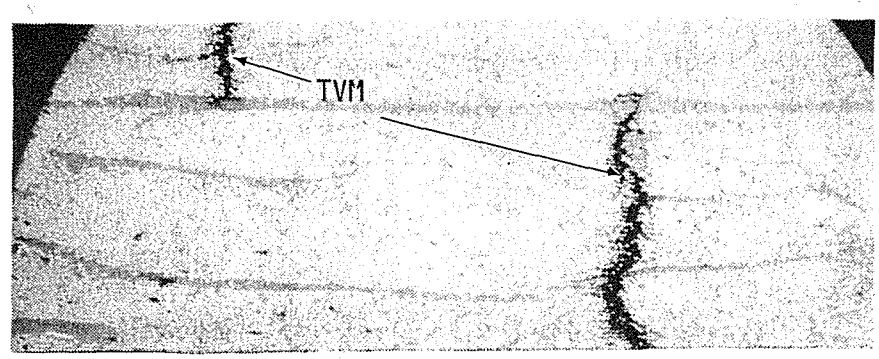

c) 45° Viewing Direction

70X

Fig. 6. Effect of Viewing Direction on TVM Observation in Type 5 Thermally Loaded $[0_3/90_3]_s$ Laminate.

stress has been attained in a ply (see Section 4.4.1). At stress levels marginally above this critical stress, microcracks do not generally penetrate a resin-rich region existing between two adjacent 90° plies, as shown in Fig. 7. However, the microcracks do propagate across the resin-rich region and the adjacent ply with the application of additional stress, as shown in Fig. 8. The TVM on the right-hand side of Figs. 7 and 8 propagated longitudinally a short distance along the resin-rich region before proceeding transversely across the next ply. This behavior was common although the longitudinal propagation occurred most frequently between plies of different fiber orientations and at higher applied stress levels.

Resin-rich regions located between plies of the same fiber angle did not exhibit a TVM-arresting effect in the thermally loaded specimens. However, the resin-rich region between plies of different orientation did appear to arrest microcrack propagation in the thermally loaded specimens as shown in Fig. 9.

The thickness of the resin-rich region had no apparent effect on its crack-arresting ability. This ability to arrest microcrack propagation for both tensile and thermal loading is a result of the transverse ultimate strength of the neat (unreinforced) PMR-15 resin being 33 percent higher than the transverse strength of the graphite-reinforced material [31-33].

4.1.3 Constraining Influences

Transverse microcracks in a ply are strongly influenced by the laminate stacking sequence. This influence is a result of constraints

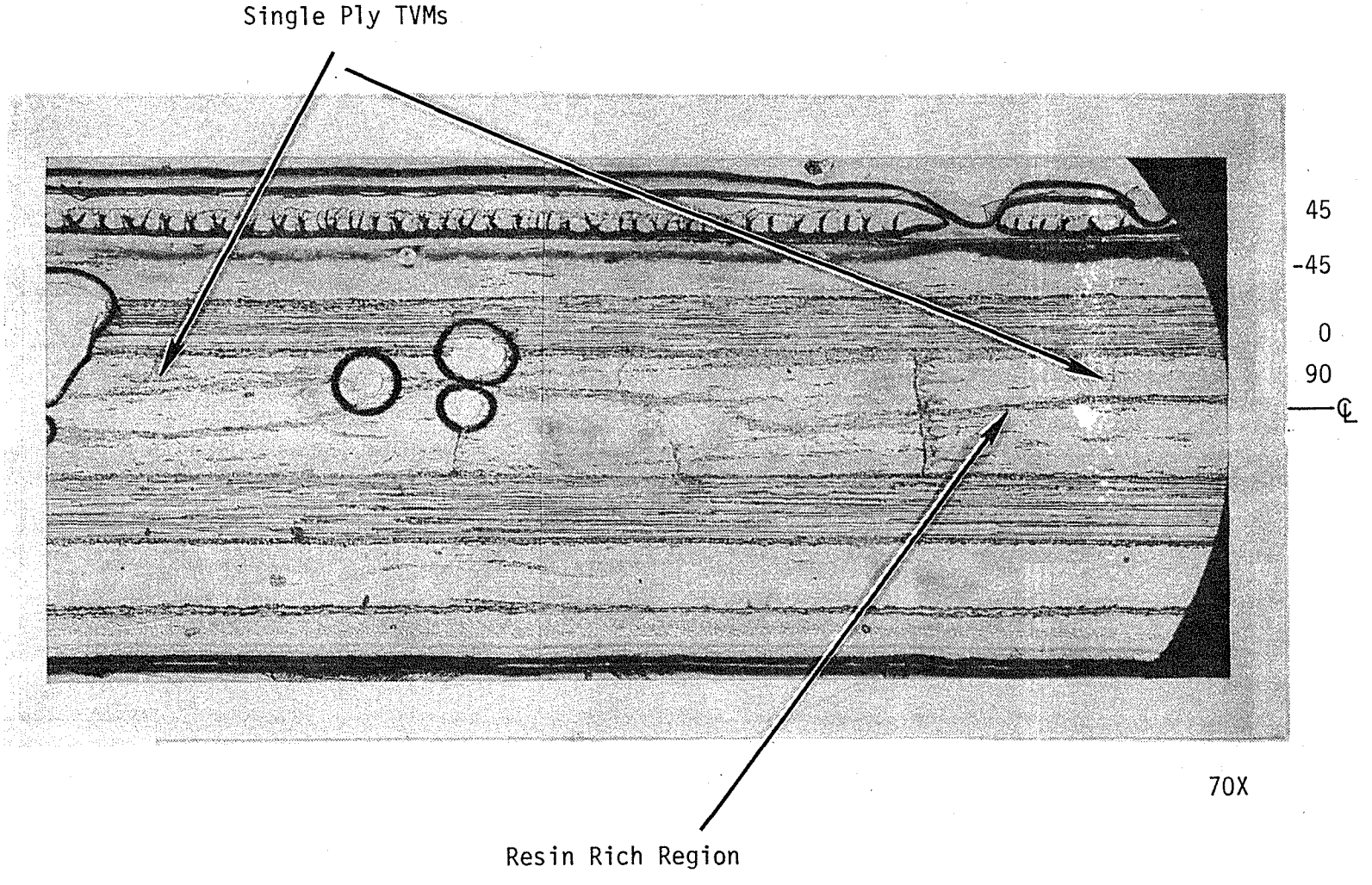

Fig. 7. Replica of $[45/-45/0/90]_s$ Tensile Specimen at 45% of of Ultimate Stress.

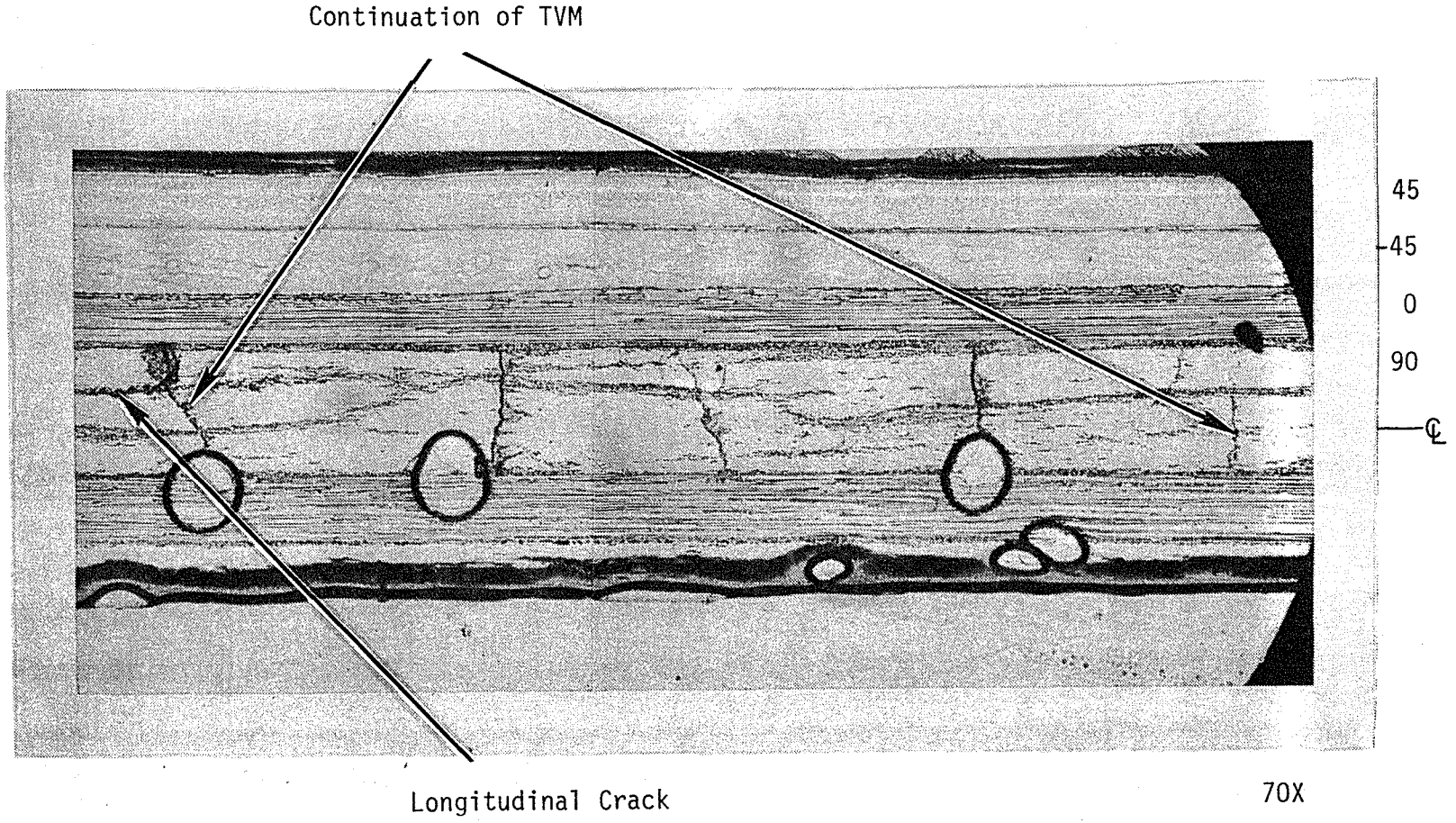

Fig. 8. Replica of $[45/-45/0/90]_s$ Tensile Specimen at 60% of Ultimate Stress.

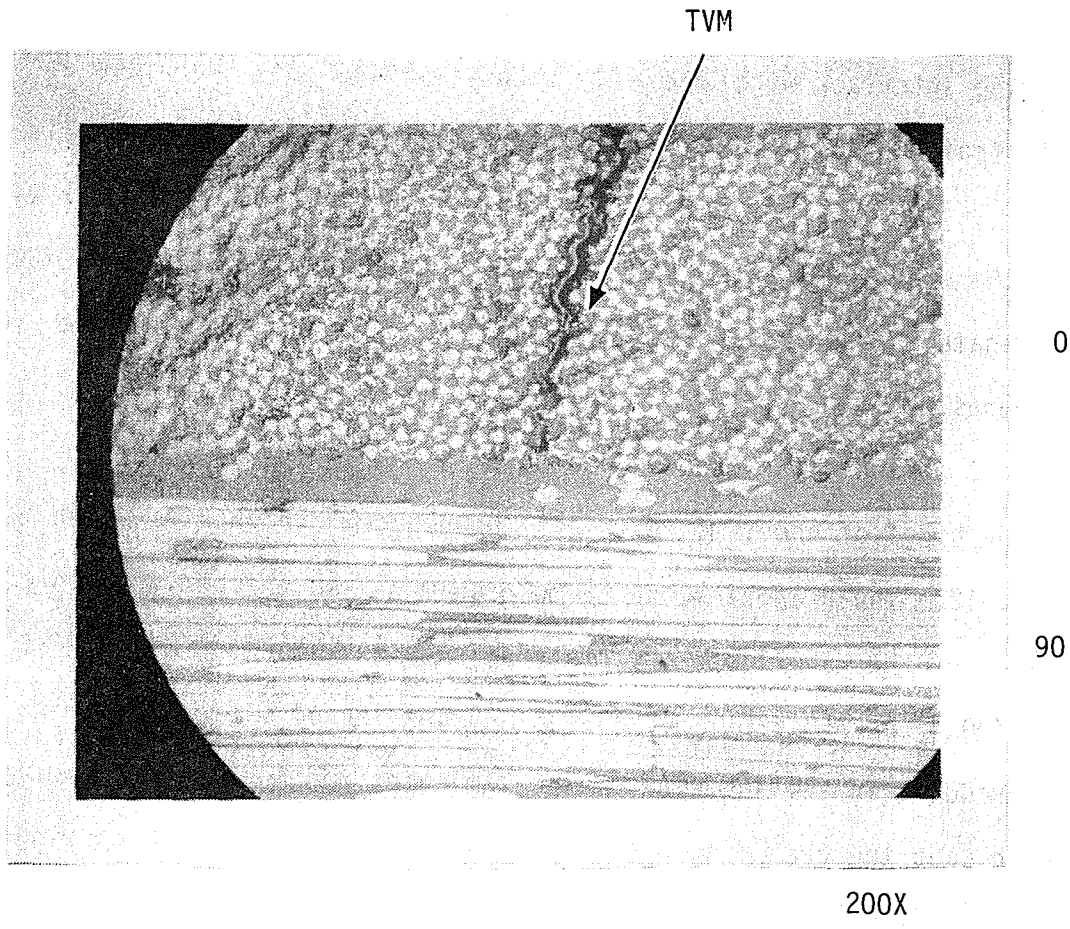

Fig. 9. TVM Near a Resin-Rich Region of a $[0_2/90_2]_s$ Laminate

imposed overall equilibrium considerations which give rise to interlaminar stresses in the boundary layer. The tapering of a transverse microcrack (Fig. 10) is an indication of this constraining effect. The microcracks in the 0° ply are wider near the mid-layer of the ply than at the interface with a 90° ply because the 90° ply exercises a constraining influence. The constraining effect of adjacent plies is also evident in Figs. 11 and 6b, which show that the mid-length width of the crack is greater for a $[0_3/90_3]_s$ laminate than for a $[(0/90)_3]_s$ laminate. Tapering of the crack width is also evident in these figures.

A common occurrence in the outer plies of a laminate is "branching" of the TVM. A typical branched microcrack is shown in Fig. 12. The branching occurs more commonly in thicker groupings of plies of the same fiber orientation, such as the outer plies of the $[0_2/90_2]_s$ and $[0_3/90_3]_s$ laminates. Branching of microcracks was infrequent in the interior of the laminate, and, when it did occur, in each case the branching was very limited. The interior branching was also limited to the thicker groups of plies having the same fiber orientation, such as the 90° plies in the $[0_3/90_3]_s$ laminate. Branching may be more common in the outer plies of a laminate because the constraint from adjacent plies is introduced only from one side, as opposed to being introduced from both sides for interior plies.

Adjacent ply constraints may determine which plies develop microcracks. After type 5 thermal loading of a $[(0/90)_3]_s$ laminate, transverse microcracks were found only in the outer 0° plies and the

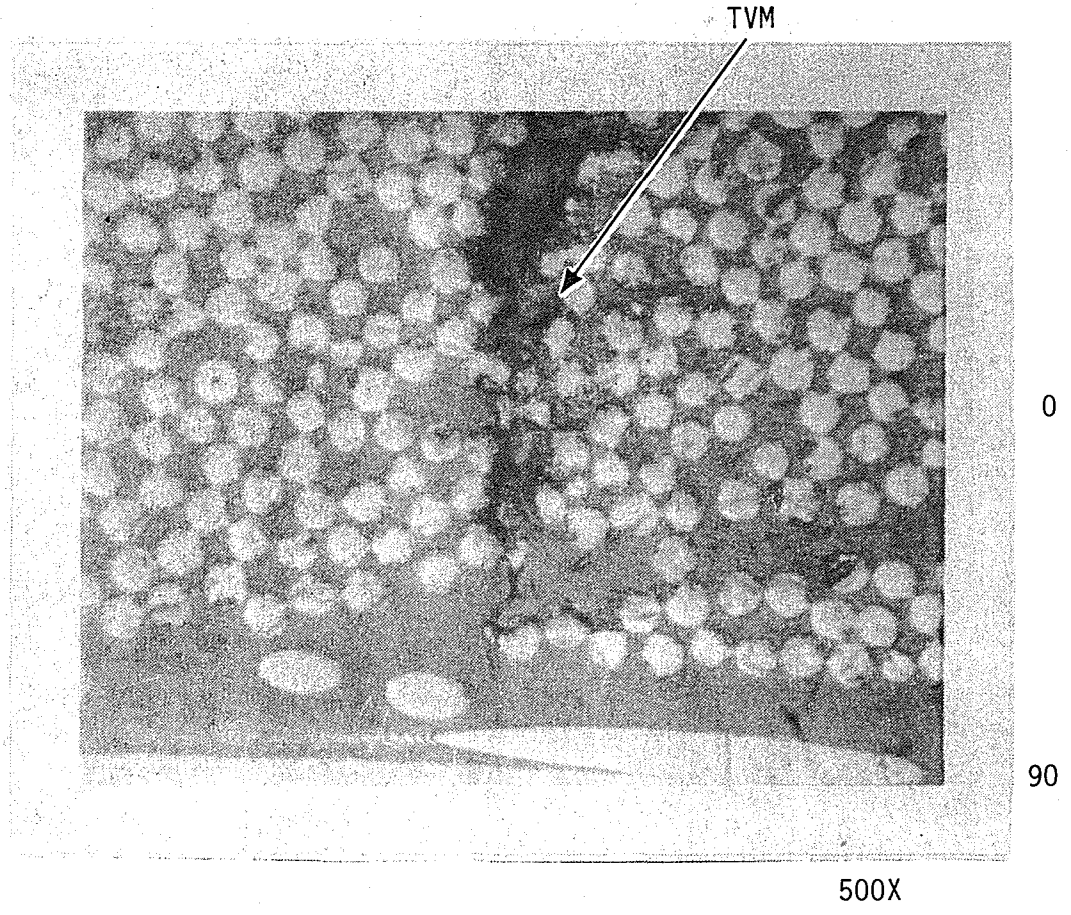

Fig. 10. TVM Tapering Near an Interface of a $[0_2/90_2]_s$ Laminate.

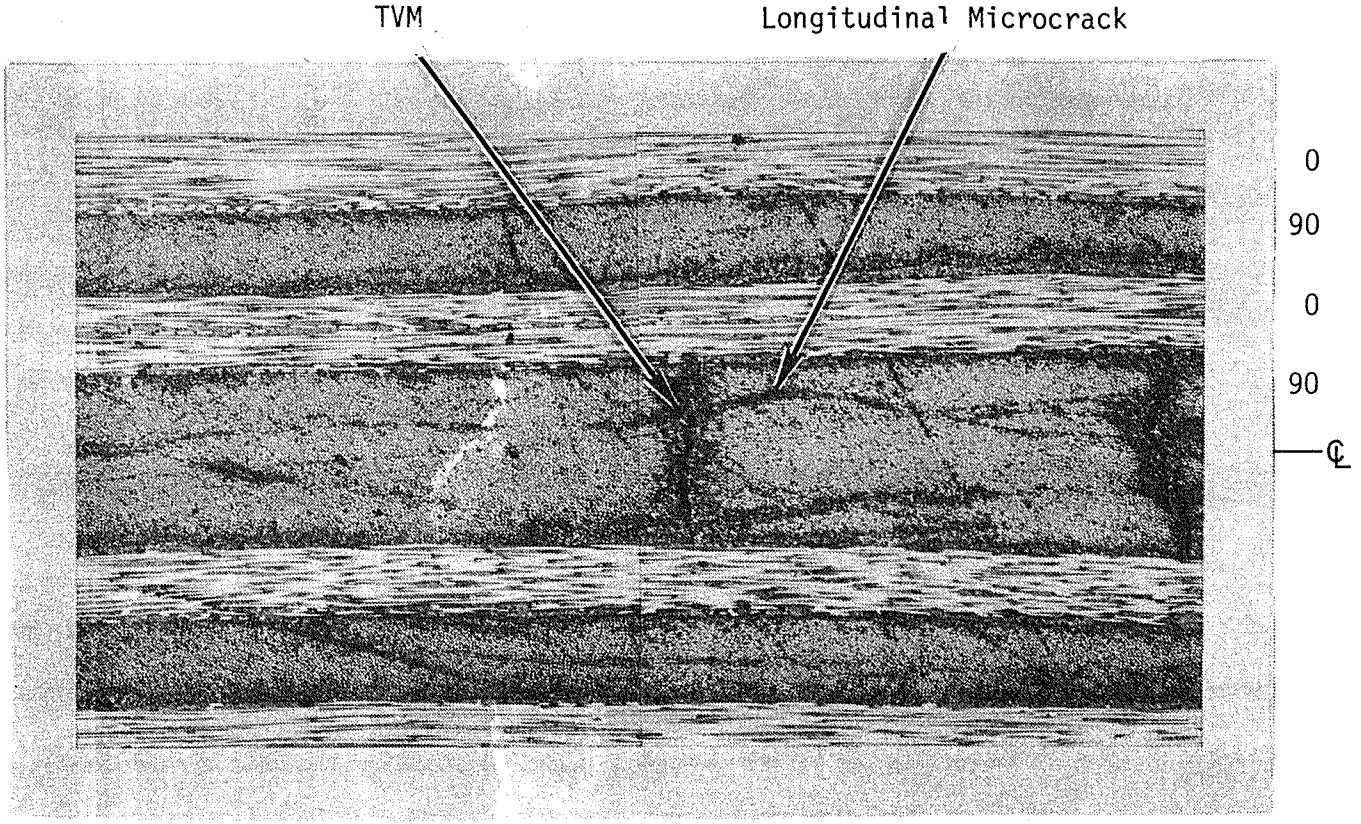

Fig. 11. 90° Viewing Direction of $[(0/90)_3]_s$ Laminate After Type 5 Thermal Loading.

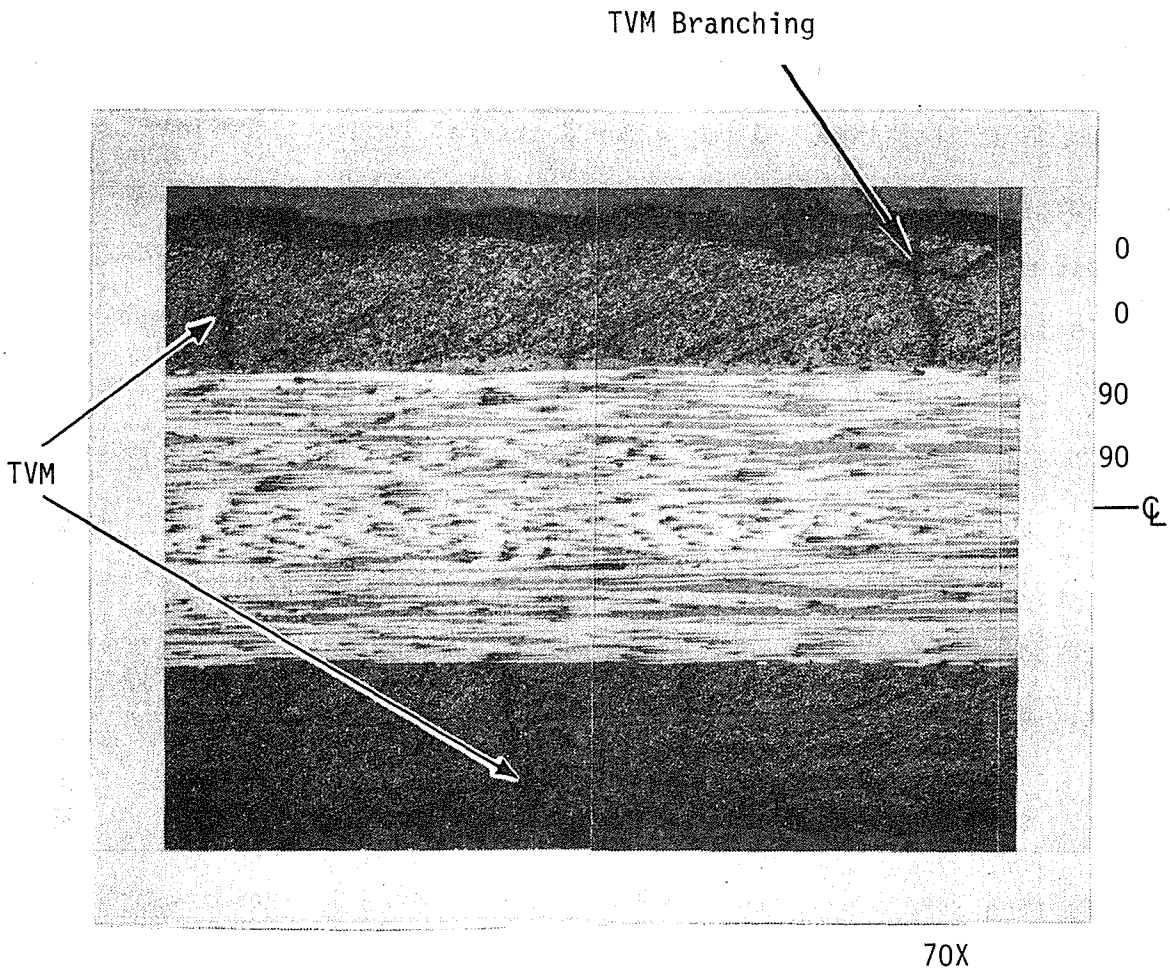

Fig. 12. TVM in a $[0_2/90_2]_s$ Laminate after Type 5 Thermal Loading.

90° plies adjacent to the midplane. Microcracks were absent in the other plies (Fig. 13). This result is inconsistent with the theory developed in Chapter 5 which predicts higher TVM density in the more heavily constrained layers. The reason for the difference is not known at this time. Also, after a thermal loading, the lower stiffness of a 45° ply does not impose the large constraint of a 0° ply, and microcracks are observed in the 90° ply of the $[0/45/90/-45]_s$ laminate shown in Fig. 14. However, when a 90° ply is bounded by 0° and 45° plies rather than two 45° plies, the 90° ply is more heavily constrained, and TVM are not observed in the 90° plies of the $[0/90/\pm45]_s$ laminate.

The longitudinal microcrack shown in Fig. 14 is discussed in detail in Section 4.2.4.

4.1.4 Extent of Microcracks from the Free Edge

The extent of transverse microcracking into the laminate from the free edges was readily observed using the X-ray method discussed in Section 3.3. X-ray photographs of cross-plied laminates subjected to a Type 5 thermal loading (fast heating to cure temperature followed by liquid nitrogen quench) are shown in Fig. 15. The microcracks generally extended completely across the 1-inch-square specimens. The few microcracks that do not extend across the specimen extend deeply into the laminate (greater than 0.1 inch [0.25 mm]). These microcracks usually stop near the tip of another TVM propagating from the opposite side of the specimen. Delaminations in the $[(0/90)_3]_s$ laminate as a result of the quench appear as dark circular shapes in Fig. 15c and,

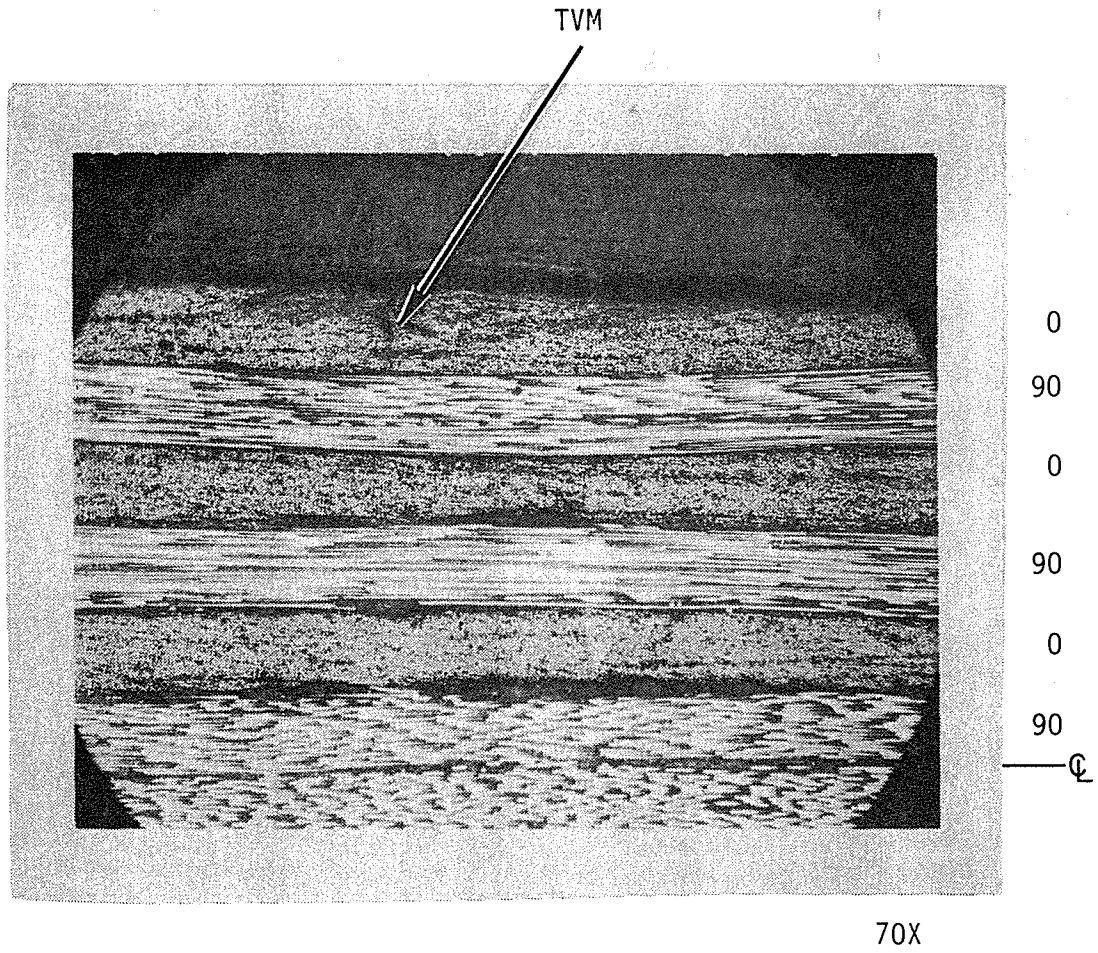

Fig. 13. TVM in a $[(0/90)_3]_s$ Laminate After Type 5 Thermal Loading.

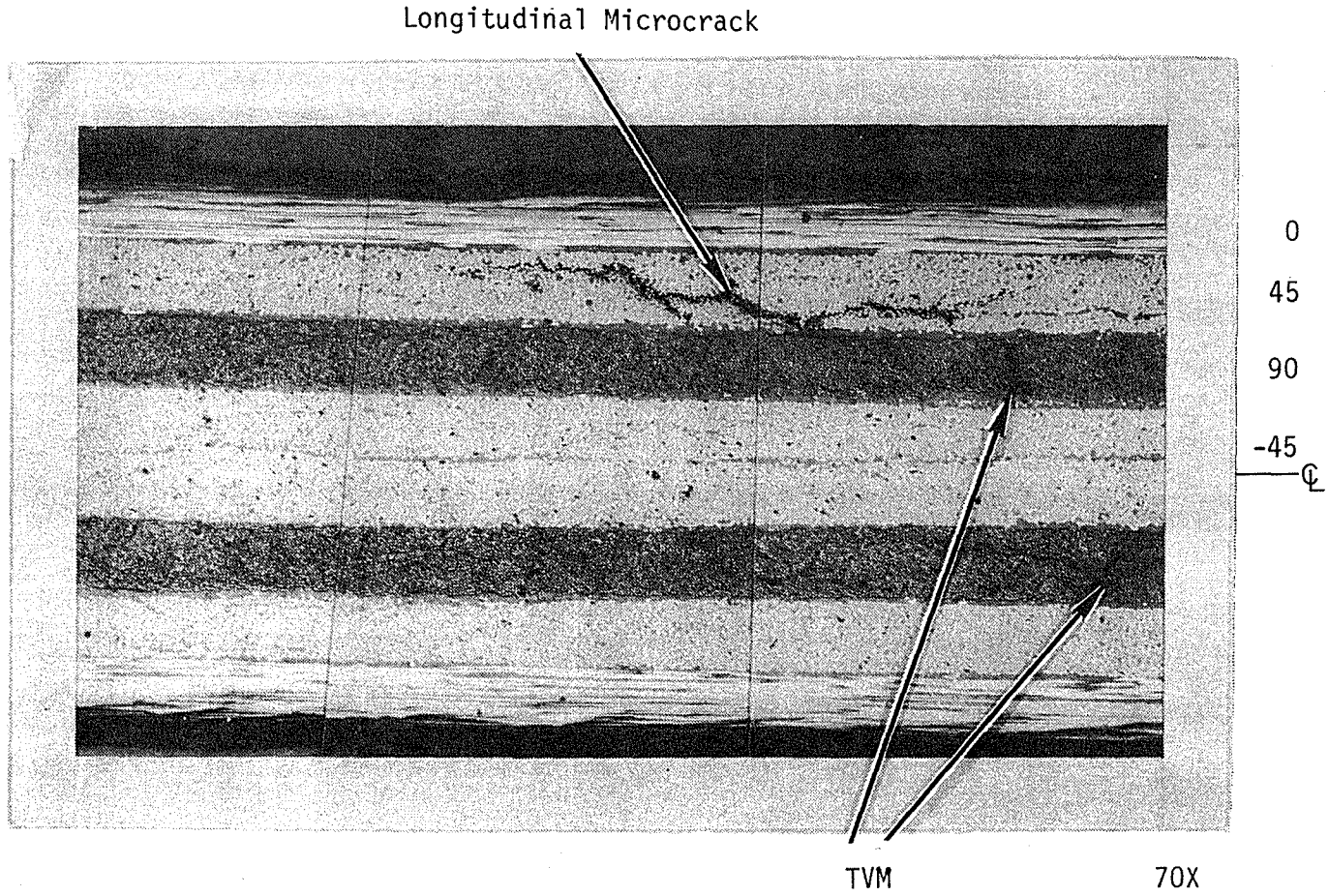

Fig. 14. 90° Viewing Direction of $[0/45/90/-45]_s$ Laminate After Type 5 Thermal Loading.

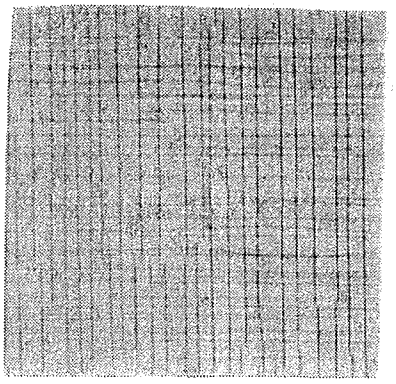

a) $[0_2/90_2]_s$

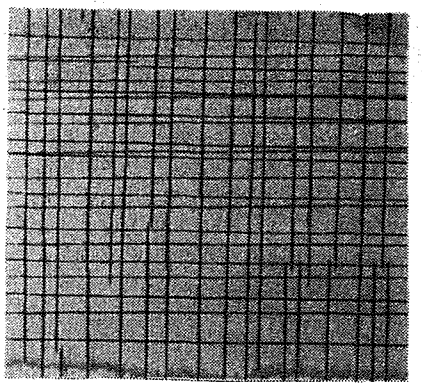

b) $[0_3/90_3]_s$

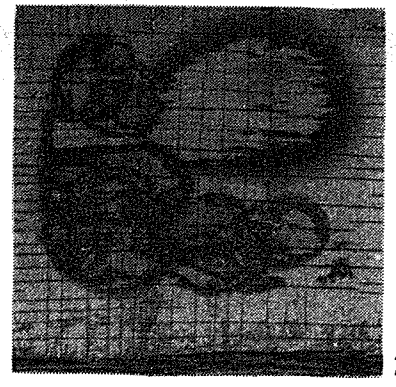

2X

c) $[(0/90)_3]_s$

Fig. 15. X-rays of Specimens Subjected to Type 5 Thermal Loading.

interestingly, do not extend to the free edges.

X-rays showed that transverse microcracks were only found in the 0° and 90° plies of the $[0/45/90/-45]_s$ laminate; microcracks were not present in the ±45° plies. Microcracks were not observed in any plies of the $[\pm45/0/90]_s$ laminate. The $[0/60/0/-60]_s$ laminate had numerous microcracks in the 0° ply, but only one in the -60° ply and none in the 60° ply. These three laminates are not shown because the contrast between microcracks and background is very poor.

The extent of the TVM from the free edge found in this investigation does not agree with the statement by Molcho and Ishai [5] that the microcracks "appear only at the edges of the laminates." The reason for this difference in TVM depth is not known for certain, but is believed to be the result of incomplete penetration of the tracer used by Molcho and Ishai.

The results of the X-ray tests show that the TVM densities observed at the edge of a laminate are the same as the densities throughout the laminate. The edge TVM densities obtained by the replica and microscopy techniques are assumed to be accurate representations of the interior laminate densities.

4.2 Thermal Loading

The specimens that were subjected to Type 1 through Type 4 thermal loadings were viewed from the 0° viewing direction only. The specimens that were subjected to a Type 5 thermal loading were observed from both the 0° and 90° viewing directions.

The TVM densities of all the specimens subjected to Type 2 through

5 thermal loadings are summarized in Figs. 16-19. Each TVM density reported in Figs. 16-19 is of the 0° plies only, except for the perpendicular view in Fig. 19, where the density is of the 90° plies only In each case, the density is the average of densities in each 0° (or 90°) ply. The densities found in the ±45° or ±60° plies are given in the text. The densities of the $[(0/90)_3]_s$ laminate are determined in a slightly different manner inasmuch as microcracks were found only in the outermost 0° plies and the 90° plies adjacent to the midplane. The TVM density reported for this laminate is the average of the two outermost 0° plies or the average of two midplane 90° plies for the 90° viewing direction.

4.2.1 Type 1 Thermal Loading - Cure Temperature to Room Temperature

This thermal loading corresponds to the cool down-to-room-temperature portion of the cure cycle (Figure 2). Five of the six laminates subjected to Type 1 loading were free of microcracks after loading. As discussed in Section 3.5, the 0° plies on one side of the $[0_3/90_3]_s$ laminate had a very few cracks which are believed to have been caused by handling while the specimens were being cut. This is in sharp contrast to the densely microcracked HTS1/PMR-15 material after its cooldown from cure, as shown in Fig. 1. This difference is attributed to the improved cure cycle and the greater transverse tensile strength of the Celion 6000/PMR-15 material as compared to the HTS1/PMR-15 material (cf. Section 5.3).

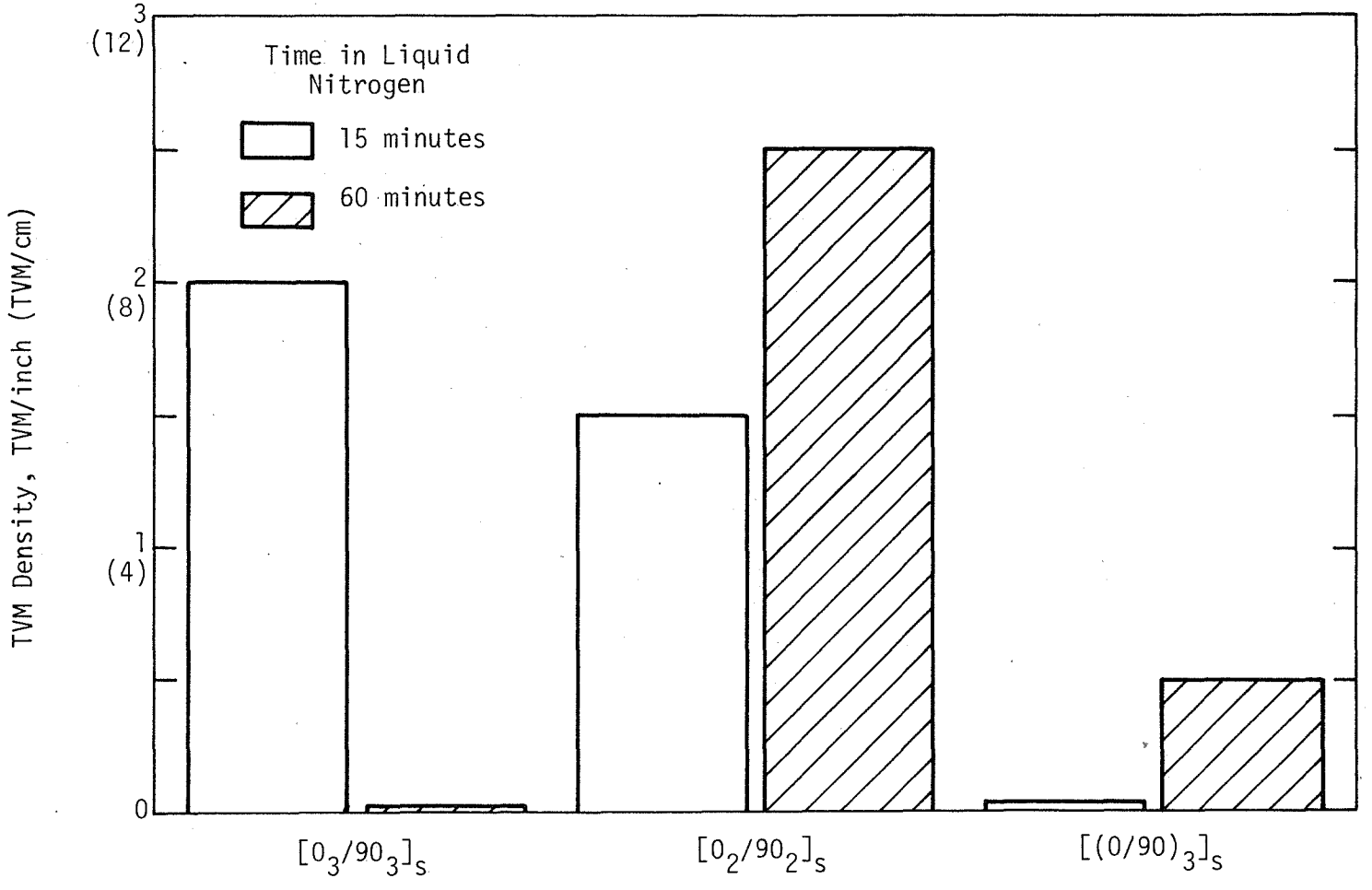

Fig. 16. TVM Densities After Type 2 Thermal Loading.

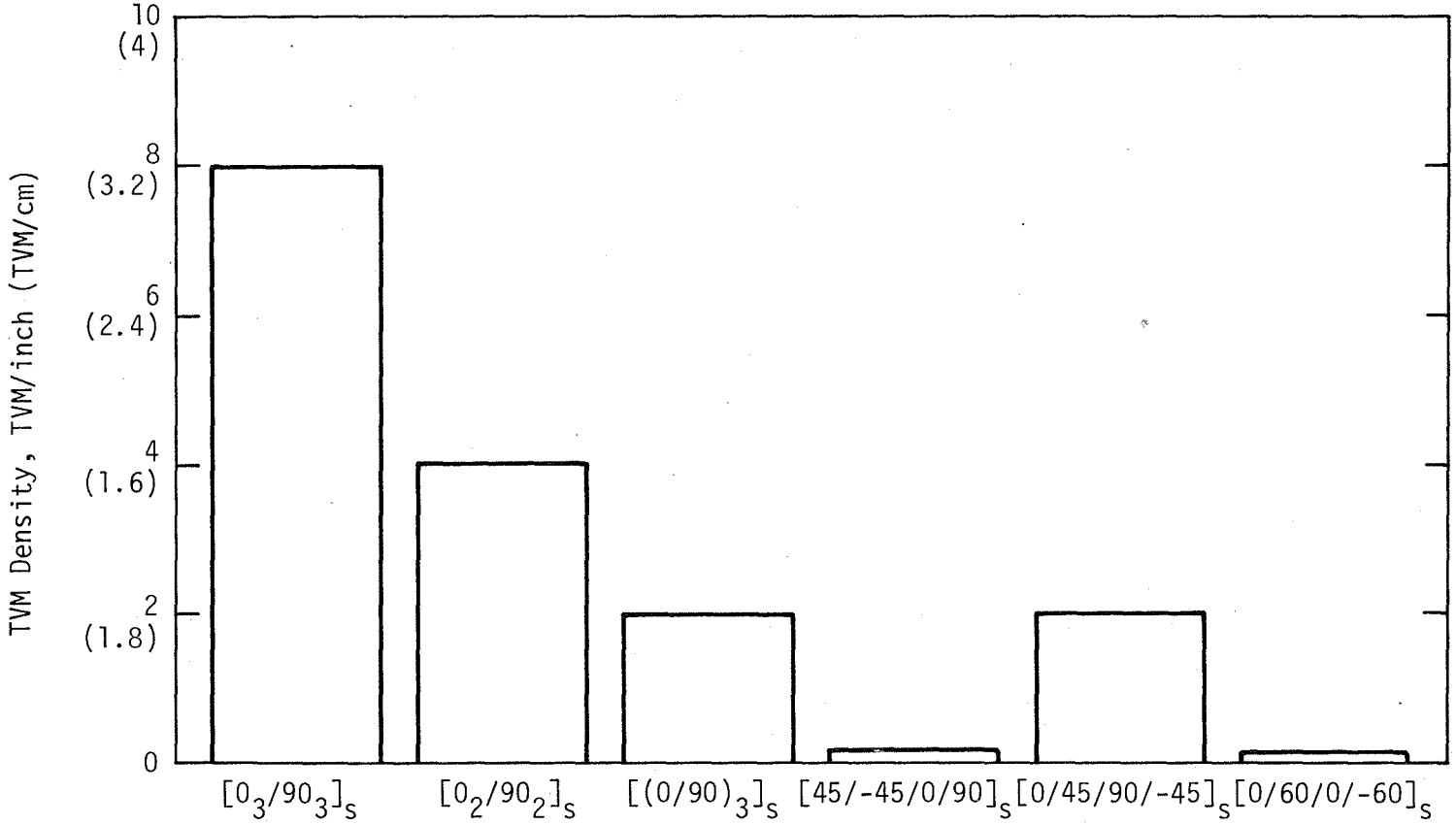

Fig. 17. TVM Densities After Type 3 Thermal Loading.

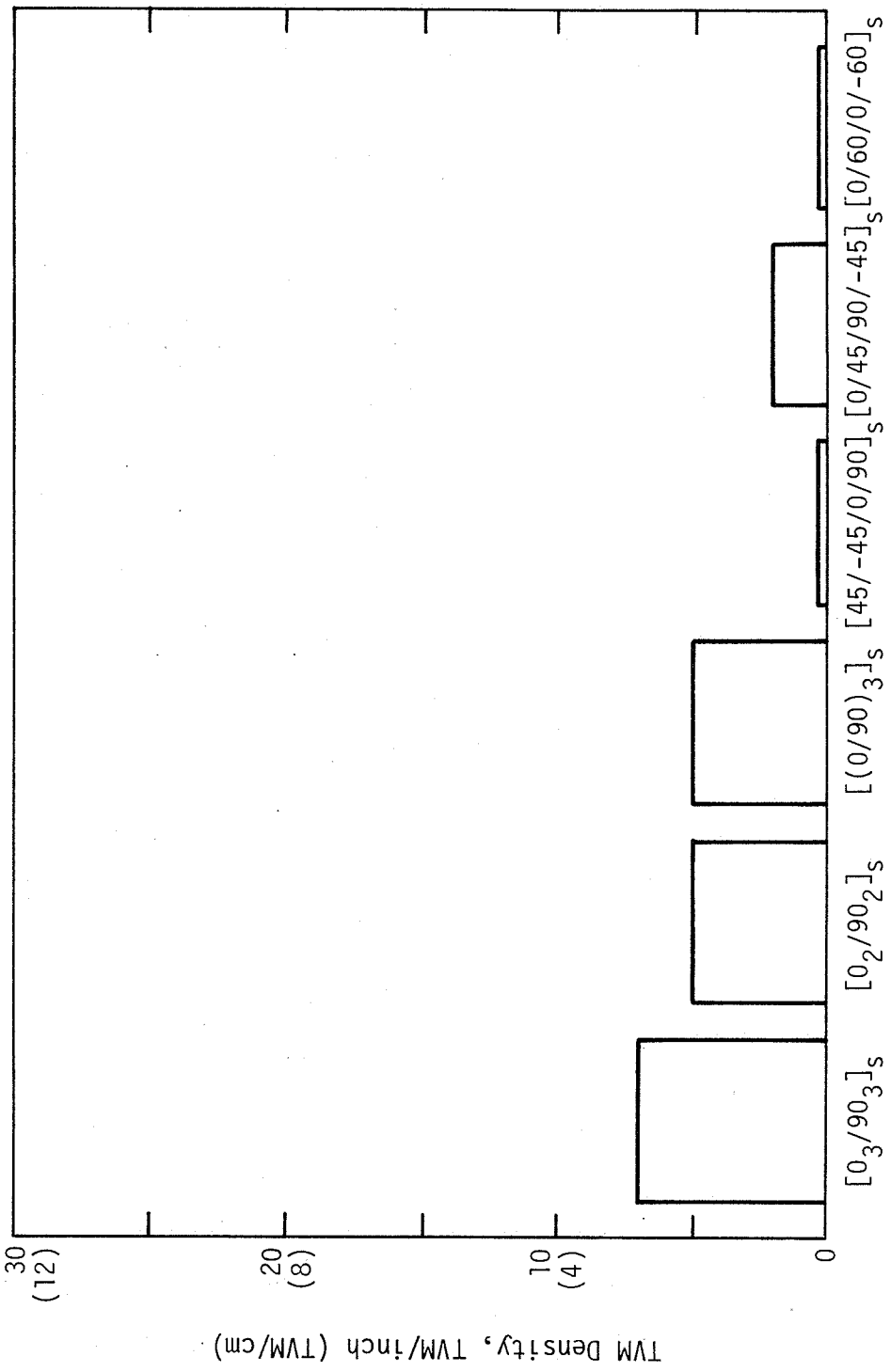

Fig. 18. TVM Densities After Type 4 Thermal Loading.

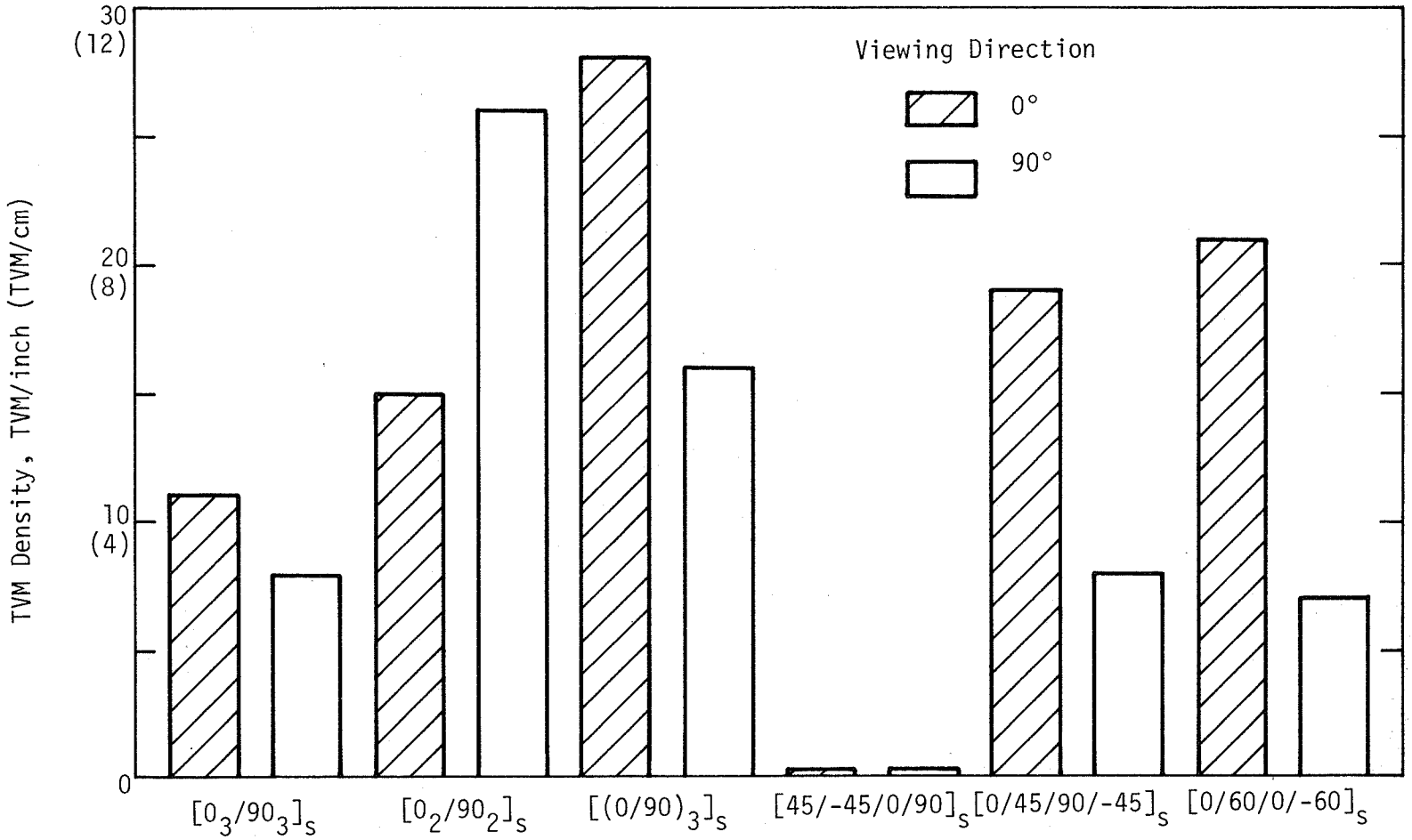

Fig. 19. TVM Densities After Type 5 Thermal Loading.

4.2.2 Type 2 Thermal Loading - Room Temperature to Liquid-Nitrogen Quench

A very low density of TVM was present in the $[0_2/90_2]_s$ and $[0_3/90_3]_s$ laminates after a Type 2 thermal loading (15 minutes in liquid nitrogen) (Fig. 16). The microcracks were observed in all 0° plies of both laminates. The $[0_2/90_2]_s$ laminate had 1-1/2 TVM/inch (0.6 TVM/cm), and the $[0_3/90_3]_s$ laminate had 2 TVM/inch (0.8 TVM/cm). The other four laminates had no detectable microcracks after this loading.

Another set of specimens was submerged into liquid nitrogen for 1 hour. Very few specimens developed microcracks; the $[0_2/90_2]_s$ laminate had 2-1/2 TVM/inch (1 TVM/cm) and the $[(0/90)_3]_s$ laminate had one TVM on one side in the outermost 0° ply. The difference in densities between tests is believed to be due to the statistical distribution of stress risers, imperfections, and strength.

4.2.3 Type 3 Thermal Loading - Room Temperature to Cure Temperature to Ice-Water Quench

Specimens that developed TVM after exposure to Type 3 thermal loading had higher TVM densities than did those specimens exposed to either a Type 1 or 2 thermal loading. The four laminates that developed microcracks were $[0_3/90_3]_s$, $[0_2/90_2]_s$, $[(0/90)_3]_s$, and $[0/45/90/-45]_s$ (Fig. 17). The $[0_3/90_3]_s$ laminate had the highest TVM density, with 8 TVM/inch (3 TVM cm).

All of the 0° plies in the $[0_3/90_3]_s$, $[0_2/90_2]_s$, and $[0/45/90/-45]_s$ laminates showed microcracking (Figs. 20-22). The $[0/45/90/-45]_s$

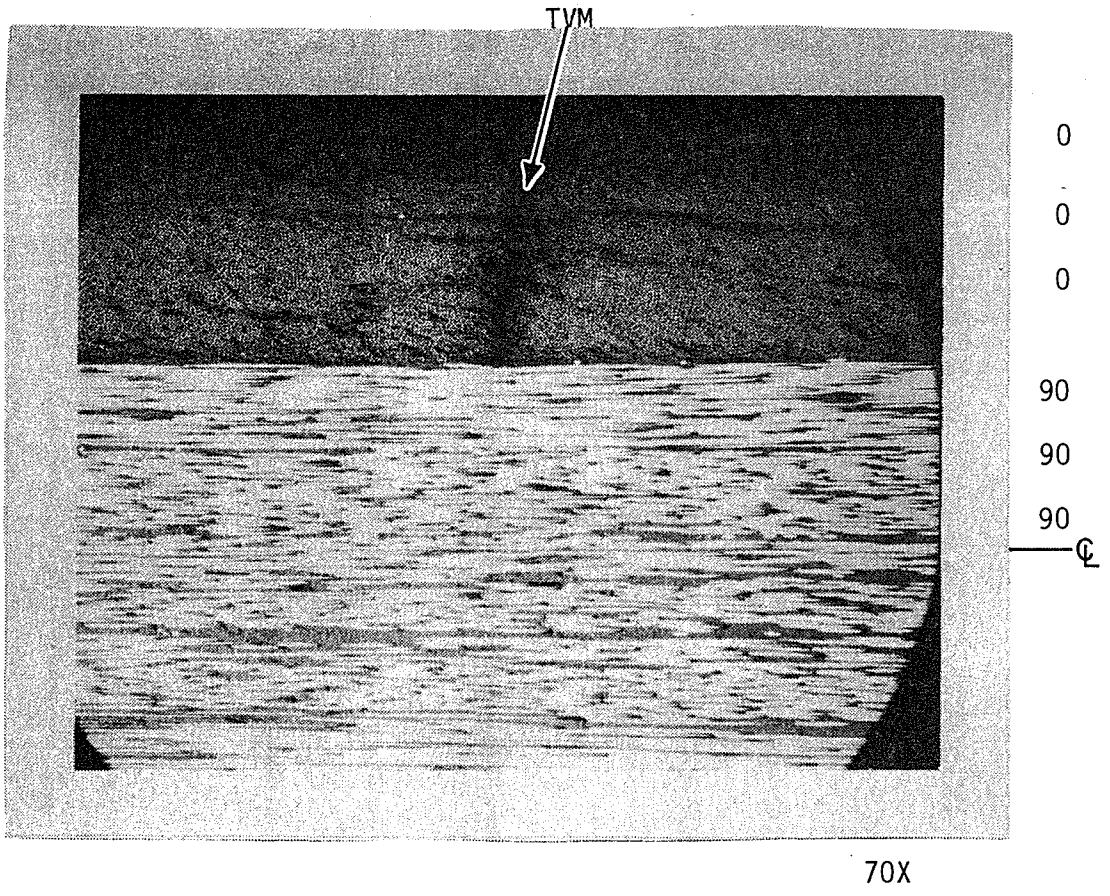

Fig. 20. TVM in a $[0_3/90_3]_s$ Laminate After Type 3 Thermal Loading.

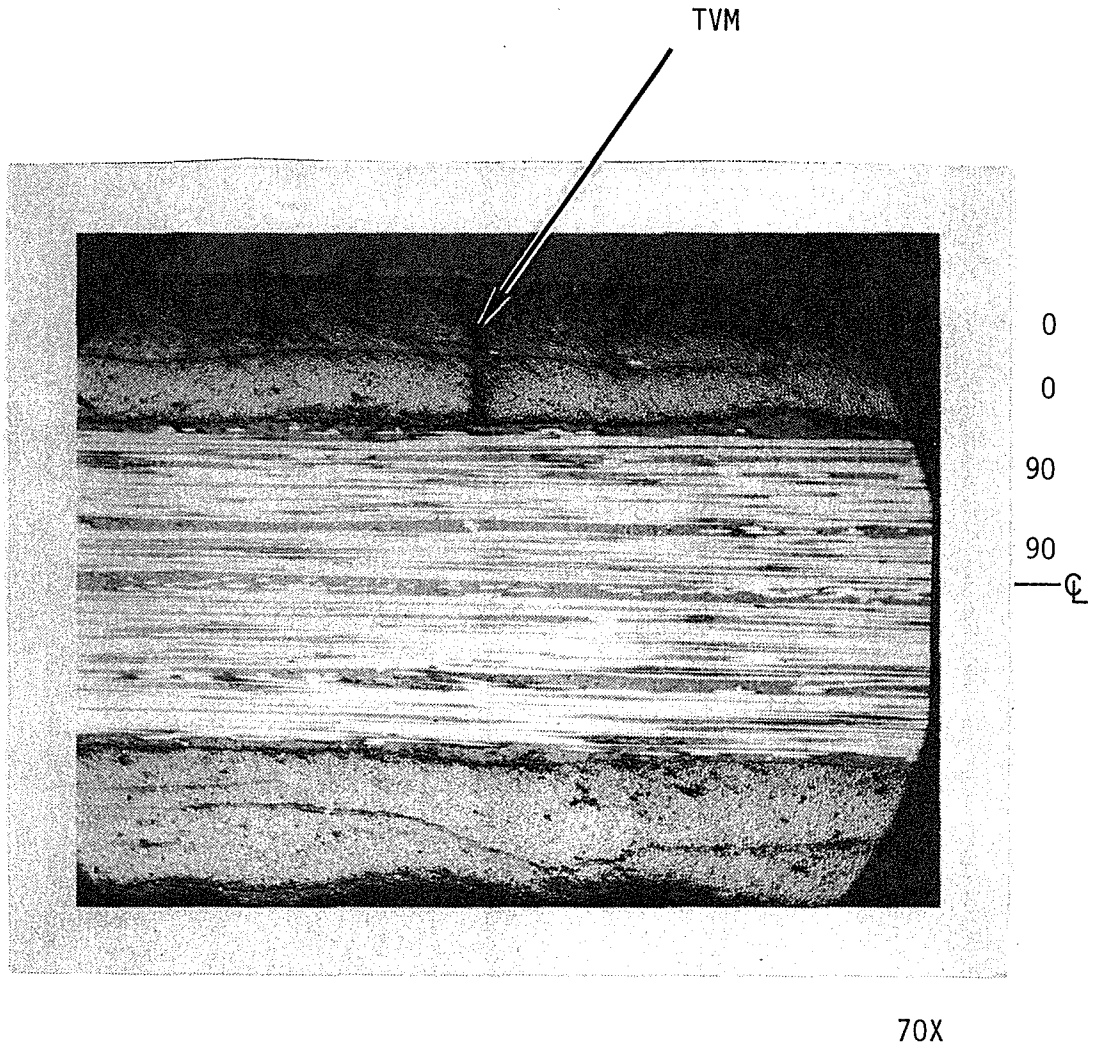

Fig. 21. TVM in a $[0_2/90_2]_s$ Laminate After Type 3 Thermal Loading.

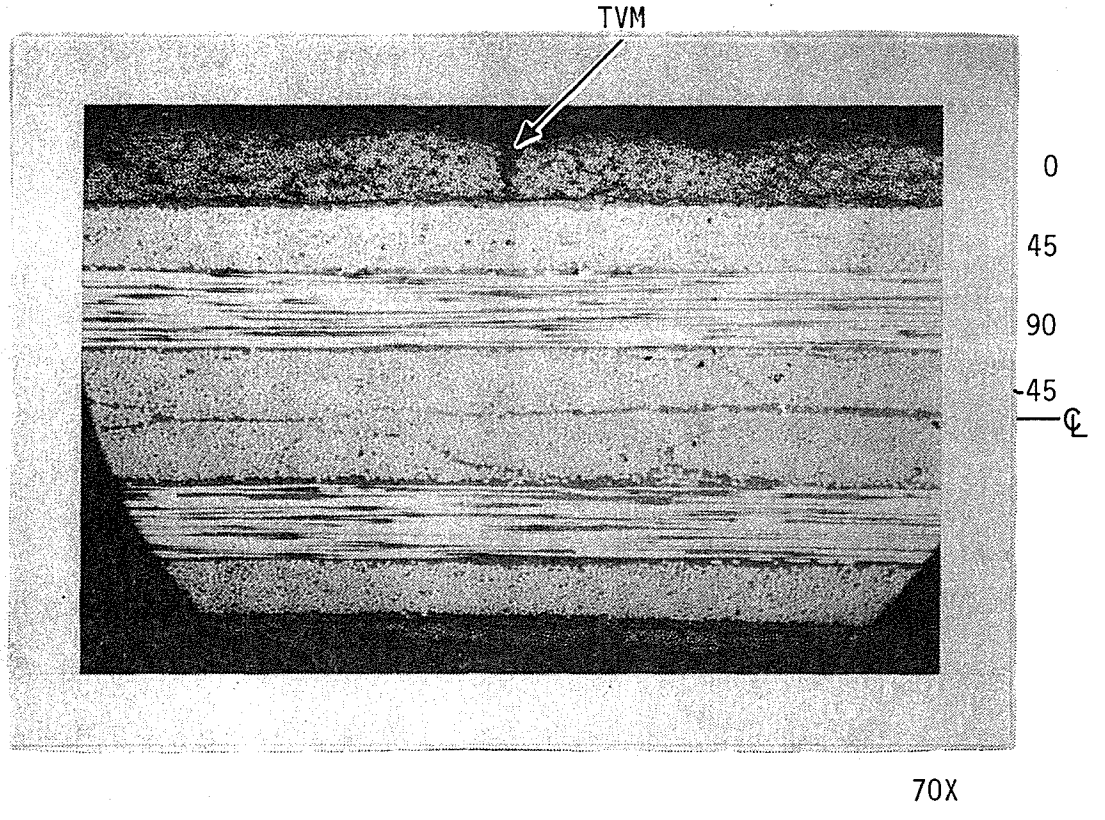

Fig. 22. TVM in a $[0/45/90/-45]_s$ Laminate After Type 3 Thermal Loading.

laminate did not have any observable microcracking in the 45° or -45° plies. Only the outermost 0° plies of the $[(0/90)_3]_s$ laminate developed microcracks as shown in Fig. 23. The other two locations of 0° plies did not contain any TVM. The microcracks in this specimen appeared only near one corner of the specimen at a localized thickening of the 0° plies. Less constraint from adjacent plies may be the cause of the localization of microcracks in this region.

4.2.4 Type 4 and 5 Thermal Loadings - Room Temperature to Cure to Liquid Nitrogen

Slowly cooling from the cure temperature to liquid nitrogen (Type 4), and quenching in liquid nitrogen from the cure temperature (Type 5) are both discussed in this section in order to better contrast and compare specimens subjected to thermal loadings differing only in the rate of cooling.

The most pronounced effect of the cooling rate was the much higher TVM density in the quenched specimens than in the slowly cooled specimens (Figs. 18 and 19). The ratio of the Type 4 to Type 5 TVM densities are: $[0_3/90_3]_s$, 7/11; $[0_2/90_2]_s$, 5/15; $[(0/90)_3]_s$, 5/28; $[0/45/90/-45]_s$, 2/19; $[0/60/00]_s$, 0/21. The $[45/-45/0/90]_s$ laminate had no observable microcracks after either type of thermal loading. The plies that contained microcracks did not vary between Type 4 and 5 loadings.

In the $[0_2/90_2]_s$, $[0_3/90_3]_s$, and $[(0/90)_3]_s$ laminates, TVM were found only in the outer 0° layers when viewed from the 0° direction for both thermal loadings. Observation from the 90° viewing direction showed that the $[0_2/90_2]_s$ and $[0_3/90_3]_s$ specimens had

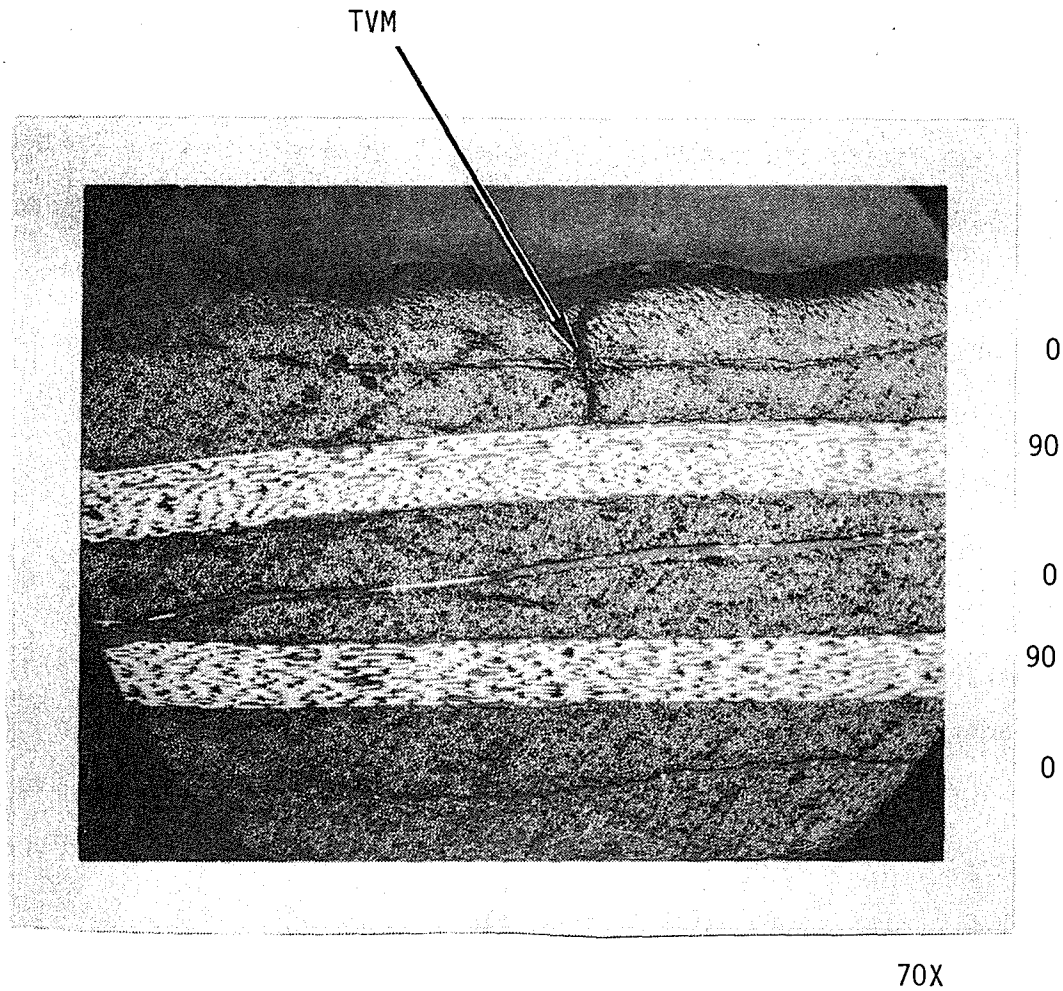

Fig. 23. TVM in a $[(0/90)_3]_s$ Laminate After Type 3 Thermal Loading.

microcracks in all the 90° plies after the Type 5 thermal loading, but the $[(0/90)_3]_s$ specimen exhibited microcracks only in the two 90° plies adjacent to the midplane. Similar results would be expected for 90° viewing of specimens subjected to Type 4 loading.

Subjecting the $[(0/90)_3]_s$ laminate to a Type 5 thermal loading caused extensive longitudinal microcracking in the 90° plies adjacent to the laminate midplane (Fig. 11). The longitudinal microcracks were not observed in the four outer 90° plies. These microcracks were only visible when observed from the 90° direction. They were not interlaminar cracks, but rather remained within the 90° plies, originating at a transverse microcrack and extending between one-third and the full distance to an adjoining TVM. The longitudinal microcracks are believed to be the result of tensile interlaminar normal stresses (σ_z) that are enhanced by the presence of the TVM.

As indicated in Figs. 16-19, the $[\pm 45/0/90]_s$ laminate was very resistant to microcracking for all thermal loadings including Types 4 and 5. For the case of Type 5 loading, this was verified from both 0° and 90° viewing directions. The $[0/45/90/-45]_s$ quasi-isotropic laminate did not exhibit this same resistance to microcracking (Figs. 18 and 19). The Type 4 loading developed 2 TVM/inch (1 TVM/cm) in the 0° ply, which is the same density as in the specimen subjected to Type 3 loading. The specimen subjected to a Type 5 thermal loading had microcracks in both the 0° and +45° plies, with densities of 19 TVM/inch (7.5 TVM/cm) for the 0° ply, and the much lower density of 4 TVM/inch (1.5 TVM/cm) for the +45° ply. The microcracks in the +45° layers were usually associated

with a microcrack in the 0° plies (Fig. 24). TVMs were not observed in the -45° plies.

Viewing the quenched $[0/45/90/-45]_s$ specimen from the 90° direction revealed a longitudinal crack approximately 0.25 inch (0.1 cm) long and near the center of the specimen in one of the 45° plies, as shown in Fig. 14. This crack was not an interlaminar crack but, rather, totally within the 45° ply, and was probably caused by shear stresses imposed by thermal gradients during the quench in liquid nitrogen or by material defects. The 90° plies had 8 TVM/inch (3.15 TVM/cm) whereas the ±45° plies were free of TVM.

The $[0/60/0/-60]_s$ laminate did not develop TVM under Type 4 thermal loading, but the Type 5 loading induced a TVM density of 21 TVM/inch (8.5 TVM/cm) in the outermost 0° plies of the specimen (Fig. 25). Microcracks were also observed in the two -60° plies adjacent to the midplane when the specimen was viewed from the 90° direction. The density of the -60° plies was 9 TVM/inch (3.5 TVM/cm).

The deleterious effects of quenching the specimens as opposed to cooling them more slowly is apparent from the results of the tests discussed in this section. In addition to the increased TVM density in the quenched specimens, quenching also caused longitudinal cracks in two laminates. The lower TVM density in the slowly cooled specimens may be due to smaller thermal gradients, partial stress relaxation and rate dependent material properties.

4.3 Tensile Loading

Tensile load was applied in the zero degree directon of the $[0_2/90_2]_s$,

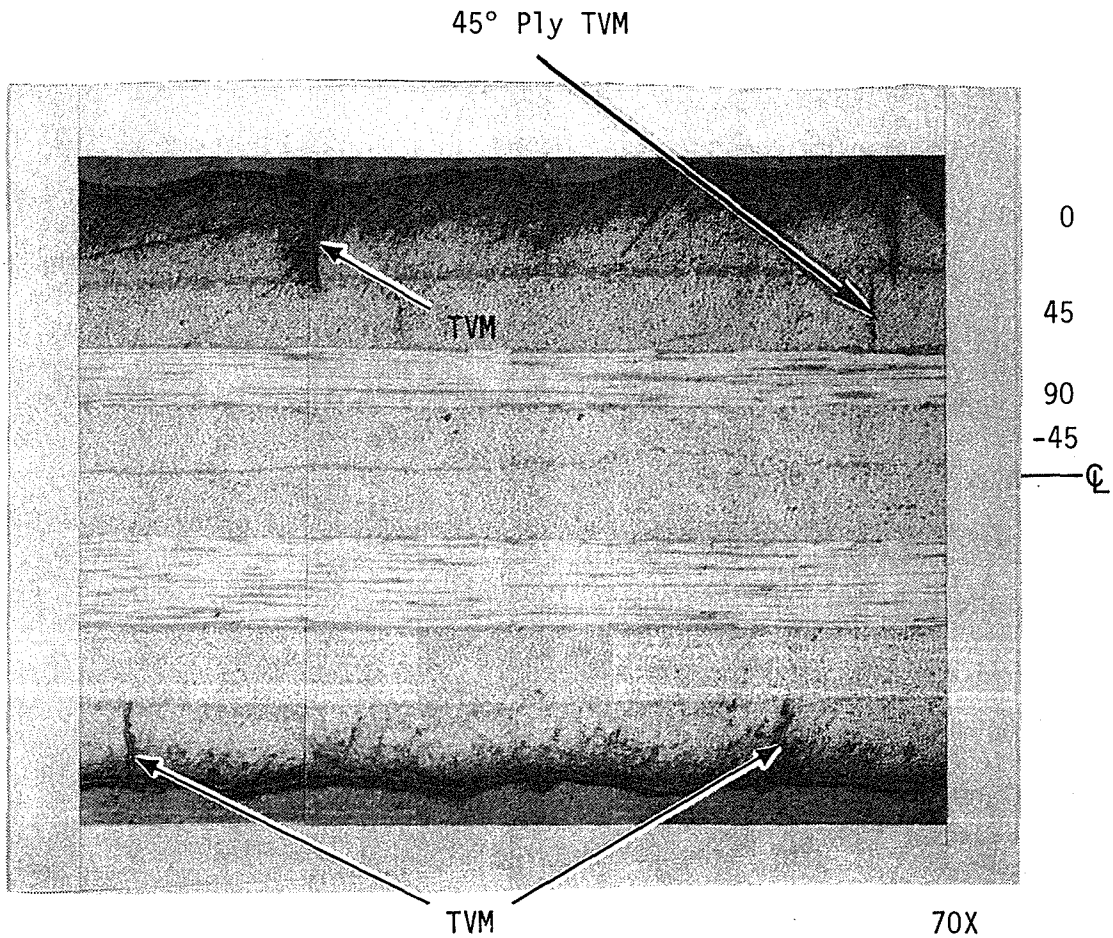

Fig. 24. TVM in a $[0/45/90/-45]_s$ Laminate After Type 5 Thermal Loading.

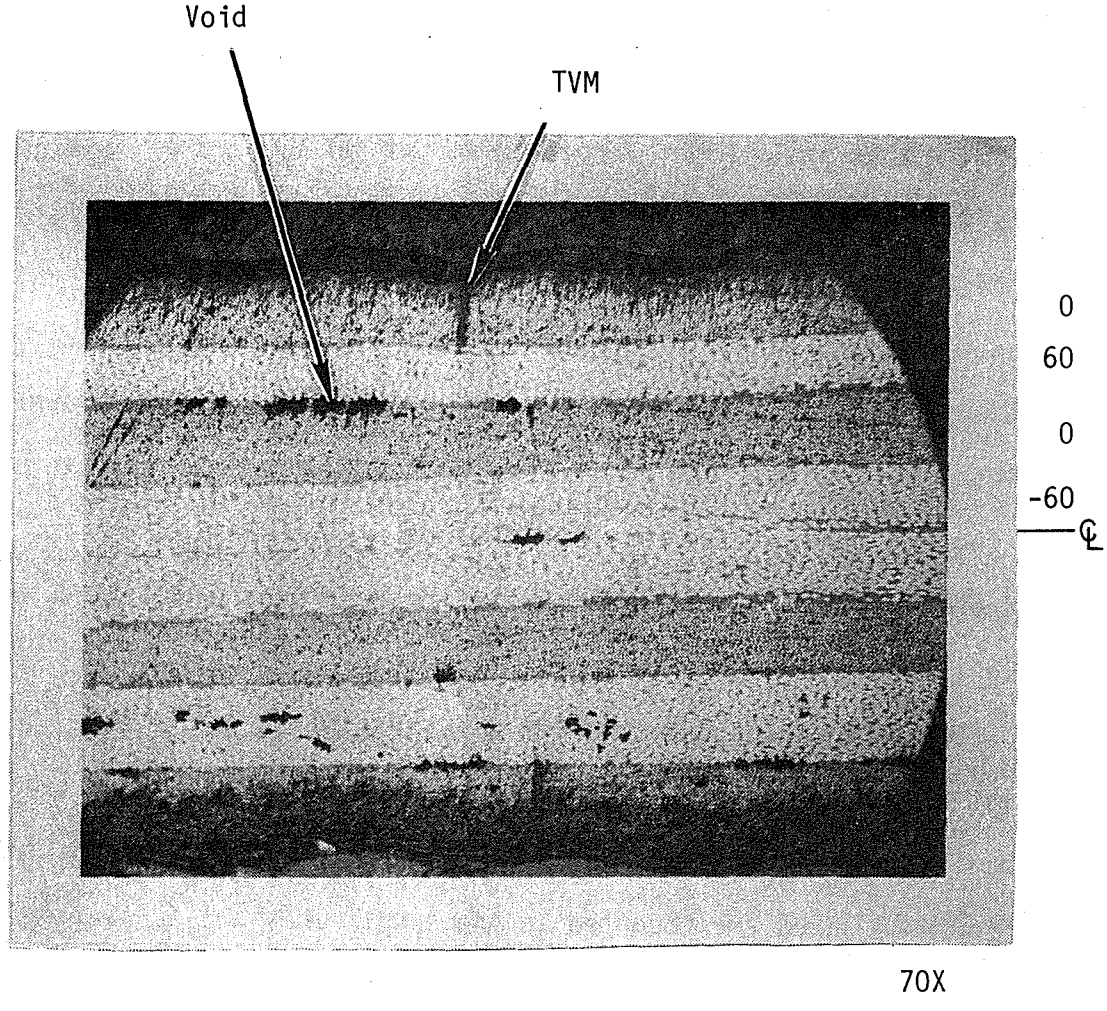

Fig. 25. TVM in a $[0/60/0/-60]_s$ Laminate After Type 5 Thermal Loading.

$[\pm 45/0/90]_s$, and $[0/45/90/-45]_s$ laminates. The microcracks along the edge of the tensile specimens were observed from the 90° viewing direction using the replicating technique discussed in Section 3.4. Numerous replicas were taken at the low stress levels in order to determine accurately when microcracking initiated. Larger load increments between replicas were used for stresses higher than the stress at which microcracking initiated. The stress dependence of TVM density is shown in Fig. 26 for all three laminate configurations tested. Three specimens of each laminate configuration were tested and all results are included in Fig. 26. The solid line through the data is only to show the general trend of the results. The average failure stress for each laminate configuration tested is shown in the figure and listed in Table 1.

Fig. 26 contains only the TVM densities of the 90° plies. The densities are an average obtained by the same method used for the thermally loaded specimens (Section 4.2). The TVM densities in the +45° or -45° plies are reported in the text. They are an average of the densities in the +45° plies or the -45° plies.

For reasons of safety and to reduce creep, the applied load was reduced before a replica was taken when the applied load was greater than 50% of ultimate load. This was discussed further in Section 3.6.2. Unloading the specimens did not close any TVM present at the higher loads. This is demonstrated by Fig. 27. Figure 27a is a replica of a $[0/45/90/-45]_s$ specimen at 50% of ultimate stress, and Fig. 27b is from the same specimen after the load was reduced to 25% of ultimate

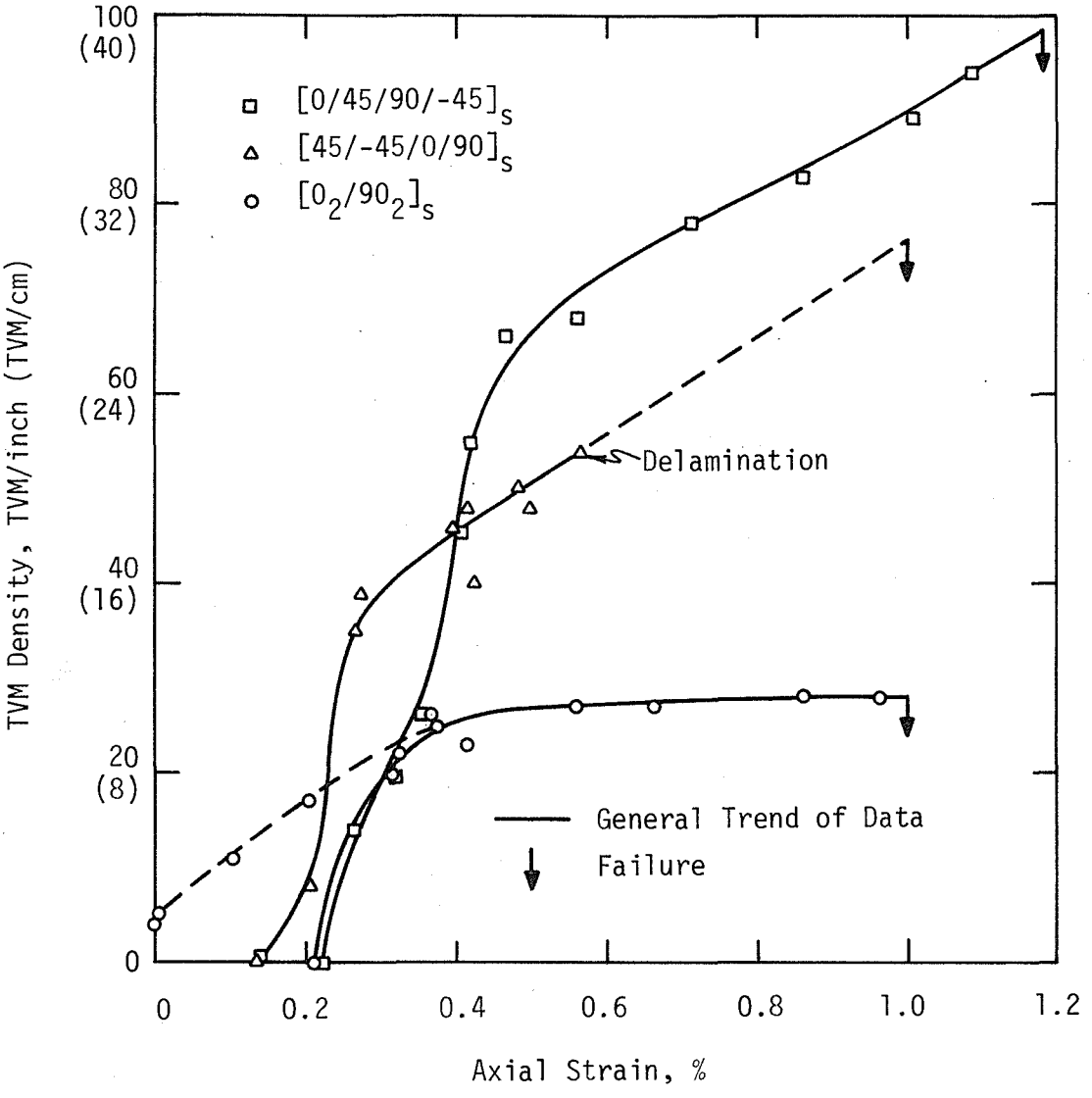

Fig. 26. 90° Ply TVM Density as a Function of Applied Strain

TABLE 1. Average Failure Stress of Tensile Specimens

Laminate Configuration	Average Failure Stress ksi (10^7 pascal)
$[0_2/90_2]_s$	94 (6.48)
$[45/-45/0/90]_s$	68 (4.69)
$[0/45/90/-45]_s$	78 (5.38)

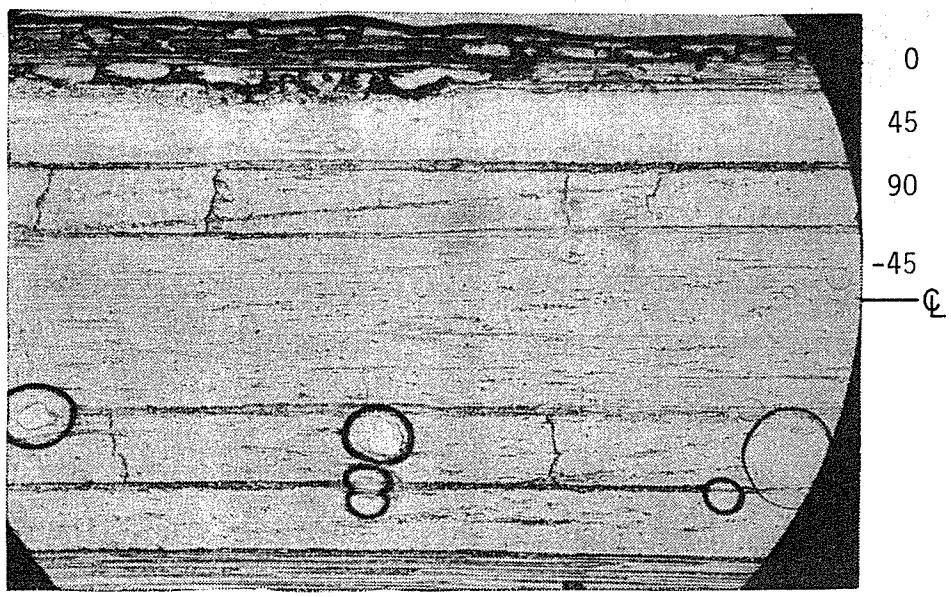

a) 50% of Ultimate Stress

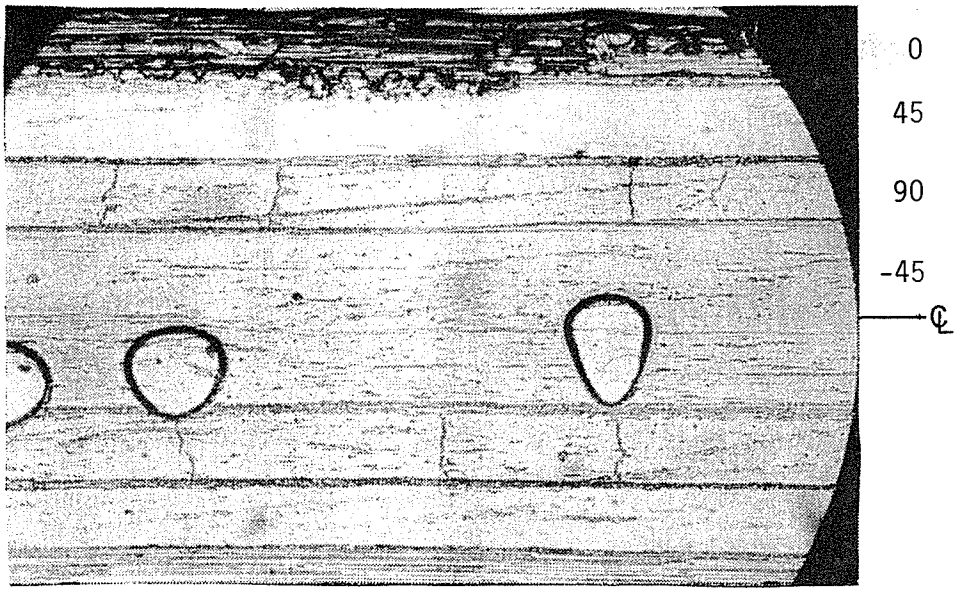

b) Reduced to 25% of Ultimate Stress

Fig. 27. Influence of Load Reduction on TVM in a $[0/45/90/-45]_s$ Laminate.

stress. As can be seen, the TVM are still present at the reduced load. The TVM were also counted on both replicas for the same 1-inch length; identical counts were obtained. The assumption was thus made that all microcracks formed at higher stress levels continue to be evident at the reduced stress of replicating for all tensile tests.

4.3.1 Transverse Microcrack Densities

4.3.1.1 $[0_2/90_2]_s$ Laminate

As Fig. 26 shows, two of the three $[0_2/90_2]_s$ specimens did not develop microcracks until a strain of 0.25% (20% of ultimate stress) was reached. After microcracking initiated, the TVM density increased rapidly to a plateau (saturation) value of 27 to 28 TVM/inch (11 TVM/cm) at 50% of ultimate stress (0.5% strain). This density remained constant until failure.

The third specimen had approximately 4 TVM/inch (2 TVM/cm) before the application of load. This specimen continued to develop microcrack until the saturation density plateau was reached at approximately the same strain as the other two specimens.

The saturation density of all three specimens closely matched, as shown in Fig. 26. This saturation density is only 3 TVM/inch (12%) higher than the density found for the most severely thermally microcracked $[0_2/90_2]_s$ specimen (Type 5 thermal loading). The microcracks from applied stress are indistinguishable from those formed during thermal loading and, hence, no photomicrographs of the replicas are presented.

4.3.1.2 $[0/45/90/-45]_s$ Laminate

In all three of these specimens, transverse microcracks first

occurred between 20% - 25% of ultimate stress (0.21% - 0.27% strain). Figure 28 shows a replica made at 26% of ultimate stress. As evident in the figure, it was difficult to obtain good replicas of the outer plies. The TVM density above 40% of ultimate stress is much higher than the density in any of the thermally loaded $[0/45/90/-45]_s$ specimens. (The short striated regions emanating from the microcracks are not a characteristic of the microcracks, but rather a result of the replicating technique (Section 3.4)). The striations are caused by the acetone incompletely wetting the specimen surface, which prevents the replicating film from softening. The globular shapes present in Fig. 28 are air bubbles, which commonly cluster around a TVM. The string of air bubbles in Fig. 28, however, is not centered over a crack. Fig. 29 does show a grouping of air bubbles near microcracks.

The microcracks appeared first in the 90° plies of the specimens and continued to increase in density to 95 TVM/inch (38 TVM/cm) through the final replica at 94% of ultimate stress. The +45° and -45° plies developed low density microcracks at 75% of ultimate stress. The TVM densities of the +45° and -45° plies were approximately 1 TVM/inch (0.4 TVM/cm) and 2 TVM/inch (0.8 TVM/cm), respectively. The microcracks in the -45° plies typically initiated at a TVM in the 90° plies or at a short longitudinal crack in the resin-rich region extending from a TVM in the 90° plies (Fig. 29). Longitudinal cracks developed in the 90° ply at 88% of ultimate stress and underwent no noticeable change as the applied stress was increased.

Microcracking initiated in the $[0/45/90/-45]_s$ laminates at a longi-

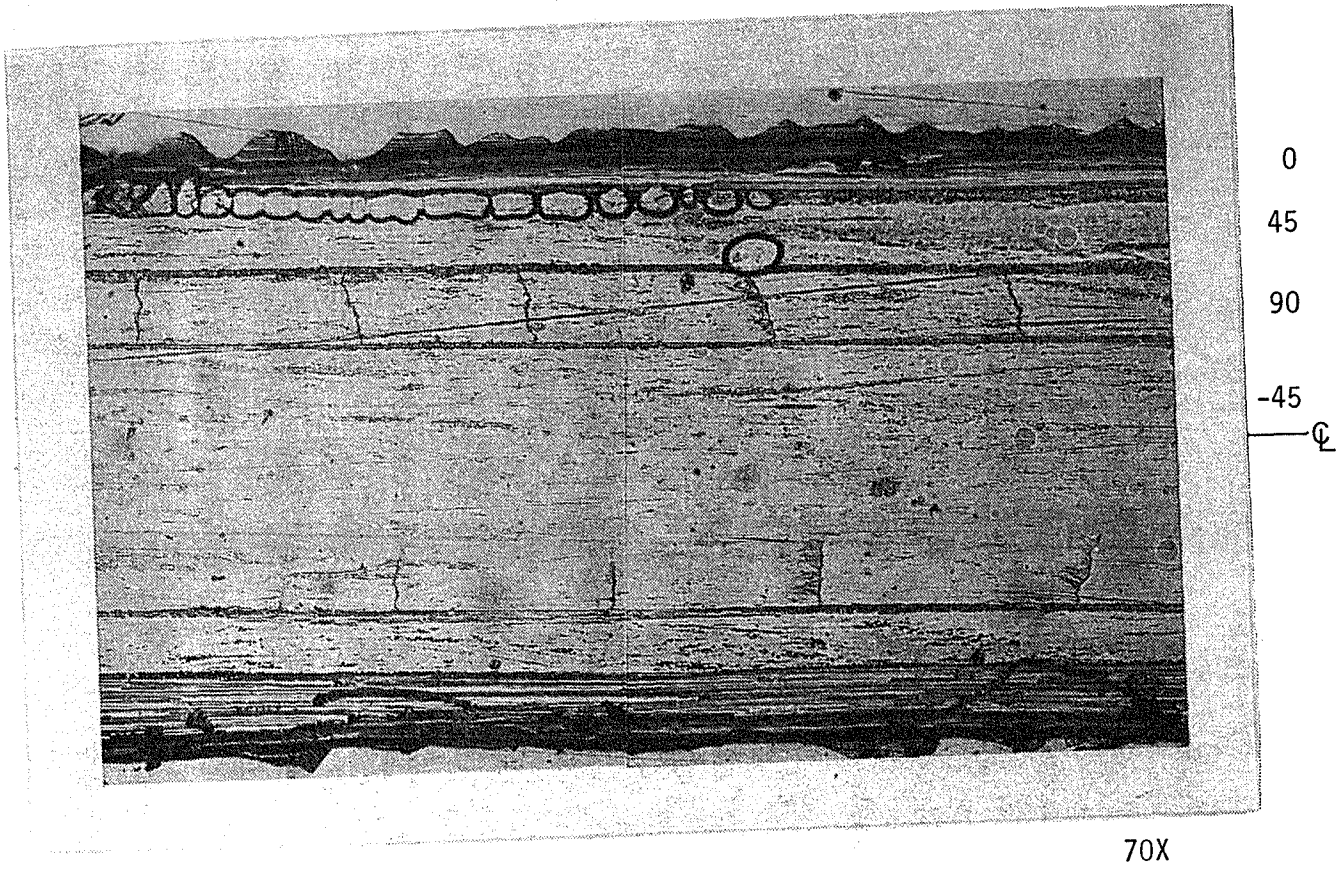

Fig. 28. Replica of $[0/45/90/-45]_s$ Tensile Specimen at 26% of Ultimate Stress.

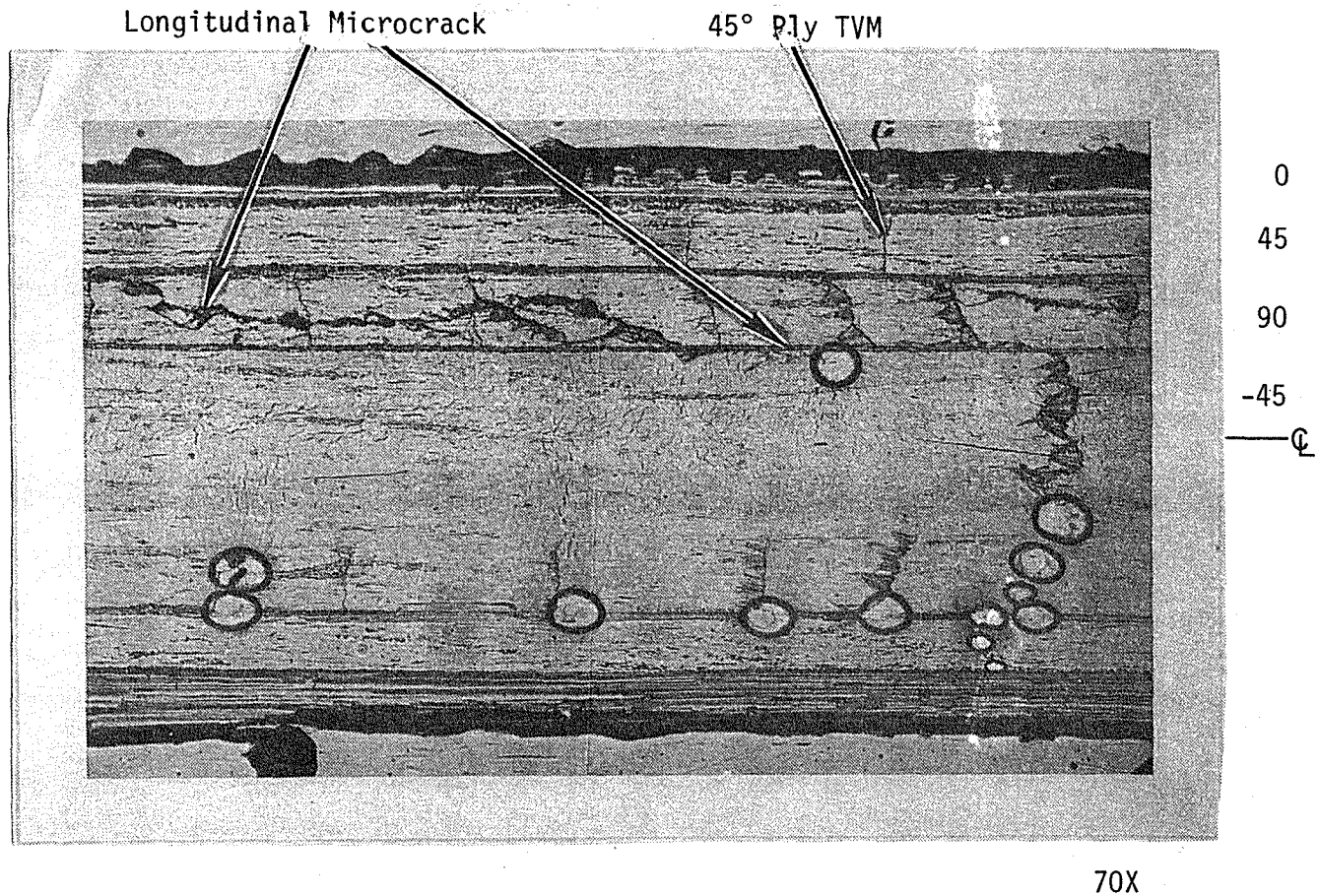

Fig. 29. Replica of $[0/45/90/-45]_s$ Tensile at 88% of Ultimate Stress.

tudinal stress between 20% - 26% of ultimate stress (0.21% - 0.27% strain). After the initial microcracking the microcrack density increased very rapidly until a stress of approximately 50% of ultimate stress (0.5% strain), and then increased at a reduced, but essentially constant rate until failure (Fig. 26). This continual microcracking to failure is in contrast to the $[0_2/90_2]_s$ laminate which reached a saturation density at a fairly low strain of approximately 0.5% (45% of ultimate stress).

4.3.1.3 $[45/-45/0/90]_s$ Laminate

In contrast to the thermally loaded specimens, microcracking was initiated in the $[45/-45/0/90]_s$ laminate under a less severe loading condition than in the $[0/45/90/-45]_s$ laminate (Fig. 26). The $[45/-45/0/90]_s$ laminate had a higher TVM density below 0.4% strain than did the $[0/45/90/-45]_s$ laminate at the same strain level. Above a strain of 0.4%, the $[45/-45/0/90]_s$ laminate exhibited a lower TVM density than did the other quasi-isotropic laminate. The slope of the TVM curve in Fig. 26 decreased at this strain also. It was not possible to take replicas of the $[45/-45/0/90]_s$ laminate above 60% of ultimate stress because the specimens developed extensive delaminations. The delamination was undoubtedly a result of free-edge effects. These effects could also be responsible for the lower failure stress of the $[45/-45/0/90]_s$ specimens as compared to the $[0/45/90/-45]_s$ specimens.

The resin-rich regions had no discernible effect upon the microcracks in the $[0_2/90_2]_s$ or the $[0/45/90/-45]_s$ laminate; however, the resin-rich regions were able to arrest microcrack propagation in the 90° plies of

the $[45/-45/0/90]_s$ laminates at an applied stress marginally above the crack-initiation stress. The effects of the resin-rich regions are discussed further in Section 4.1.2.

4.3.2 Mechanical Properties and Microcrack Densities

4.3.2.1 Elastic Modulus

The elastic modulus of the $[0_2/90_2]_s$ and $[0/45/90/-45]_s$ tensile specimens demonstrated no significant dependence upon TVM density. The modulus of both laminates changed only minimally with stress. This is the same result obtained by Doner and Novak [2] for graphite fiber/epoxy composites. No step increases in strain on the stress-strain curve were observed while TVM were developing. Such increases were expected for high TVM density because the decreased stiffness in the region of microcracks causes an increase in strain at a constant applied stress. The only stair-step-type effect observed was associated with the specimen creeping while a replica was being taken. The Epikote 828 epoxy/E-glass composite tested by Parvizi and Bailey [27], and the epoxy/AS3501 graphite composite tested by Reifsnider and Masters [9] did exhibit a stair-stepping of the stress-strain curve. These results indicate that the correlation between modulus and TVM density may be material or experimental procedure dependent.

Only the $[45/-45/0/90]_s$ specimens demonstrated nonlinearity in the stress-strain curve (Fig. 30). The strain at which the curve displays initial nonlinearity ($\varepsilon = 0.6\%$) corresponds to the same strain at which a $[\pm 45]_s$ laminate displays a decrease in modulus when the residual stresses within the $[45/-45/0/90]_s$ laminate are considered. The

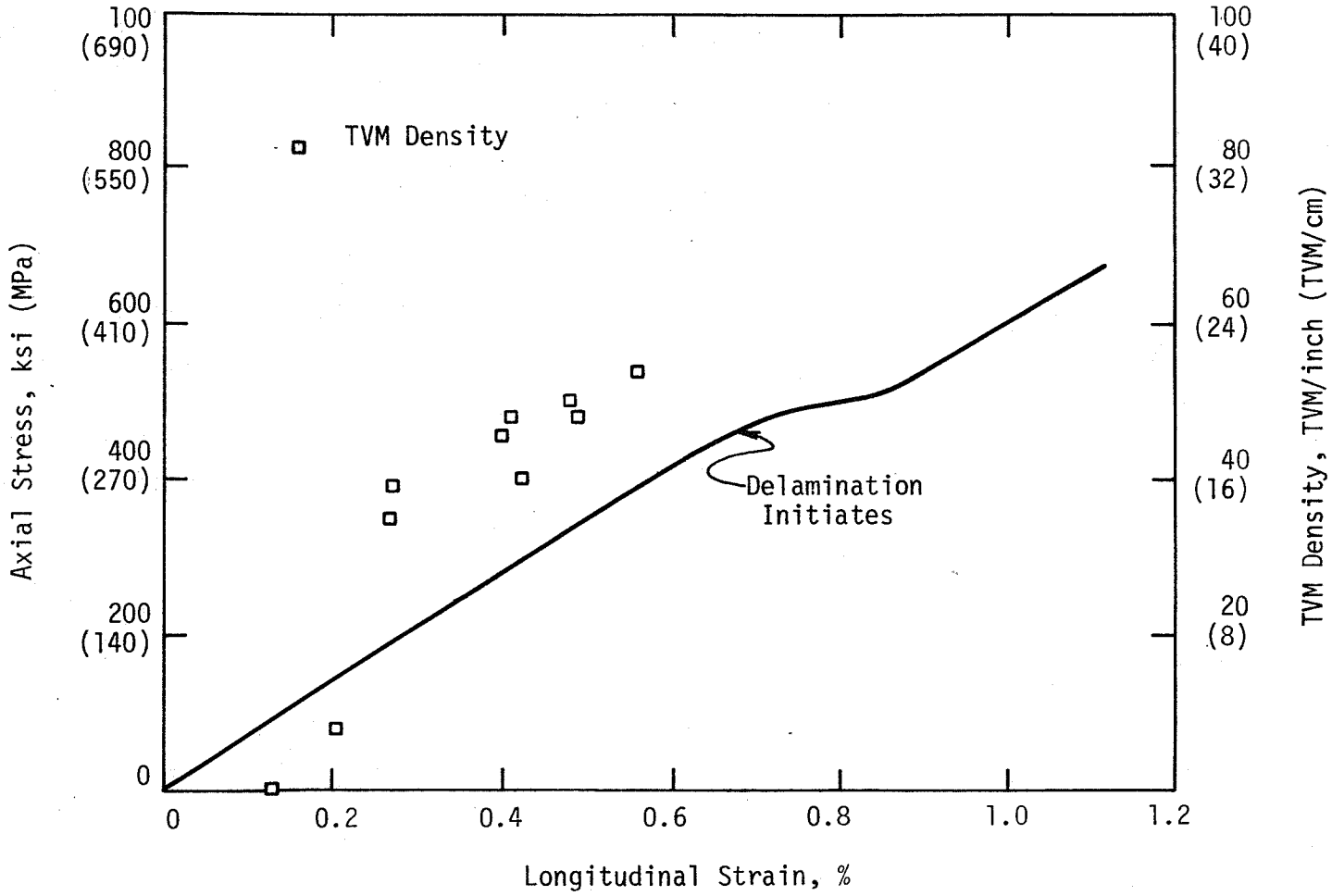

Fig. 30. Stress-Strain - TVM Density for a $[45/-45/0/90]_s$ Laminate.

delamination of the laminate undoubtedly also affected the stress-strain curve. Dependence of the modulus upon TVM density was not found in the laminate prior to delamination.

4.3.2.2 Poisson's Ratio

Transverse strain and TVM density as functions of longitudinal strain are shown in Figs. 31 through 33 for the three laminates tested. Poisson's ratio of the $[45/-45/0/90]_s$ tensile specimens did not change during the range of longitudinal strain in which replicas could be taken. This laminate did have a sudden, rapid increase in transverse strain at a longitudinal strain of about 0.8% (Fig. 31). This is believed to result from the large curvature of the delaminated portion of the specimen. The curvature was large enough to subject the transverse strain gages to additional compressive strain.

Poisson's ratio of the $[0/45/90/-45]_s$ laminate increased from 0.284 to 0.33 at a strain of approximately 0.28% (Fig. 32). This is approximately the strain at which the TVM density exhibited a sharp increase during mechanical loadings (Fig. 26). After this initial change, Poisson's ratio remained essentially constant until failure.

Poisson's ratio of the $[0_2/90_2]_s$ specimens decreased from 0.04 to 0.018 at a longitudinal strain of 0.4% (Fig. 33). This is approximately the strain at which the TVM density plateau region begins in Fig. 26, indicating that Poisson's ratio of this laminate decreases with increased TVM density. This would result from the 90° ply not carrying load in the axial (loading) direction because of the microcracks. This in turn reduces the transverse compressive strain of

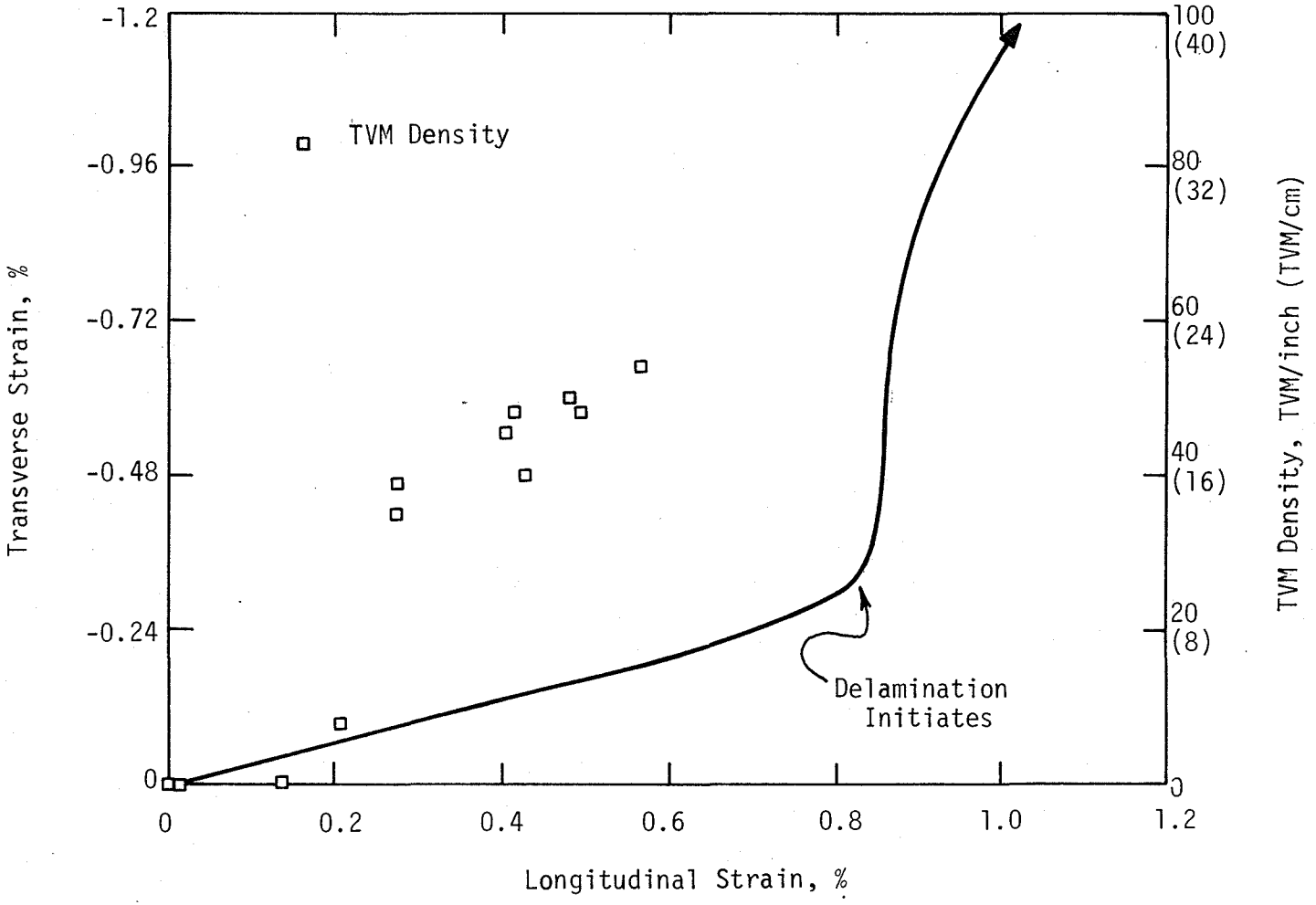

Fig. 31. Transverse Strain - TVM Density - Longitudinal Strain for a $[45/-45/0/90]_s$ Laminate.

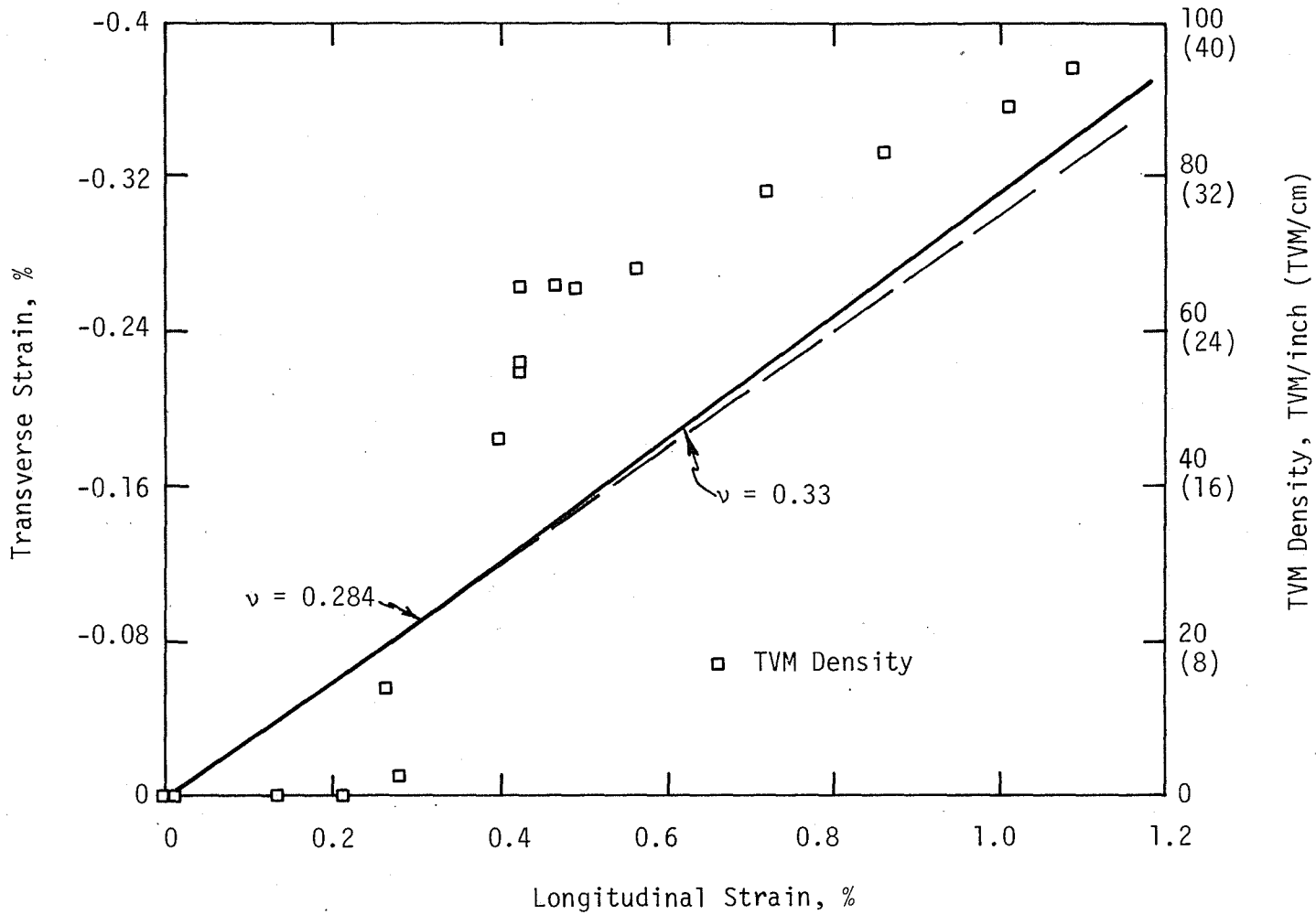

Fig. 32. Transverse Strain - TVM Density - Longitudinal Strain for a $[0/45/90/-45]_s$ Laminate.

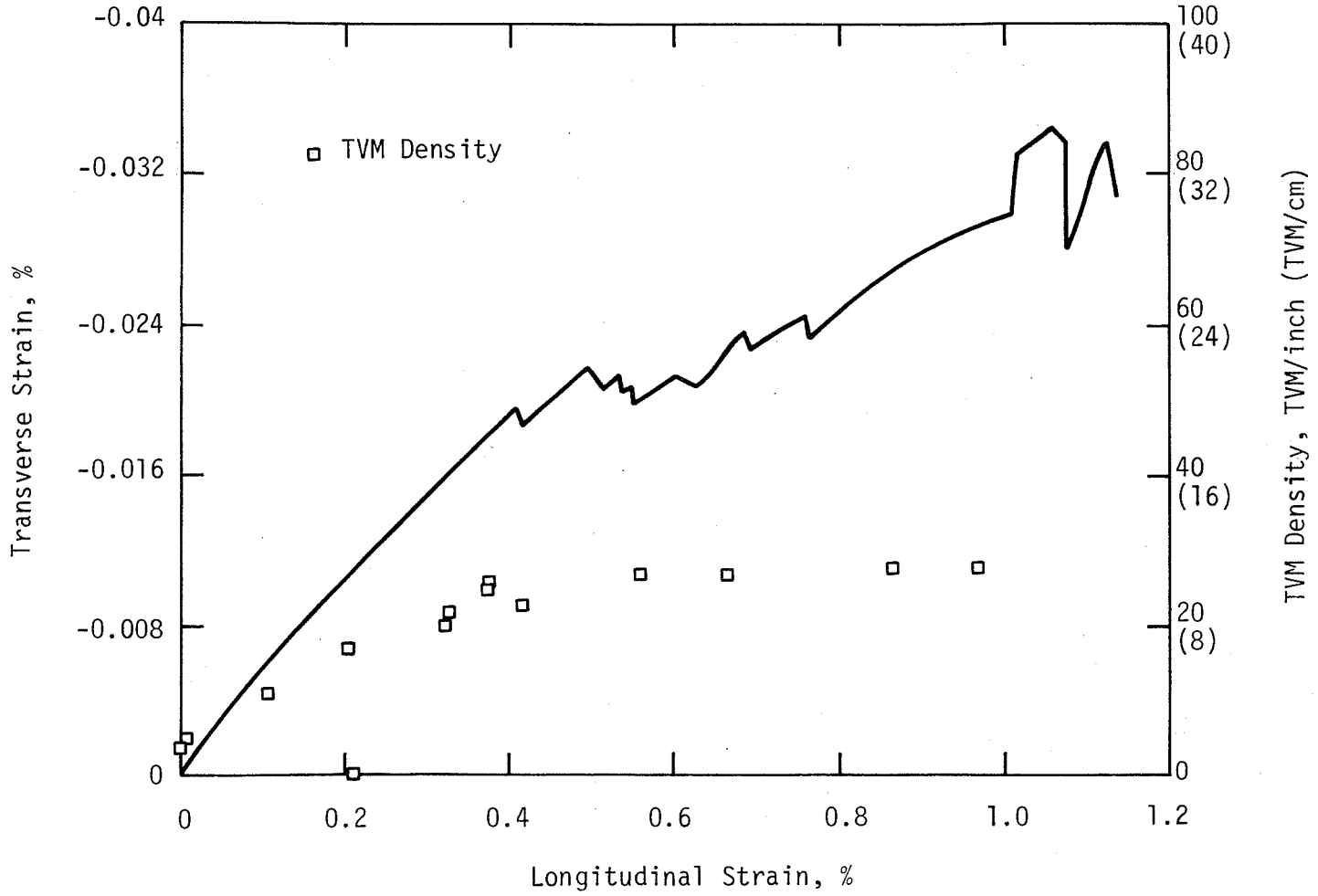

Fig. 33. Transverse Strain - TVM Density - Longitudinal Strain for a $[0_2/90_2]_s$ Laminate.

the 90° ply and of the laminate. In fact, the increment of transverse strain can be positive due to axial stress relief in the 90° ply. This explains erratic behavior of the curve in Fig. 33.

The discontinuities present in the central portion of the curve in Fig. 33 are believed to be the result of longitudinal cracks forming and reducing the transverse compressive strains in the 0° plies. The scattered data at a strain above 1% were common to all three specimens of this laminate, as well as for another that was loaded at 0.005 in/min (33.9 μm/sec). Local failures forming in the 0° plies under the strain gage are believed to be the cause of the erratic transverse strain behavior. Splitting and peeling of the 0° plies was common near the failure stress.

4.4 Stress-Free Temperature

Six unsymmetric $[0_3/90_3]$ specimens were used to determine the stress-free temperature. They displayed a high rate of curvature decrease during the 50°F (30°C) before zero curvature, thus ensuring precision in determining the temperature of zero curvature to within ±10°F (5°C). The values for curvature and stress-free temperature are shown in Table 2. A wide variation in curvature of the specimens is evident from Fig. 5 and Table 2. The nonuniformity of curvature along the length of each specimen and in different specimens, is believed to be due to variations in thickness of either the 0° or 90° plies. These nonuniformities did not affect the precision of the method. The measured stress-free temperatures range from 570-625°F (300-330°C). The average value for seven specimens was 599°F (315°C).

TABLE 2. Stress-Free Temperature and Curvature of a $[0_3/90_3]$ Laminate

Specimen	Curvature, $inch^{-1}$ (cm^{-1})	Stress-Free Temperature, °F (°C)
1-1	0.17 (0.0669)	610 (320)
1-2	0.15 (0.0591)	625 (330)
1-3	-	-
1-4	-	610 (320)
2-1	0.12 (0.0472)	570 (300)
2-2	0.13 (0.0912)	580 (305)
2-3	0.11 (0.0433)	590 (310)
2-4	0.18 (0.0709)	605 (320)

The temperature of each specimen was increased to 625°F (330°C) after the stress-free temperature had been determined. This temperature was maintained for one hour, then the specimens were cooled at 15°F/min (8°C/min) to ambient temperature. After this exposure, they exhibited a slightly increased, more uniform curvature along their length, a sharply decreased elastic flexure strength, and an increased TVM density. The latter two effects are attributed to a decrease in ultimate stress of the matrix. Cavano and Winters [49] have reported that a 650°F (345°C) postcure will decrease the room-temperature tensile strength of the neat resin, PMR-15.

Chapter 5

ANALYTICAL METHODS AND RESULTS

5.1 Laminate Analysis

5.1.1 Classical Derivation

Classical laminate analysis predicts the elastic behavior of a plate composed of numerous orthotropic laminae. The two basic assumptions employed in classical lamination theory are that all the laminae are perfectly bonded together, and that Kirckhoff's plate hypothesis applies. The primary result of making these assumptions is that normals to the midplane remain normal and of constant length. This implies that ε_z, γ_{xz}, and γ_{yz} are zero throughout the plate. A general formulation of the governing equations is briefly outlined below; a more detailed development is presented in references [35,36].

Lamina stress-strain relationships constitute the basis for laminate analysis. Assuming that each lamina is a homogeneous, orthotropic material, the lamina stress-strain relation in the material coordinate system (Fig. 34) is

$$\begin{Bmatrix} \sigma_1 \\ \sigma_2 \\ \tau_{12} \end{Bmatrix} = \begin{bmatrix} Q_{11} & Q_{12} & 0 \\ Q_{12} & Q_{22} & 0 \\ 0 & 0 & Q_{66} \end{bmatrix} \begin{Bmatrix} \varepsilon_1 \\ \varepsilon_2 \\ \gamma_{12} \end{Bmatrix} \tag{5.1}$$

or, in condensed matrix notation,

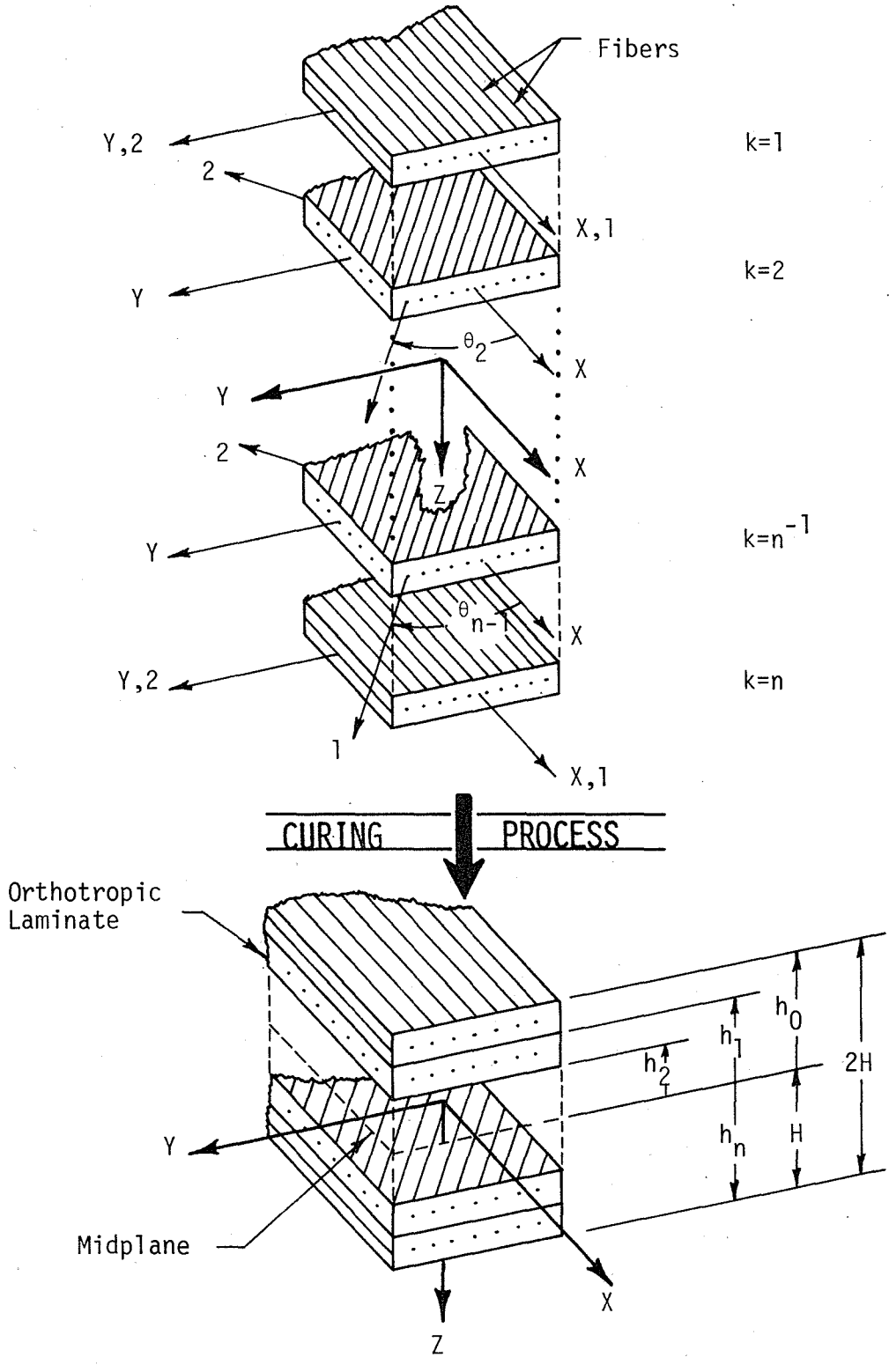

Fig. 34. Lamina and Laminate Coordinates.

$$\{\sigma\}_{1,2} = [Q]\{\varepsilon\}_{1,2} \tag{5.2}$$

where the subscripts 1,2 indicate material coordinates.

Expressing these relations in terms of a principal laminate coordinate system, one obtains

$$\begin{Bmatrix} \sigma_x \\ \sigma_y \\ \tau_{xy} \end{Bmatrix} = \begin{bmatrix} \bar{Q}_{11} & \bar{Q}_{12} & \bar{Q}_{16} \\ \bar{Q}_{12} & \bar{Q}_{22} & \bar{Q}_{26} \\ \bar{Q}_{16} & \bar{Q}_{26} & \bar{Q}_{66} \end{bmatrix} \begin{Bmatrix} \varepsilon_x \\ \varepsilon_y \\ \gamma_{xy} \end{Bmatrix} \tag{5.3}$$

or, in condensed notation,

$$\{\sigma\} = [\bar{Q}]\{\varepsilon\} \tag{5.4}$$

where $[\bar{Q}]$ is defined as

$$[\bar{Q}] = [T_1]^{-1}[Q][T_2] \tag{5.5}$$

and, $[T_1]$ and $[T_2]$ are transformation matrices for stress and strain, respectively. Invoking Kirckhoff's assumptions, the strain in the k^{th} layer can be defined as the midplane strain plus the strain due to bending. The equation in this form is

$$\begin{Bmatrix} \varepsilon_x \\ \varepsilon_y \\ \gamma_{xy} \end{Bmatrix} = \begin{Bmatrix} \varepsilon_x^o \\ \varepsilon_y^o \\ \gamma_{xy}^o \end{Bmatrix} + z^k \begin{Bmatrix} \kappa_x^b \\ \kappa_y^b \\ \kappa_{xy}^b \end{Bmatrix} \tag{5.6}$$

or, in condensed notation,

$$\{\varepsilon\}^k = \{\varepsilon^\circ\} + z^k\{\kappa\} \tag{5.7}$$

where $\{\varepsilon^\circ\}$ are the midplane strains, and $\{\kappa\}$ are the midplane curvatures, in laminate coordinates.

The stress-strain relation for the k^{th} layer is

$$\{\sigma\}^k = [\bar{Q}]^k(\{\varepsilon^\circ\} + z^k\{\kappa\}) \tag{5.8}$$

The resultant forces $\{N\}$ and moments $\{M\}$ per unit length are obtained by integrating the stresses through the laminate,

$$\begin{Bmatrix} N_x \\ N_y \\ N_{xy} \end{Bmatrix} = \sum_{k=1}^{n} [\bar{Q}]^k \left(\int_{z_{k-1}}^{z_k} \{\varepsilon^\circ\} dz + \int_{z_{k-1}}^{z_k} \{\kappa\} z dz \right) \tag{5.9}$$

$$\begin{Bmatrix} M_x \\ M_y \\ M_{xy} \end{Bmatrix} = \sum_{k=1}^{n} [\bar{Q}]^k \left(\int_{z_{k-1}}^{z_k} \{\varepsilon^\circ\} z dz + \int_{z_{k-1}}^{z_k} \{\kappa\} z^2 dz \right) \tag{5.10}$$

Simplifying and expressing in condensed form,

$$\begin{Bmatrix} N \\ M \end{Bmatrix} = \begin{bmatrix} A & B \\ B & D \end{bmatrix} \begin{Bmatrix} \varepsilon^\circ \\ \kappa \end{Bmatrix} \tag{5.11}$$

where

$$A_{ij} = \sum_{k=1}^{n} \bar{Q}_{ij}^k (z_k - z_{k-1})$$

$$B_{ij} = \frac{1}{2} \sum_{k=1}^{n} \bar{Q}_{ij}^{k}(z_k^2 - z_{k-1}^2) \qquad (5.12)$$

$$D_{ij} = \frac{1}{3} \sum_{k=1}^{n} \bar{Q}_{ij}^{k}(z_k^3 - z_{k-1}^3)$$

with i,j = 1,2,6.

5.1.2 Temperature-Dependent Material Properties

The analysis of most laminates requires the consideration of residual thermal stresses and strains, especially if the laminate fabrication temperature is high. For temperature independent properties, thermal effects are included simply by adding a free thermal strain term to the left-hand side of equation 5.7. This term is the product of the coefficients of thermal expansion and the temperature change from cure. This method does not include any variation in material properties that occur as a result of temperature change. Such variations can be included by the method proposed by Hahn and Pagano [23] and developed briefly below.

The total strain in the k^{th} layer is assumed to be the sum of mechanical $\{\varepsilon^M\}^k$ and thermal $\{\varepsilon^T\}^k$ strains,

$$\{\varepsilon\} = \{\varepsilon^M\}^k + \{\varepsilon^T\}^k \qquad (5.13)$$

where the free thermal strains for a temperature change T_o to T are

$$\{\varepsilon^T(T)\}^k = \int_{T_o}^{T} \{\alpha(\xi)\}^k d\xi \qquad (5.14)$$

and $\{\alpha(T)\}^k$ are the temperature dependent coefficient of thermal expansion of the k^{th} layer.

From equations (5.4) and (5.13), the thermal stresses for a temperature change from T_o, the stress-free temperature, to the temperature of interest T are

$$\{\sigma(T)\}^k = [\bar{Q}(T)]^k(\{\varepsilon\}^k - \{\varepsilon^T\}^k)$$

or using (5.7) for the total strains

$$\{\sigma(T)\}^k = [\bar{Q}(T)]^k(\{\varepsilon^\circ\} + z^k\{\kappa\} - \{\varepsilon^T\}^k) \tag{5.15}$$

where $\bar{Q}_{ij}(T)$ are the stiffnesses at temperature T and $\{\varepsilon^T\}^k$ are given by (5.14).

The thermal-mechanical laminate constitutive equations are

$$\begin{aligned} \{N+N^T\} &= [A(T)]\{\varepsilon^\circ\} + [B(T)]\{\kappa\} \\ \{M+M^T\} &= [B(T)]\{\varepsilon^\circ\} + [D(T)]\{\kappa\} \end{aligned} \tag{5.16}$$

where

$$([A],[B],[D]) = \int_{-H}^{H} [\bar{Q}(T)]^k(1,z,z^2)dz$$

$$(\{N^T\},\{M^T\}) = \int_{-H}^{H} [\bar{Q}(T)]^k\{\varepsilon^T(T)\}^k(1,z)dz =$$

$$\int_{-H}^{H} [\bar{Q}(T)]^k \int_{T_o}^{T} \{\alpha(\xi)\}^k d\xi(1,z)dz \tag{5.17}$$

The inplane strains and curvatures for given loading conditions may be found by inverting equations (5.16) to obtain

$$\begin{Bmatrix} \varepsilon^\circ \\ \kappa^0 \end{Bmatrix} = \begin{bmatrix} A & B \\ B' & D \end{bmatrix}^{-1} \begin{Bmatrix} N+N^T \\ M+M^T \end{Bmatrix} = \begin{bmatrix} A' & B' \\ B' & D' \end{bmatrix} \begin{Bmatrix} N+N^T \\ M+M^T \end{Bmatrix} \tag{5.18}$$

The exact integration of $\{\alpha(T)\}^k$, as opposed to an incremental or numerical integration, is accomplished by assuming a polynomial function

for $\alpha(T)$. The functional representation of all the material properties is discussed in the following section.

5.1.3 Stress- and Temperature-Dependent Material Properties

An incremental load method was employed to represent nonlinear material properties in the laminate analysis. The assumptions used in the analysis are: (1) the material properties are constant during each load increment; and (2) the material properties have the functional dependence,

$$E_1 = \frac{d\sigma_1}{d\varepsilon_1} = f(\sigma_1,T) \qquad E_2 = \frac{d\sigma_2}{d\varepsilon_2} = f(\sigma_2,T)$$

$$\nu_{12} = f(\sigma_1,T) \qquad G_{12} = \frac{d\tau_{12}}{d\gamma_{12}} = f(\tau_{12},T) \tag{5.19}$$

$$\alpha_{11} = f(T) \qquad \alpha_{22} = f(T)$$

where the properties for each load increment are calculated from the stresses after the previous increment. References [37,39,40] used incremental loading, with the material properties being a function of strain.

The incremental form of equation (5.15) for the i^{th} stress increment is obtained from the Taylor series expansion to be

$$\{\sigma\}_i^k = \{\sigma\}_{i-1}^k + \{\Delta\sigma\}_i^k$$

$$= \{\sigma\}_{i-1}^k + [\tilde{\bar{Q}}(\{\sigma\}_{i-1}^k,T)](\{\Delta\varepsilon^\circ\}_i + z^k\{\Delta\kappa\}_i - \{\Delta\varepsilon^T\}_i^k) \tag{5.20}$$

where $\{\Delta\varepsilon^\circ\}_i$ and $\{\Delta\kappa\}_i$ can be found from equation (5.18), i.e.,

$$\begin{Bmatrix} \Delta\varepsilon^{\circ} \\ \Delta\kappa \end{Bmatrix}_i = \begin{bmatrix} A' & B' \\ B' & D' \end{bmatrix}_{i-1} \begin{Bmatrix} \Delta N+\Delta N^T \\ \Delta M+\Delta M^T \end{Bmatrix}_i \tag{5.21}$$

where

$$[A',B',D'] = [A'(\{\sigma\}^k_{i-1},T),\ B'(\{\sigma\}^k_{i-1},T),\ D'(\{\sigma\}^k_{i-1},T)]$$

$$\{\Delta N^T,\Delta M^T\}_i = \int_{-H}^{H} [\bar{Q}(\{\sigma\}^k_{i-1},T)]\{\Delta\varepsilon^T\}^k_i(1,z)dz \tag{5.22}$$

The material properties used in the analysis were expressed as polynomial equations of two independent variables -- stress and temperature. The general form of the equations was

$$P = C_1 + C_2\sigma + C_3T + C_4\sigma^2 + C_5T^2 + C_6\sigma T + C_7\sigma^3 + C_8T^3 + C_9\sigma^2T + C_{10}\sigma T^2 \tag{5.23}$$

The coefficients for each equation (Table 3) were found by a least-squares-fit to the available data which was obtained from a number of different sources. The stress-strain curves at various temperatures were obtained by adjusting the results for HTS1/PMR-15 of Shuart and Herakovich [20]. Their results were adjusted based upon room-temperature data for Celion 6000/PMR-15 as follows: the HTS1 longitudinal stress-strain data were not modified since the values were nearly the same as the Celion 6000 material; the transverse stress data were multiplied by the factor 1.14; the shear modulus of the unidirectional material was obtained from tensile tests of ±45 laminates by a method described by Hahn [38]; the HTS1/PMR-15 shear modulus at -250°F (-155°C) was

Table 3. Material Property Polynomials for Celion 6000/PMR-15

Coefficient	C_1	C_2	C_3	C_4	C_5
	C_6	C_7	C_8	C_9	C_{10}
$\frac{1}{E_1(\sigma_{11},T)}$	5.903×10^{-8}	-1.112×10^{-13}	1.111×10^{-12}	2.915×10^{-19}	-6.647×10^{-15}
	1.782×10^{-17}	-	-	-	-
$\frac{1}{E_2(\sigma_{22},T)}$	7.117×10^{-7}	8.014×10^{-12}	2.930×10^{-10}	8.505×10^{-16}	3.748×10^{-13}
	9.203×10^{-14}	-	-	-	-
$G_{12}(\sigma_{12},T)$	8.682×10^{6}	-4.809×10^{1}	-6.406×10^{2}	3.195×10^{-3}	-3.131×10^{0}
	-2.177×10^{-1}	-7.979×10^{-7}	5.281×10^{-3}	2.377×10^{-5}	-2.128×10^{-5}
$\nu_{12}(T)$	3.359×10^{-1}	-	-7.082×10^{-5}	-	-5.679×10^{-9}
	-	-	2.715×10^{-10}	-	-
$X_T(T)$	1.910×10^{5}	-	8.196×10^{1}	-	-1.471×10^{-1}
	-	-	-	-	-
$Y_T(T)$	7.569×10^{3}	-	5.650×10^{-1}	-	-7.799×10^{-3}
	-	-	-	-	-

Table 3 (continued)

Coefficient	C_1	C_2	C_3	C_4	C_5
	C_6	C_7	C_8	C_9	C_{10}
S(T)	9.237×10^{3}	-	-3.539×10^{0}	-	-2.492×10^{-2}
	-	-	3.614×10^{-5}	-	-
$\alpha_{11}(T)$	-1.234×10^{-7}	-	1.934×10^{-9}	-	-
	-	-	-	-	-
$\alpha_{22}(T)$	10.09×10^{-6}	-	1.022×10^{-8}	-	-
	-	-	-	-	-

Polynomial Equation

$$P = C_1+C_2\sigma+C_3T+C_4\sigma^2+C_5T^2+C_6\sigma T+C_7\sigma^3+C_8T^3+C_9\sigma^2T+C_{10}\sigma T^2$$

Units

$E_1, E_2, G_{12}, X_T, Y_T, S, \sigma$-PSI

T-°F

α_1, α_2-1/°F

increased by 1.09. ~~Some~~ THE Celion 6000/PMR-15 properties used were taken from results of current investigations by G. Farley of NASA Langley Research Center.

The Poisson's ratio used was that of the HTS1/PMR-15, which is nearly the same as that of the Celion 6000 material. The longitudinal, transverse, and shear ultimate strengths of the HTS1/PMR-15 composite were multipled by 1.0, 1.545, and 1.0, respectively. The Poisson's ratio and strength polynomials were functions only of temperature.

5.1.4 Residual Stress Predictions

The chosen functional form of the material property dependence (constant, temperature-dependent, or stress- and temperature-dependent) obviously affects the results of the laminate analysis. The significance of these effects is demonstrated in Table 4, where the residual stress predictions for a $[0/90]_s$ laminate are compared using three different assumed forms of material behavior. (Residual stresses in the material coordinates are identical in each ply.) The results of the analysis for cross-ply and quasi-isotropic laminates indicate that: (1) the residual stresses do not exceed the ultimate transverse ply strength if constant (room-temperature) properties are used; (2) the residual stresses predicted using temperature-dependent properties exceed the ultimate transverse stress by 15%; (3) stress- and temperature-dependent behavior predicts that the residual stresses are marginally large enough for microcracks to develop. (Transverse microcracks are assumed to develop whenever the transverse strength of a ply is exceeded by the ply's transverse stress.) The stress- and

Table 4. Predicted Transverse Residual Curing Stresses for $[0/90]_s$ Gr/Pi Laminates

Form of Mechanical Properties	Residual Stresses ksi (MPa)	Percent of Transverse Failure Stress
Constant	7.15 (49.3)	95%
Temperature Dependent	8.65 (59.6)	115%
Stress- and Temperature-Dependent	7.98 (55.0)	106%

NOTE: Stress-Free Temperature = 625°F (330°C)
Y_T = 7.523 ksi (51.9 MPa)

temperature-dependent material properties should best represent the actual material behavior and give the most accurate predictions of the stresses. These properties were used in all subsequent laminate analyses. Identical results were obtained for a $[0/90/\pm45]_s$ laminate, since the residual stresses are the same as for a cross-plied laminate.

The assumed stress-free temperature significantly influences the predicted room-temperature residual stresses (Fig. 35). Laminate analysis using stress- and temperature-dependent properties predicts that there will be no microcracks at room temperature if the stress-free temperature is below 595°F (310°C) for cross-plied laminates. The stress-free temperature of Celion 6000/PMR-15 laminates was reported in Section 4.5 to range from 570°F (300°C) to 625°F (330°C), indicating that some laminates may not develop microcracks at room temperature if no additional loads are applied. Also, the percentage of 90° plies in a cross-plied laminate influences the magnitude of the residual stresses in the laminate, as shown in Fig. 36. The residual stress exceeds the transverse tensile strength when the percentage of 90° plies is greater than 35 and less than 65, for a stress-free temperature of 625°F (330°C). This range would, of course, be smaller for a lower stress-free temperature or higher strength.

The specimens used in this investigation had no significant TVM densities after curing, but four specimens did develop microcracks after being reheated to the cure temperature and quenched in ice water (Fig. 17). Laminate analysis using a stress-free temperature of 625°F (330°C) predicts that the room-temperature transverse residual

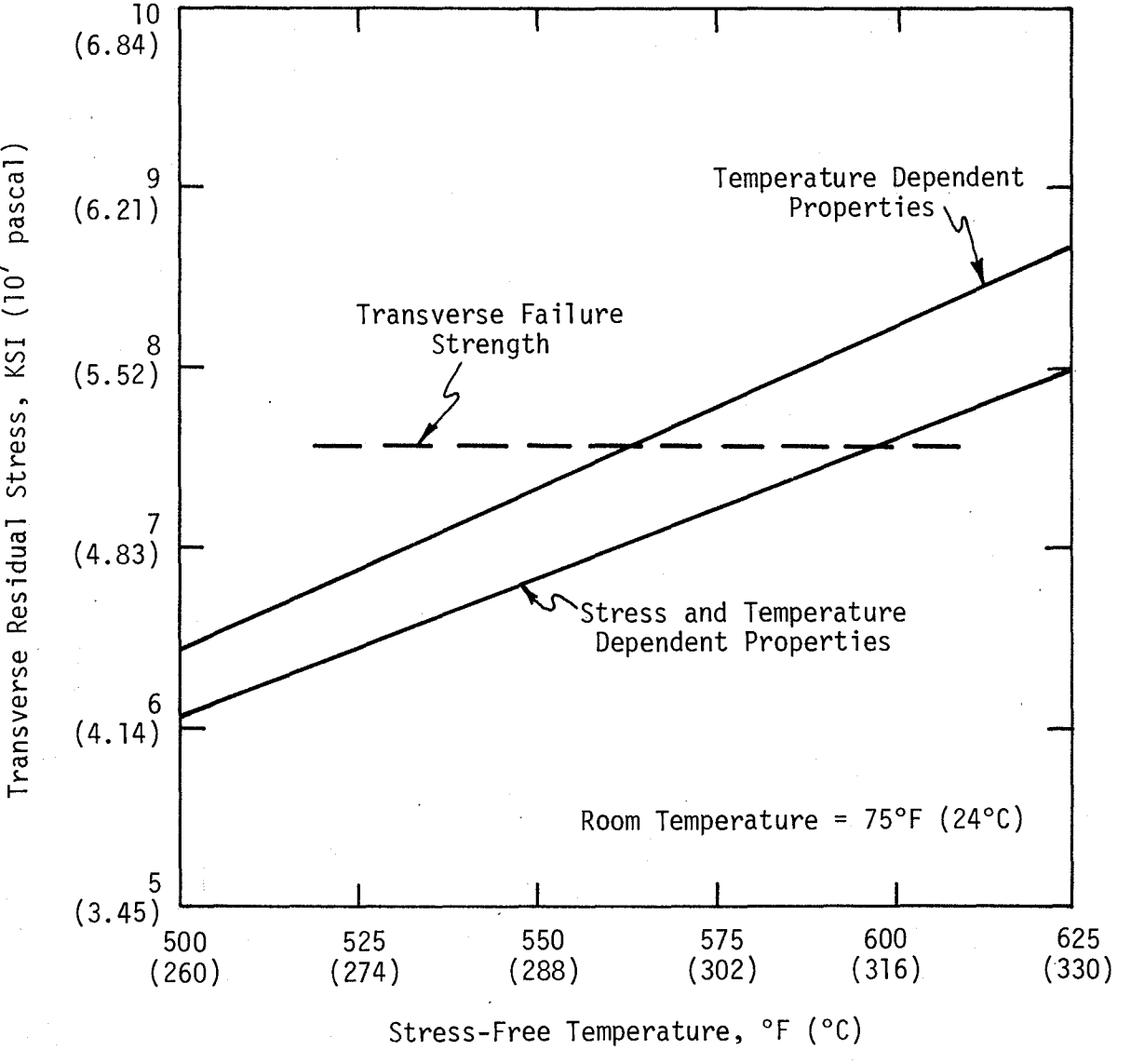

Fig. 35. Residual Stresses for $[0/90]_s$ and $[0/90/\pm45]_s$ Laminates as a Function of Stress-Free Temperature.

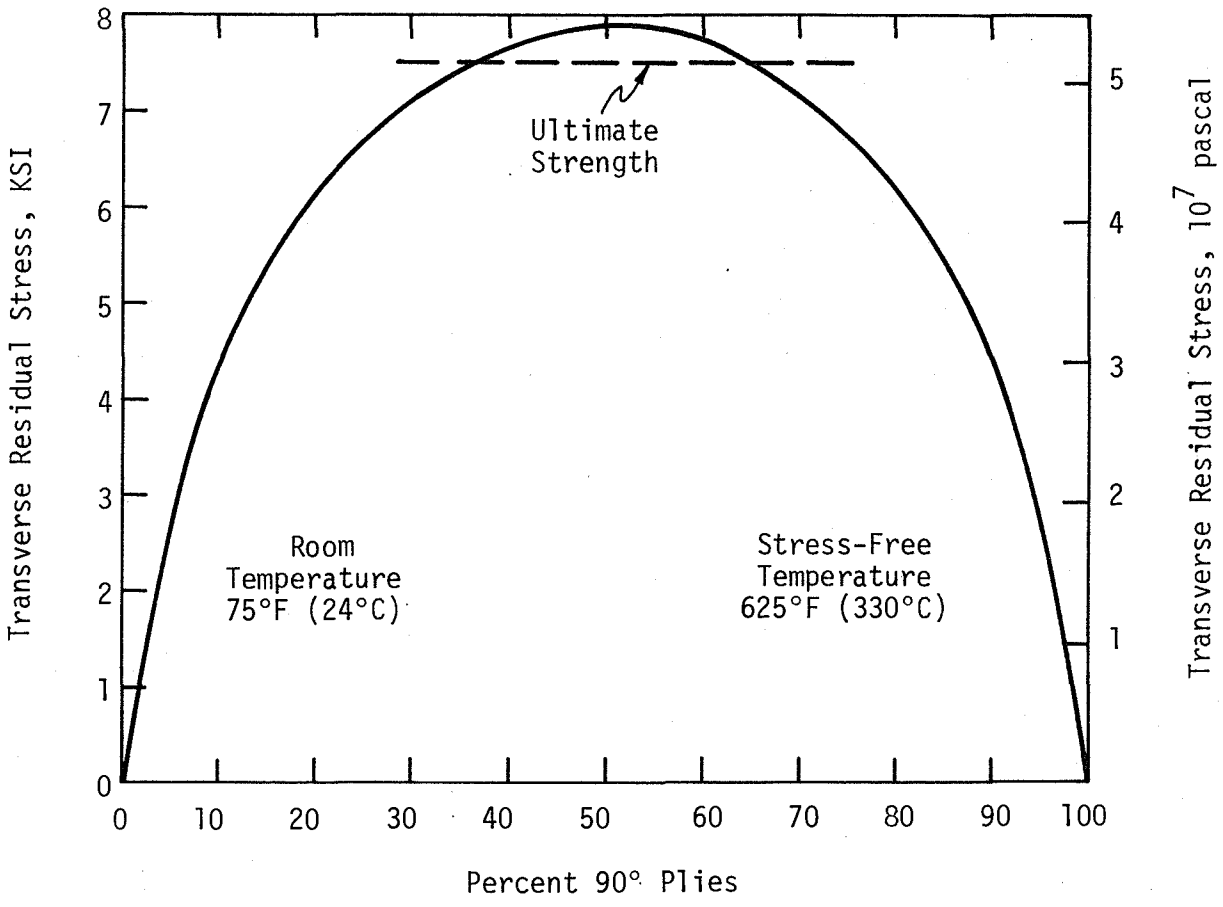

Fig. 36. Transverse Residual Stress in Cross-Ply Laminates as a Function of Percent 90° Plies.

stress will exceed the transverse ply strength by less than 6%. The absence of the microcracks at room temperature indicates that the stress-free temperature is lower than 625°F (330°C) or that other effects such as stress relaxation are important. Also, the specimens may have been fabricated using a batch of preimpregnated material that had a higher transverse failure strength than that of the material used to obtain material properties. The microcracks present after the ice-water quench are the result of the predicted 10% higher residual stresses at 32°F (0°C) than at room temperature. Additionally, the reduction in transverse ply strength due to the re-exposure to 625°F (330°C), as discussed in Section 4.4, could have contributed to the cracking of the specimens quenched in ice water.

Inasmuch as laminate analysis predicts that the transverse residual stresses exceed the ply strength at 32°F (0°C), it follows that all the specimens should develop microcracks after the Type 2 exposure (liquid nitrogen quench from room temperature). However, after this exposure, only three of the six laminates were found to contain microcracks, the densities of which were low. The possible cause of this discrepancy is stress relaxation during the slow cool from cure coupled with the extended period of time at room temperature before the liquid nitrogen quench.

Unlike the specimens that experienced a Type 2 exposure, the specimens subjected to a Type 4 or 5 thermal exposure developed significant TVM densities. The difference in densities for the different exposures is believed to result from the relaxation of the

thermal stresses at the cure temperature and then the rapid cooling to the liquid nitrogen temperature. The cooling is sufficiently rapid that no significant stress relaxation occurs before the liquid nitrogen temperature is reached. The residual stresses then greatly exceed the ply transverse strength.

The influence of edge effects on the development of microcracking is clearly demonstrated by a comparison of the results from the $[0/45/90/-45]_s$, $[\pm 45/0/90]_s$ and cross-plied laminates. The interior (away from free edges) residual stresses are predicted by laminate analysis to be the same in all such laminates. However, the experimental results indicated significant microcracking in the $[0/45/90/-45]_s$ laminate after Type 4 and Type 5 thermal loading, but no TVM in the $[45/-45/0/90]_s$ laminate. Cross-plied laminates exhibited significant TVM similar to the $[0/45/90/-45]_s$ laminate. These differences can only be attributed to edge effects.

The residual stresses in the $[0/60/0/-60]_s$ laminate are predicted to be 15% above the ply transverse strength at 32°F (0°C). The absence of microcracks after the Type 3 and 4 exposure (Fig. 17 and 18) is attributed to the other effects discussed above including stress-free temperature, stress relaxation and variable strength.

5.1.5 Resin-Rich Region Effects

Laminate analysis was also used to determine the possible effects a resin-rich region may have on the residual stresses in a laminate. The resin-rich regions are not uniformly thick throughout a laminate. Such nonuniformities were investigated by considering two resin-rich

regions that were 0.10 h_o and 0.05 h_o inch thick. The stress-free temperature was assumed to be 625°F (330°C). Two laminates were analyzed, $[0/R/90]_s$ and $[0/R/90/\pm45]_s$, where R is an abbreviation for resin-rich region.

The transverse stresses in a ply were virtually unaffected by the presence of the resin-rich regions for both thicknesses of resin-rich regions and types of laminates. The only noticeable effect of the resin-rich regions was to increase the longitudinal stresses in a ply. The 0.05-ply-thick region increased the longitudinal compressive stress by 5%, and the 0.1-ply-thick region doubled that increase in stress. The residual stresses in the resin-rich regions were very high. The stress was predicted to be 11 ksi (7.6×10^7 pascal), which exceeds the 10 ksi (6.9×10^7 pascal) ultimate stress reported by Cavano and Winters [33] for the neat resin. In spite of the high residual stress predictions in the resin-rich regions, the transverse microcracks did not appear to originate from, or to penentrate deeply into, the resin-rich regions (cf. Section 4.2.1). A micromechanics analysis may render a more precise prediction of crack initiation.

5.2 Multiple Cracking Theory

The multiple cracking theory was developed by Garrett and Bailey [26], and improved by Parvizi and Bailey [27], to predict the spacing between TVMs as load is applied to a $[0/90]_s$ laminate. This differs from the theory of Reifsnider [11], which predicts the minimum (saturation) microcrack spacing in a laminate. The multiple cracking

theory was originally developed only for cross-plied laminates. The method is shown in Section 5.2.2 to also predict the TVM spacing in a quasi-isotropic laminate with the 90° plies adjacent to the midplane.

5.2.1 Theoretical Development

The theory is based upon the modified shear-lag analysis by Cox [41]. The modified shear-lag analysis determines the stress in the 0° longitudinal ply of a $[0/90]_s$ laminate after the first crack has occurred in the 90° transverse ply. A perfect bond is assumed to exist between plies in the cross-ply laminate shown in Figure 37.

The laminate will have a laminate-analysis-type behavior until the transverse ultimate strain of the 90° ply, ε_{tu}, has been reached. At this strain, the first TVM will develop in the transverse ply. This causes a stress increment, $\Delta\sigma(y)$, to be transferred to the longitudinal plies. The maximum value of $\Delta\sigma$ is $\Delta\sigma_o$. It occurs in the plane of the TVM and decreases with distance y as the load is transferred back into the transverse ply. Assuming a uniform load distribution in the longitudinal plies, the constant $\Delta\sigma_o$ is found to be

$$\Delta\sigma_o = \sigma_a \left[\frac{b+d}{b} - \frac{E_\ell}{E_c}\right] \qquad (5.24)$$

where σ_a is the applied stress on the sample, E_ℓ and E_c are the Young's moduli of the longitudinal ply and composite, respectively, and b and d are as defined in Figure 37.

The value of the stress increment $\Delta\sigma$ at a distance y from the crack is determined using the modified shear-lag analysis. This analysis

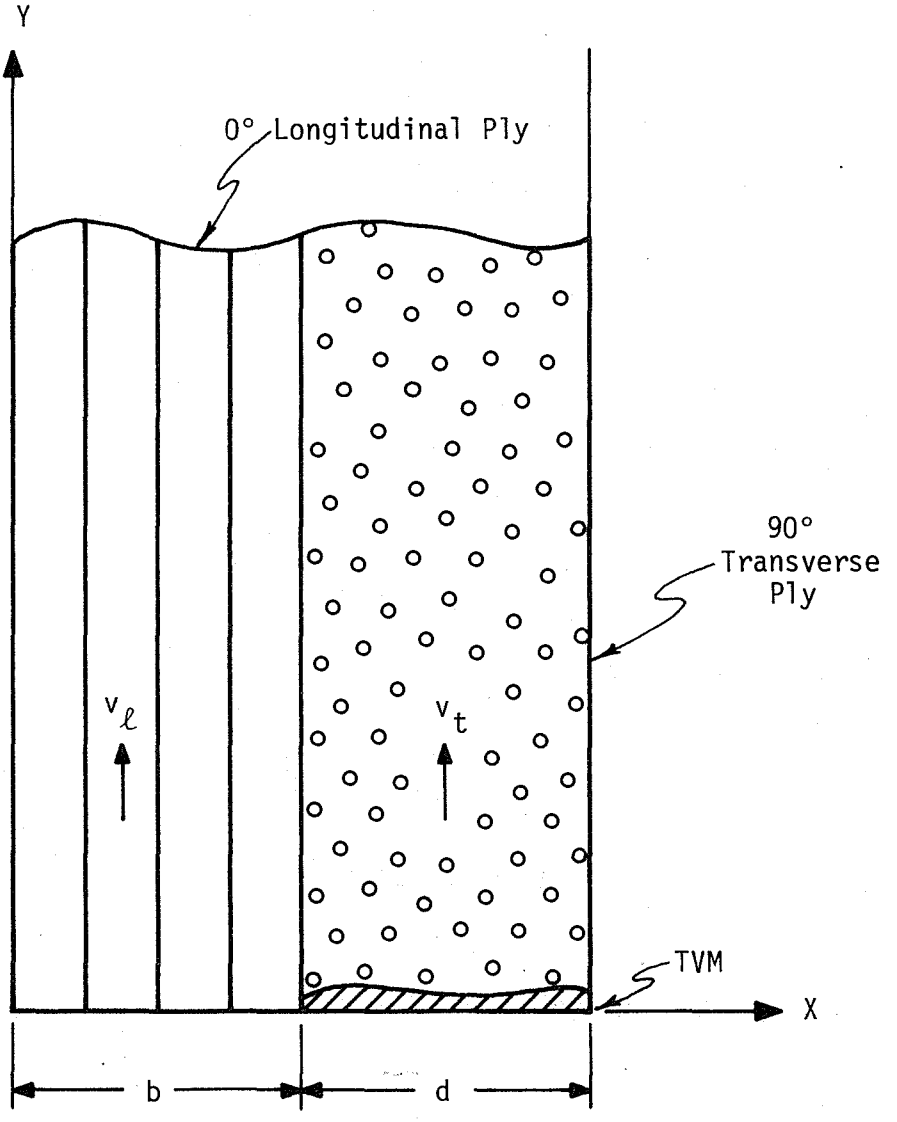

Fig. 37. Multiple Cracking Theory Model

assumes that the shear stress, τ_{xy}, is directly proportional to the difference in v_ℓ and v_t (the average y component of displacements in the longitudinal and transverse plies, respectively),

$$-\frac{\tau_{xy}}{b} = H\,(v_\ell - v_t) \tag{5.25}$$

where H is a proportionality constant. From a simple force balance, (Fig. 38),

$$\tau_{xy} = -b\,\frac{d(\Delta\sigma)}{dy} \tag{5.26}$$

Combining (5.25) and (5.26), the governing differential equation for $\Delta\sigma$ is

$$\frac{d(\Delta\sigma)}{dy} = H(v_\ell - v_t) \tag{5.27}$$

Differentiating with respect to y,

$$\frac{d^2(\Delta\sigma)}{dy^2} = H\left(\frac{\sigma_\ell}{E_\ell} - \frac{dv_t}{dy}\right) \tag{5.28}$$

where σ_ℓ is the stress in the longitudinal ply at a distance y from the TVM.

The following simplification is assumed,

$$\frac{dv_t}{dy} = \bar{\varepsilon}_t \tag{5.29}$$

where $\bar{\varepsilon}_t$ is the average axial strain in the transverse ply. The total load carried by the laminate is equivalent to the sum of the loads carried by the individual plies. Thus giving at the strain ε_{tu},

$$\frac{d\bar{v}_t}{dy} = \bar{\varepsilon}_t = \frac{1}{E_t d}\left[E_c \varepsilon_{tu}(b+d) - \sigma_\ell b\right] \tag{5.30}$$

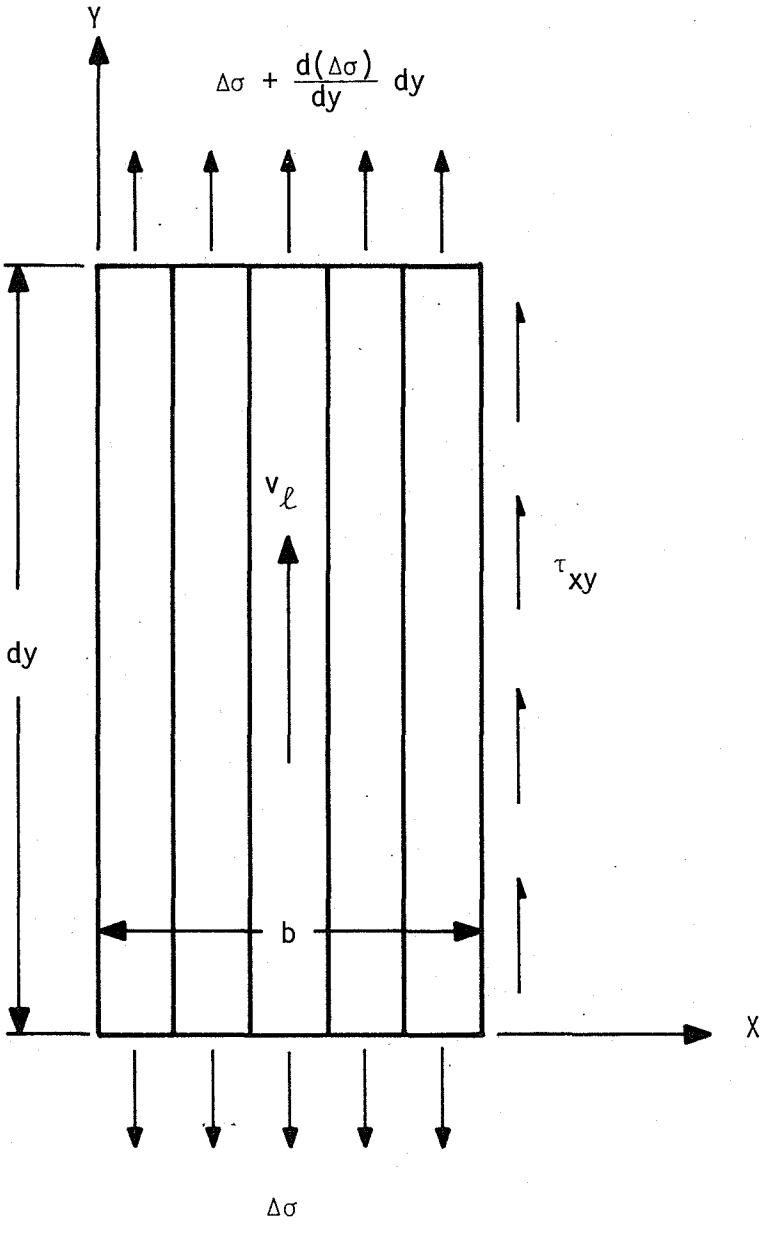

Fig. 38. Free-Body Diagram for Multiple Cracking Theory.

where E_t is the Young's modulus for the transverse ply in the y direction.

Substituting equation (5-30) into (5-28), the second-order differential equation is obtained,

$$\frac{d^2(\Delta\sigma)}{dy^2} = \phi\Delta\sigma \tag{5.31}$$

where

$$\phi = \frac{HE_c(b+d)}{E_\ell E_t d} \tag{5.32}$$

The general solution of this equation using the boundary conditions that $\Delta\sigma = 0$ at large y and $\Delta\sigma = \Delta\sigma_o$ at $y = 0$ is

$$\Delta\sigma = \Delta\sigma_o \exp(-\phi^{1/2} y) \tag{5.33}$$

The constant, H, is found as follows. Equation (5.25) implies the stress condition

$$\frac{\partial\tau_{xy}}{\partial x} = 0 \tag{5.34}$$

Now, let v be the actual displacement of the transverse ply close to the longitudinal ply. At the ply interface, $v = v_\ell$ and at larger x, $v = v_t$. The following relationship then results,

$$\frac{dv}{dx} = \frac{\tau_{xy}}{G_{12}} \tag{5.35}$$

where G_{12} is the shear modulus of the transverse ply in the x-y plane of Figure 37. Integration of equation (5.35) from the ply interface to the midplane yields

$$\Delta v = v_t - v_\ell = \frac{\tau_{xy} d}{G_{12}} \tag{5.36}$$

Substitution of equations (5.26) and (5.36) into equation (5.27) yields H to be,

$$H = \frac{G_{12}}{bd} \tag{5.37}$$

Therefore,

$$\phi = \frac{E_c G_{12}}{E_\ell E_t} \frac{b+d}{bd^2} \tag{5.38}$$

The second TVM will develop first at the end of the specimen most distant from the first microcrack. This occurs when the applied stress causes σ_t (the y component of stress in the transverse ply) to exceed $E_t \varepsilon_{tu}$. This value of σ_a is found from a summation of forces to be

$$\sigma_a = E_t \varepsilon_{tu} \frac{E_c d}{(b+d)E_c - bE_\ell} [1 - \exp(-\phi^{1/2} y)]^{-1} \tag{5.39}$$

Determining the relationship between σ_a and σ_t is more complex when microcracks are developing between two pre-existing cracks. From a force balance of a segment of the longitudinal ply (free-body shown in Fig. 38),

$$\tau_{xy} = -b \frac{d(\Delta\sigma)}{dy} \tag{5.40}$$

Substituting from equation (5.33), this becomes

$$\tau_{xy} = \Delta\sigma_o \phi^{1/2} b \exp(-\phi^{1/2} y) \tag{5.41}$$

The shear stresses from both cracks add together but are of different

signs. If the crack spacing is t, the total shear stress between two cracks will be

$$\tau_{xy} = b\Delta\sigma_o \phi^{1/2} [\exp(-\phi^{1/2} y) - \exp(\phi^{1/2} (y-t))] \qquad (5.42)$$

Substituting equation (5.42) into equation (5.40), and integrating between 0 and y, $\Delta\sigma(y)$ between two microcracks is found to be

$$\Delta\sigma(y) = \Delta\sigma_o [-\exp(-\phi^{1/2} t) + \exp(-\phi^{1/2} y) + \exp(\phi^{1/2} (y-t))] \qquad (5.43)$$

Using summation of forces and equation (5.24), equation (5.43) becomes the relationship between applied stress and the stress in the transverse ply,

$$\sigma_t = \sigma_a \frac{(b+d)E_c - bE_\ell}{E_c d} [1 + \exp(-\phi^{1/2} t) - \exp(-\phi^{1/2} y)$$

$$- \exp(\phi^{1/2} (y-t))] \qquad (5.44)$$

A TVM will develop when σ_t again is equal to $E_t\varepsilon_{tu}$. This first occurs midway between the current two microcracks because σ_t is maximum there. Substituting $E_t\varepsilon_{tu}$ into equation (5.44), the applied stress required to cause a TVM between two cracks of spacing, t, is found to be

$$\sigma_a = E_t\varepsilon_{tu} R[1 + \exp(-\phi^{1/2} t) - 2 \exp(-\phi^{1/2} \tfrac{t}{2})]^{-1} \qquad (5.45)$$

where

$$R = \frac{E_c d}{(b+d)E_c - bE_\ell} \qquad (5.46)$$

The applied stress required to produce additional microcracks is

determined by substituting t/2 for t in equation (5.45). This process is continued until either the ultimate strength of the longitudinal plies is exceeded, or debonding occurs at the transverse-longitudinal ply interface.

The microcrack spacing depends upon the position of the first crack as well as the length of the specimen. Specimens of length $\ell = 2nr$, where n is any integer and r is a given length, will have the same crack spacing for a given applied stress if the first crack developed in the middle of the specimen. If the first microcrack develops at a distance g from one end of the specimen, the subsequent cracking behavior will be similar to that of two different specimens of lengths g and $(\ell-g)$, e.g., one part of the specimen will have a different crack spacing than the other. Regardless of the length of the specimen and the position of the first microcrack, the TVM spacing at a given stress will be bounded by two forms of equation (5.45). The upper bound on crack spacing is obtained from equation (5.45). The lower bound is found by substituting t/2 for t in equation (5.45),

$$\sigma_a = E_t \varepsilon_{tu} R[1 + \exp(-\phi^{1/2} \frac{t}{2}) - 2 \exp(-\phi^{1/2} \frac{t}{4})]^{-1} \qquad (5.47)$$

Crack density will be used instead of crack spacing in the next section, crack density being merely the inverse of crack spacing.

5.2.2 TVM Density Predictions

The upper and lower bounds of TVM densities at a given applied stress will be presented rather than the "stepwise" changes in TVM

density curves predicted by the theory for a specific specimen. The results will thus be more general, not just for a specific specimen. Additionally, imperfections in a laminate would cause it to deviate from the specific predictions for it, because microcracks would not always develop midway between pre-existing microcracks. Although the results may deviate from the predictions for the specific laminate, the results will remain bounded by the more general predictions. In Figs. 39 to 43, the maximum TVM density predicted is the solid line; the minimum density is the broken line.

The thickness of a laminate and the percentage of 0° plies are predicted to have an important influence on the TVM density of a laminate. TVM density at an applied stress greater than the TVM initiation stress decreases as laminate thickness increases as shown in Fig. 39. Changing laminate thickness does not affect crack initiation stress if the percentage of 0° plies remains constant. However, an increase in the percentage of 0° plies increases significantly the crack initiation stress, as shown in Fig. 40. This increase in crack initiation stress results primarily from the increased modulus of the laminate due to the greater percentage of 0° plies. At equal increases in stress above the crack initiation stress, the laminate having the higher percentage of 0° plies will have a greater TVM density.

The multiple cracking theory predictions are compared to the experimental results of Section 4.3.1.1 in Fig. 41 for a 0.048-inch (0.122 cm) thick $[0_2/90_2]_s$ laminate. The experimental data in Fig.

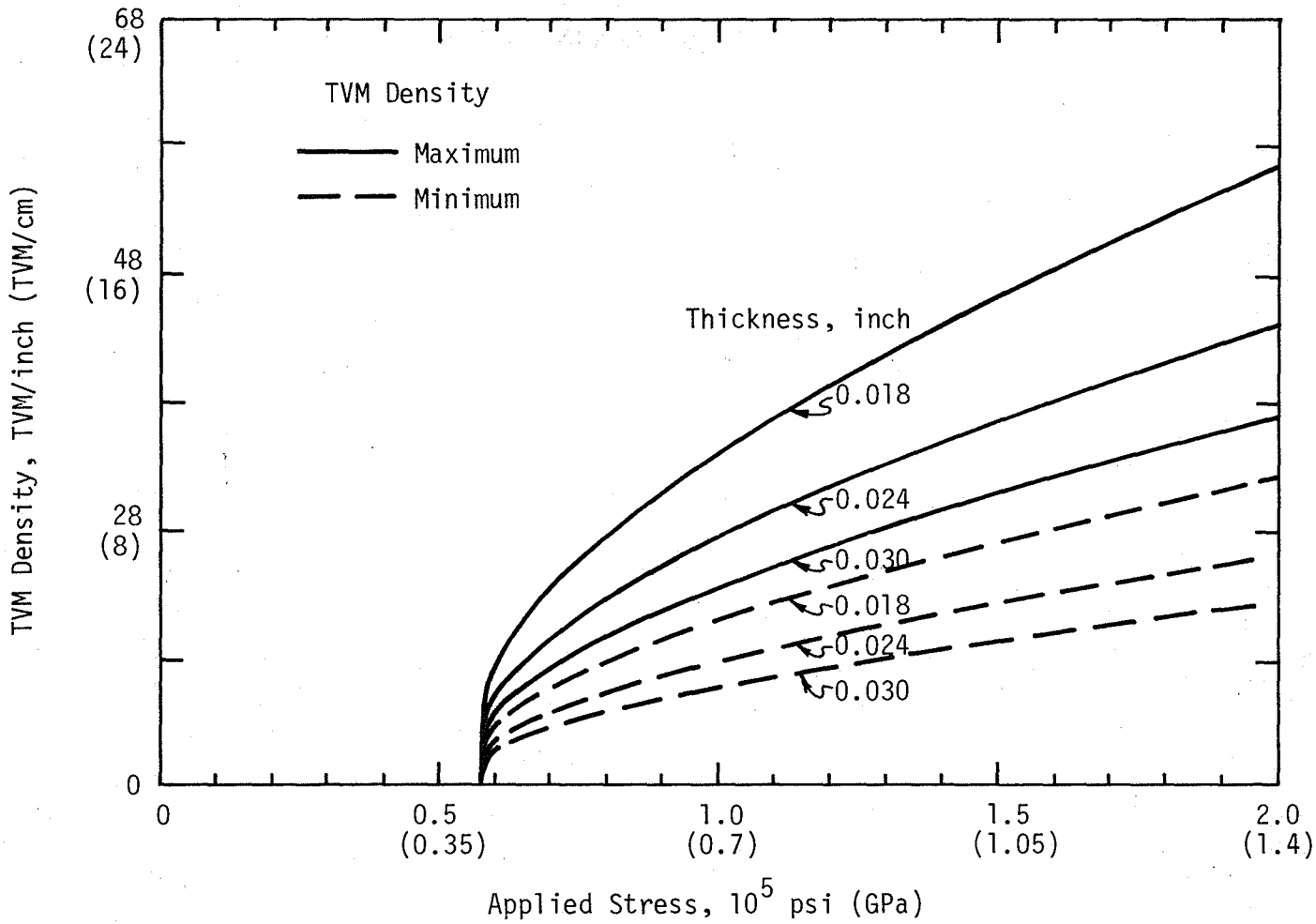

Fig. 39. Effect of Laminate Thickness on TVM Density in a $[0/90]_s$ Laminate.

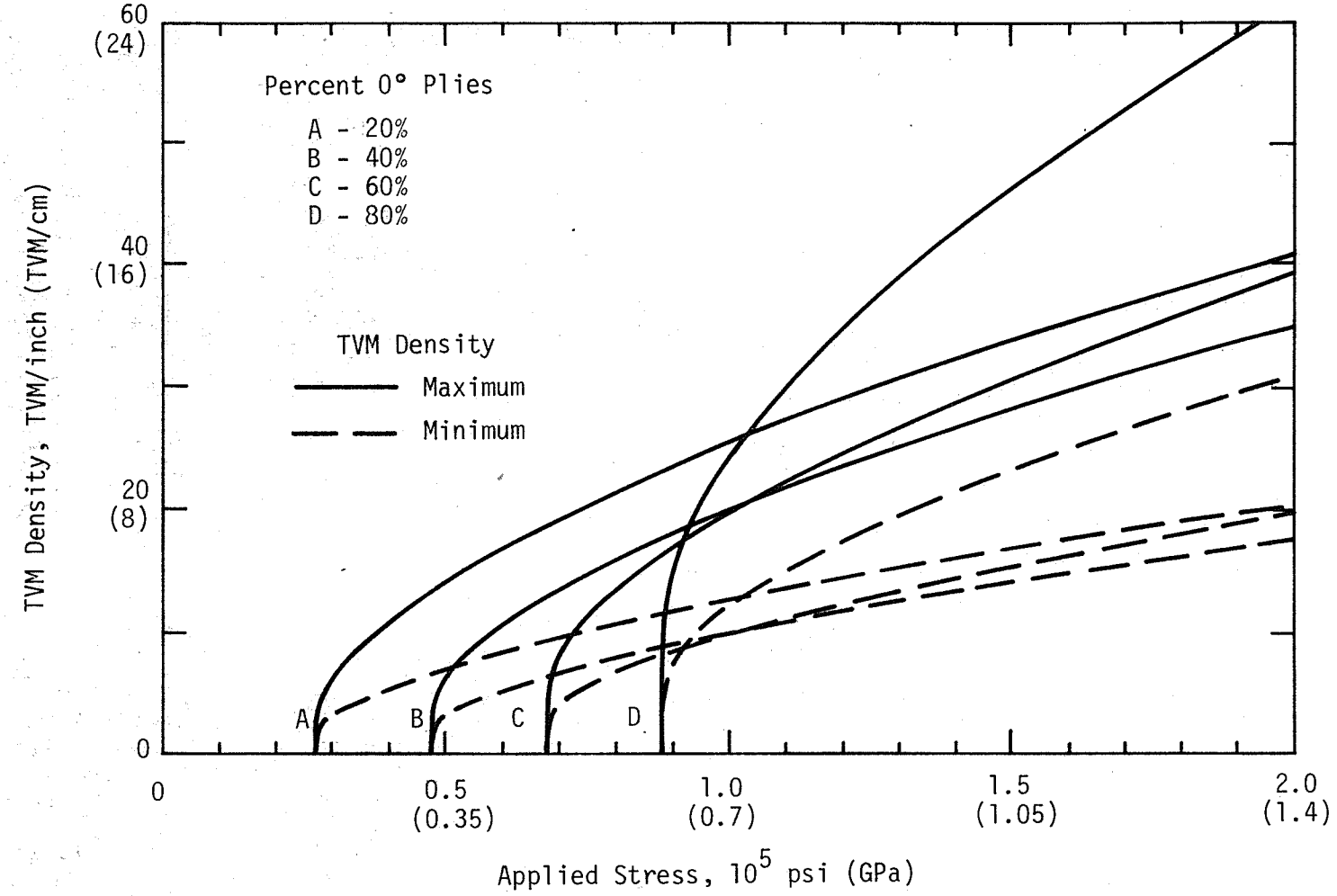

Fig. 40. Predicted TVM Density in a $[0/90]_s$ Laminate as a function of percent 0° plies and applied stress.

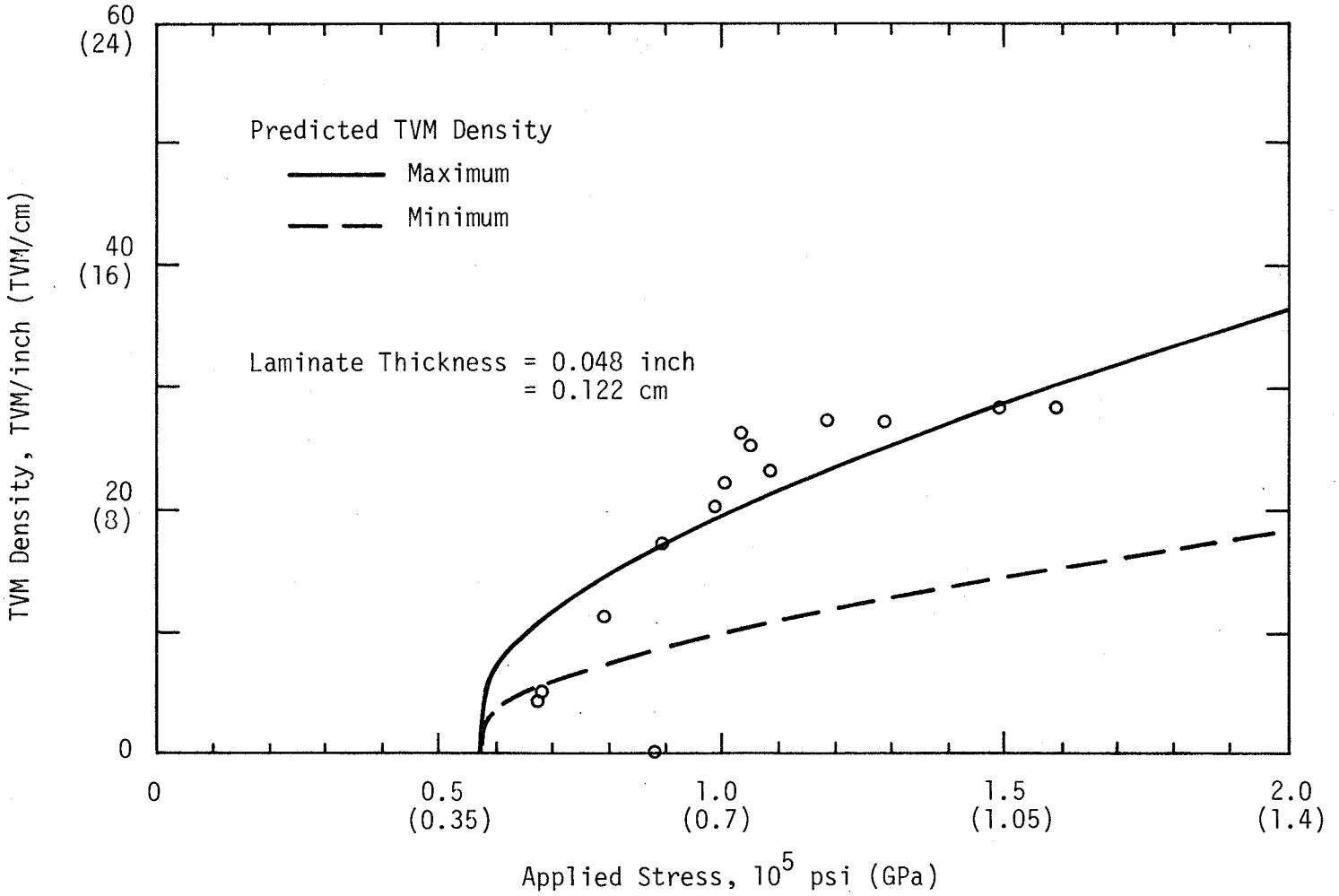

Fig. 41. Comparison of Multiple Cracking Theory Predictions and Experiment for a $[0_2/90_2]_s$ Laminate.

41 have been adjusted to include residual stresses determined by laminate analysis using stress- and temperature-dependent material properties, as in Section 5.1.3. The effect of the residual stresses was included by adding the product of the transverse residual strain in the 90° ply times the laminate modulus to the applied stress on the laminate. Any Poisson effect was neglected. As can be seen from Fig. 41, comparison between theory and experiment is not particularly good. The experimental results exceed the upper bound prior to attaining the saturation density.

The equations used for the cross-plied laminates are readily applicable to one type of quasi-isotropic laminate -- the $[\pm 45/0/90]_s$. This laminate has the same boundary conditions as the cross-plied laminates for which the theory was derived. The longitudinal Young's modulus in equations (5.45) through (5.47) is replaced by the longitudinal modulus of a $[\pm 45/0]$ laminate (obtained by rule of mixtures); the rest of the analysis remains the same.

The quasi-isotropic laminate exhibits a thickness dependence similar to that of the cross-plied laminates (Fig. 42). The applied stress necessary to initiate microcracking is less in the quasi-isotropic laminate than in a cross-plied laminate due to the lower stiffness of the quasi-isotropic laminate. The lower laminate stiffness also results in the quasi-isotropic laminate having a higher TVM density than a cross-plied laminate of the same thickness with less than 80% 0° plies. The multiple cracking theory predictions are compared to the experimental results for the $[\pm 45/0/90]_s$ laminate in

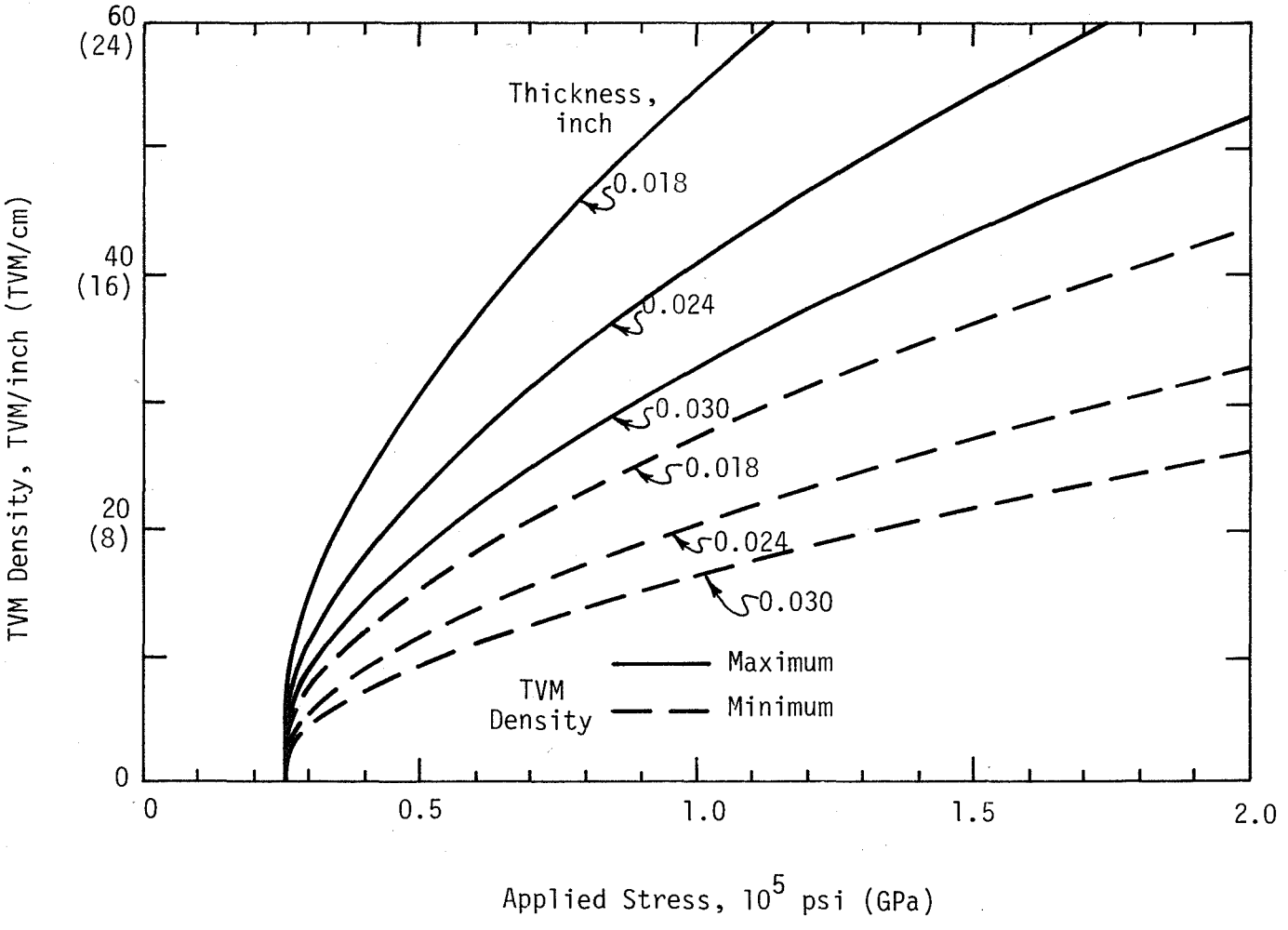

Fig. 42. Effect of Laminate Thickness on TVM Density in a $[\pm 45/0/90]_S$ Laminate.

Fig. 43. The experimental results compare very closely to the upper bound predictions for TVM densities above 10 TVM/inch (4 TVM/cm). The experimental data were adjusted for residual stresses as in the $[0_2/90_2]_s$ laminate described previously.

The sequence in which the layers are stacked in a laminate greatly affects the TVM density. Predictions for $[0_2/90_2]_s$ and $[(0/90)_2]_s$ laminates are compared in Fig. 44. Although both laminates initiate microcracking at the same applied stress, the innermost two 90° plies of the $[(0/90)_2]_s$ laminate are predicted to have twice the TVM density of the 90° plies in the $[0_2/90_2]_s$ laminate.

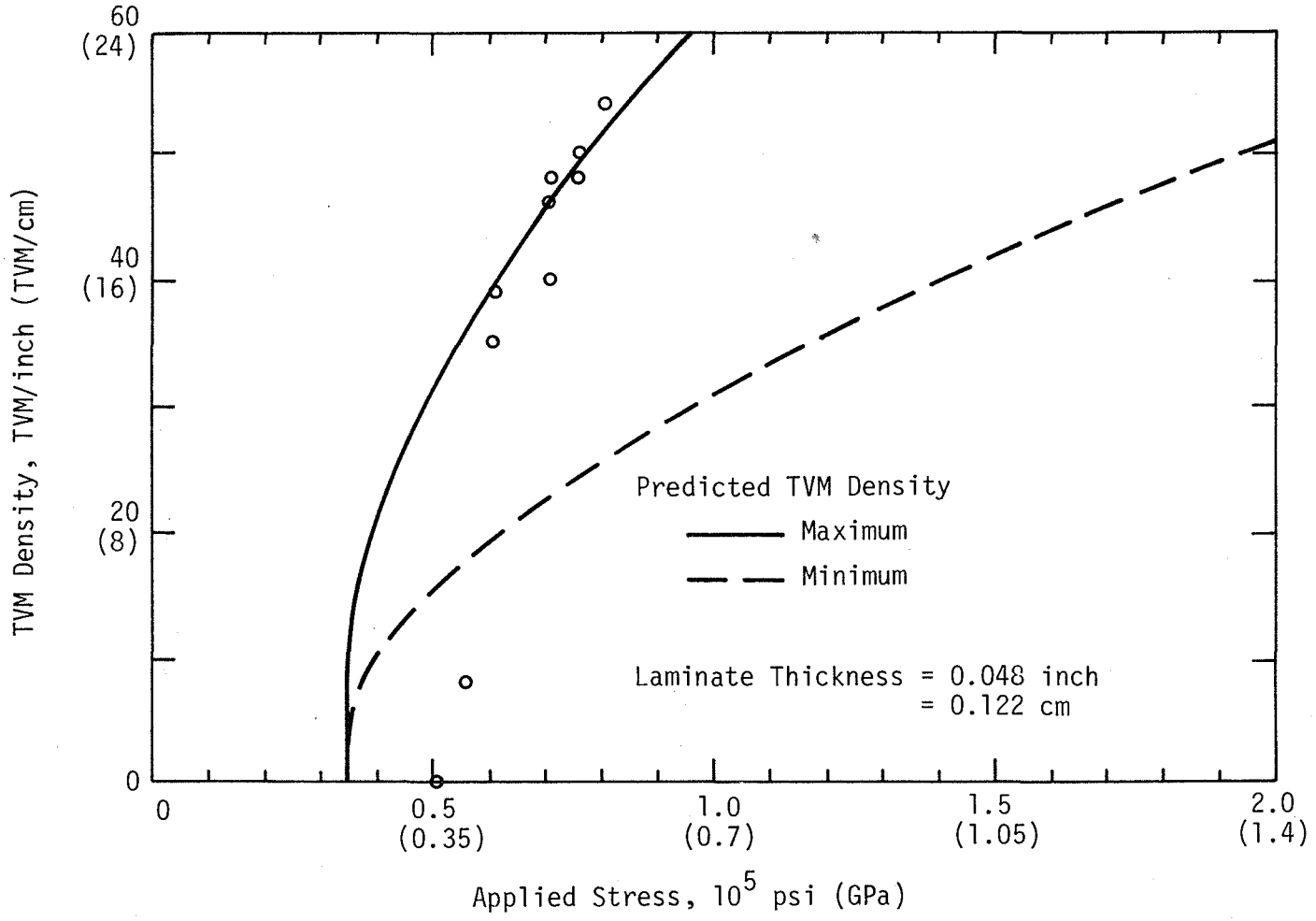

Fig. 43. Comparison of Multiple Cracking Theory Predictions and Experiment for a $[\pm 45/0/90]_s$ Laminate.

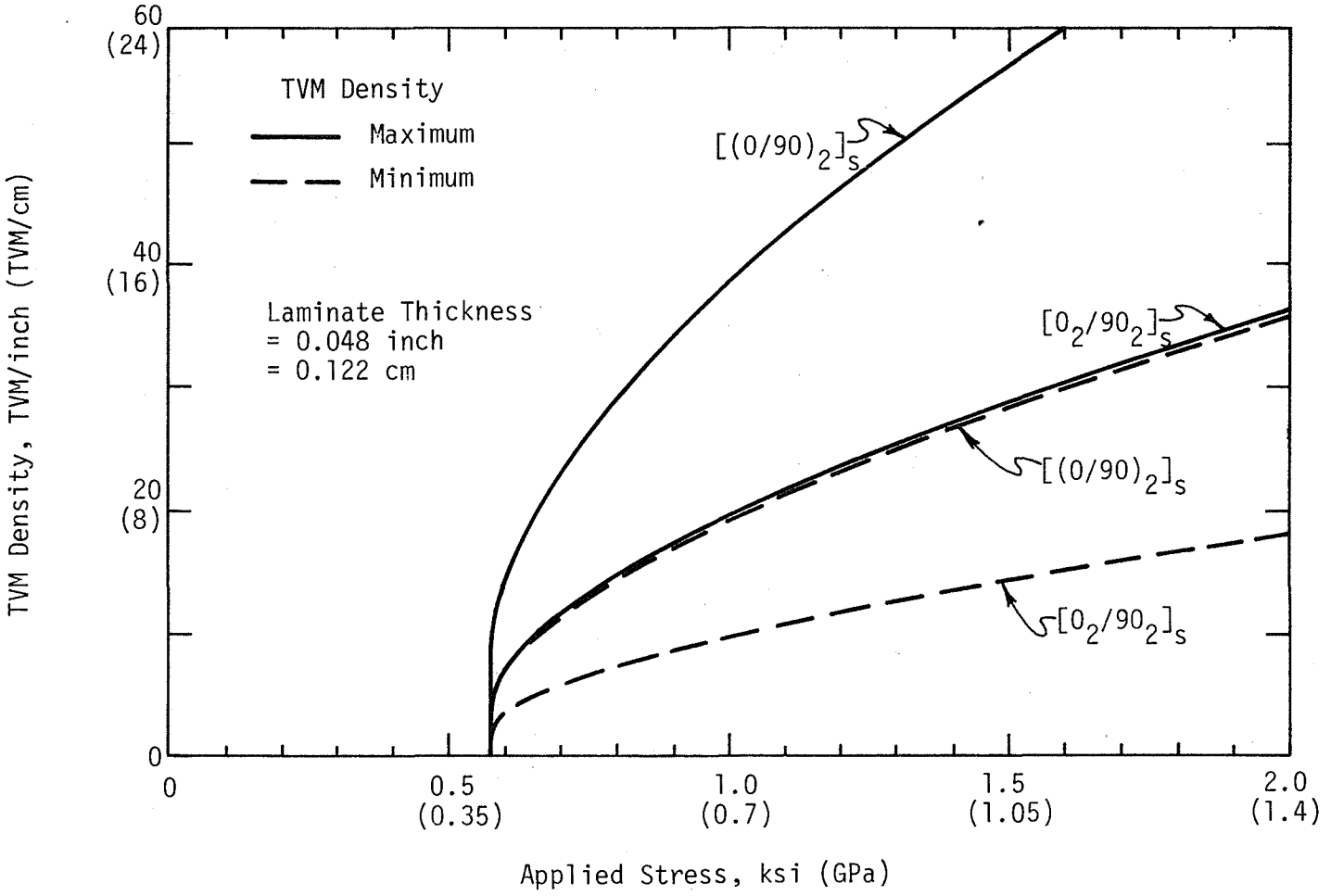

Fig. 44. Effect of Stacking Sequence on TVM Density in Cross-Plied Laminates.

Chapter 6

CONCLUSIONS

This study has investigated, both experimentally and analytically, transverse microcracks (TVM) in Celion 6000/PMR-15 graphite-polyimide composites. TVM resulting from both thermal and tensile loading was studied in cross-plied and quasi-isotropic laminates. Two analytical methods were used: laminate analysis including stress- and temperature-dependent material properties, and the multiple cracking theory developed by Parvizi, Garrett, and Bailey.

The following major conclusions have been reached as a result of the investigation:

1. The Celion 6000/PMR-15 laminates studied in this investigation are free of cracks after curing.

2. Quenching laminates into liquid nitrogen from room temperature does not produce significant TVM densities; however, this quench from the cure temperature does cause significant TVM densities in all the laminates tested except the $[\pm 45/0/90]_s$ laminate which had no observable microcracks after any thermal loading.

3. Laminate configuration (stacking sequence, fiber angles, layer thickness) strongly influences TVM density.

4. Laminate analysis using stress- and temperature-dependent material properties predicts that the residual curing stresses are marginally large enough to initiate microcracking.

5. Free edge effects and rate of loading significantly influence TVM densities.

6. TVM densities determined by observations of the edges of laminates accurately represent densities in the interior regions of laminates.

7. The stress-free temperature of preimpregnated composite materials varies from batch to batch. The stress-free temperature of two batches of Celion 6000/PMR-15 was found to range from 610° to 625°F (320° to 330°C) and 570° to 605°F (300° to 320°C).

8. Resin-rich regions act as crack arresters, but generally do not stop crack propagation through adjacent layers of the same fiber orientation.

9. Mechanical loading induces higher TVM densities than does thermal loading.

10. The Young's modulus of the laminates investigated was not appreciably affected by TVM density.

11. The Poisson's ratios of $[0_2/90_2]_s$ and $[0/45/90/-45]_s$ laminates varies with TVM density. The $[0_2/90_2]_s$ laminate exhibited a 55% decrease in Poisson's ratio after the saturation density was reached. The Poisson's ratio of the $[0/45/90/-45]_s$ laminate increased 16% after microcracking initiated.

12. Tensile mechanical loading causes significantly higher TVM densities in $[0/45/90/-45]_s$ and $[\pm45/0/90]_s$ laminates than in $[0_2/90_2]_s$ laminates.

13. While reasonably good correlation between theory and experiment was obtained for TVM density as a function of load, additional work is needed to develop an improved general theory.

REFERENCES

1. "Integrated Research on Carbon Composite Materials," Technical Report AFML-TR-66-310, Part II, pp. 143, December, 1967.

2. Doner, D. R. and Novak, R. C., "Structural Behavior of Laminated Graphite Filament Composites," 24th Annual Technical Conference, Reinforced Plastics/Composites Division, The Society of the Plastics Industry, Inc., Section 2-D, pp. 1-8, 1969.

3. Spain, R. G., "Thermal Microcracking of Carbon Fibre/Resin Composites," Composites, pp. 33-37, March, 1971.

4. McGarry, F. J. and Willner, A. M., "Microcracking in Fibrous Glass Reinforced Resin Composites," 23rd Annual Technical Conference Reinforced Plastics/Composites Division, The Society of the Plastics Industry, Inc., Section 14-B, pp. 1-11, 1968.

5. Novak, R. C. and DeCrescente, M. A., "Fabrication Stresses in Graphite-Resin Composites," J. of Engineering for Power, Vol. 92, pp. 377-380, October, 1970.

6. Novak, R. C., "Fabrication Stresses in Fiber-Resin Composites," UARL J213186-9, pp. 1-14, 1970.

7. Molcho, A. and Ishai, O., "Thermal Cracking of C.F.R.P. Laminates," Society for the Advancement of Material and Process Engineering, Vol. 10, pp. 255-262, October, 1978.

8. Lee, B. L. and McGarry, F. J., "Study of Processing and Properties of Graphite Fiber/High Temperature Resin Composites," AMMRC CTR 76-10, April, 1976.

9. Reifsnider, K. L. and Masters, J. E., "Investigation of Characteristic Damage States in Composite Laminates," presented at the ASME Winter Annual Meeting, San Francisco, Ca., December 10-15, 1978.

10. Quackenbush, N. E. and Doner, D. R., "Graphite Filament Reinforced Plastics," Contract Naval Air System Command, Department of the Navy, N00019-69-C-0135, January, 1970.

11. Reifsnider, K. L., "Some Fundamental Aspects of the Fatigue and Fracture Response of Composite Materials," 14th Annual Meeting, Soc. of Engr. Sci., pp. 1-12, November, 1977.

12. Stalnaker, D. O. and Stinchcomb, W. W., "Load History - Edge Damage Studies in Two Quasi-isotropic Graphite Epoxy Laminates," Composite Materials: Testing and Design (Fifth Conference), ASTM STP 674, S. W. Tsai, Ed., American Society for Testing and Materials, 1979, pp. 620-641.

13. Daniel, I. M., Liber, T., and Chamis, C. C., "Measurement of Residual Strains in Boron-Epoxy and Glass-Epoxy Laminates," Composite Reliability, ASTM STP 580, American Society for Testing and Materials, pp. 340-351, 1975.

14. Daniel, I. M. and Liber, T., "Laminated Residual Stresses in Hybrid Composites," Final Report Part 1, Contract II, NAS3-16766, pp. 15-80, June, 1976.

15. Daniel, I. M. and Liber, T., "Effect of Laminate Construction on Residual Stresses in Composites," Society for Experimental Stress Analysis, Spring Meeting, Paper No. WR-45-1975, pp. 1-22, May, 1976.

16. Daniel, I. M. and Liber, T., "Effect of Laminate Construction on Residual Stresses in Graphite/Polyimide Composites," Experimental Mechanics, Vol. 17, No. 1, pp. 21-25, January, 1977.

17. Daniel, I. M. and Liber, T., "Lamination Residual Strains and Stresses in Hybrid Laminates," Composite Materials: Testing and Design (Fourth Conference), ASTM STP 617, American Society for Testing and Materials, pp. 331-343, 1977.

18. Chamis, C. C., "Residual Stresses in Angle plied Laminates and Their Effects on Laminate Behavior," NASA TM-78835, April, 1978.

19. Hashin, Z., Rosen, B. W., and Pipes, R. B., "Nonlinear Effects on Composite Laminate Thermal Expansion," Material Sciences Corporation, MSC/TFR/808/1015, NASA contract No. NAS1-14964, July, 1978.

20. Shuart, M. J. and Herakovich, C. T., "An Evaluation of the Sandwich Beam in Four-Point Bending as a Compressive Test Method for Composites," NASA TM-78783, September, 1978.

21. Hashin, Z., Bagchi, D., and Rosen, B. W., "Nonlinear Behavior of Fiber Composite Laminates," NASA CR-2313, April, 1974.

22. Serafini, T. T. and Delvigs, P., "A Review of Processable High Temperature Resistant Addition-Type Laminating Resins," Applied Polymer Symposium, No. 22, pp. 89, 1973.

23. Hahn, H. T. and Pagano, N. J., "Curing Stresses in Composite Laminates," J. Composite Materials, Vol. 9, pp. 91-107, January, 1975.

24. Herakovich, C. T., "On Thermal Edge Effects in Composite Laminates," Int. J. Mech. Sci., Vol. 18, pp. 129-134, 1976.

25. Herakovich, C. T. and Wong, D. M., "Influence of Residual Stresses on the Tensile Strength of Composite-Metal Sandwich

Laminates," Experimental Mechanics, Vol. 17, No. 11, pp. 404-414, November, 1977.

26. Garrett, K. W. and Bailey, J. E., "Multiple Transverse Fracture in 90° Cross-Ply Laminates of a Glass Fibre-Reinforced Polyester," Journal of Materials Science, Vol. 12, pp. 157-168, 1977.

27. Parvizi, A. and Bailey, J. E., "On Multiple Transverse Cracking in Glass Fibre Epoxy Cross-Ply Laminates," Journal of Materials Science, Vol. 13, pp. 2131-2136, 1978.

28. Delvigs, P., Serafini, T. T., and Lightsey, G. R., "Addition-Type Polyimides from Solutions of Monomeric Reactants," NASA TN D-6877, August, 1972.

29. Serifini, T. T., Delvigs, P., and Lightsey, G. R., "Thermally Stable Polyimides from Solutions of Monomeric Reactants," Journal of Applied Polymer Science, Vol. 16, pp. 905-915, 1972.

30. Winters, W. E. and Serafini, T. T., "PMR Polyimides - Processable High Temperature Composite Matrix Resins," 20th National SAMPE Symposium and Exhibition, Science of Advanced Materials and Process Engineering Series, Vol. 20, pp. 629-643, 1975.

31. Cavano, P. J. and Winters, W. E., "PMR Polyimide/Graphite Fiber Composite Fan Blades," NASA-CR-135113, December 15, 1976.

32. Cavano, P. J., "Second Generation PMR Polyimide/Fiber Composites," Quarterly Technical Progress Narrative No. 2 for June 1, 1978 through August 31, 1978, Contract NAS3-21349, September, 1978.

33. Hansen, M. P. and Chamis, C. C., "Experimental and Theoretical Investigation of HT-S/PMR-PT Composites for Application to Advanced Aircraft Engines," NASA-TM-X-71459, February 5-8, 1974.

34. Knauss, J. F., Starnes, J. H., Jr., and Henneke, E. G., II, "The Compressive Failure of Graphite/Epoxy Plates with Circular Holes," VPI-E-78-5, February, 1978.

35. Jones, R. M., Mechanics of Composite Materials, Scripta Book Company, 1975.

36. Ashton, J. E., Halpin, J. C., and Petit, P. H., Primer on Composite Materials: Analysis, Technomic Publishing Co., Inc., 1969.

37. Renieri, G. D. and Herakovich, C. T., "Nonlinear Analysis of Laminated Fibrous Composites," VPI&SU Report VPI-E-76-10, June, 1976.

38. Hahn, H. T., "A Note on Determination of the Shear Stress-Strain Response of Unidirectional Composites," Journal of Composite Materials, Vol. 7, pp. 383, July, 1973.

39. Kaminski, B. E., Lemon, G. H., and McKague, E. L., "Development of Engineering Data for Advanced Composite Materials," AFML-TR-70-108, 1972.

40. Hashin, Z., Bagchi, D., and Rosen, B. W., "Non-linear Behavior of Fiber Composite Laminates," NASA CR, NAS1-11284, September, 1973.

41. Cox, H. L., British Journal of Applied Physics, Vol. 3, pp. 72, 1952.

APPENDIX

USER'S GUIDE FOR THE COMPUTER CODE LAST

USER'S GUIDE FOR THE COMPUTER CODE LAST

The Fortran computer code LAST, Laminate Analysis with Stress- and Temperature-dependent material properties, was developed to calculate the lamina stresses and strains in a laminate due to applied loads and temperature change. LAST uses the laminate analysis equations developed in Section 5.1.1 which are applicable to both symmetric and unsymmetric laminates. The code includes the capability for stress- and temperature-dependent material properties which are input in the form of a least-squares polynomial of the two independent variables, stress and temperature.

Up to 20 plies and 5 materials may be input. This may be easily increased by changing dimension statements.

Data Input Format

Card Number	Variable, Format	Description
1	A,F1.0	A=1 if a catalog of problems desired. If so, a 1 should appear in col. 79 of the next card.
2,3	TITLE,20A4	Two 80 column cards for problem titles
4	KEY(I),19I2	= 1, Print or execute option = 0, Do not print or execute option
	I=1	Print $[Q]^k$
	I=2	Print $[\bar{Q}]^k$
	I=3	Print [A], [B], [D], and inverse matrices
	I=4	Print material properties
	I=5	Print cumulative midplane strain and curvature in nonlinear problems

Card Number	Variable, Format	Description
	I=6	Print cumulative thermal expansion and averaged thermal expansion coefficient
	I=7	= 1 if only tensile material properties are being input
	I=8	Print average laminate engineering constants
	I=9	Determine if the maximum lamina stresses have been exceeded and to read in the failure polynomials
	I=10	Print the maximum stresses at the desired temperature from the failure polynomials
	I=11	= 0, 1/E1 and 1/E2 material polynomials are input for E1 and E2
		= 1, E1 and E2 are obtained directly from material polynomials.
5	NMAT,I5	Number of different materials used in problem
	NLAYP,I5	Number of layers in laminate
	IHALF,I5	≠ 0, Inputting only half of a symmetric laminate
	HALF,F10	Laminate half thickness
6	MAT(I),I5	Material number of I^{th} layer
	THICK(I),F10	Thickness of I^{th} layer
	THETA(I),F10	Fiber orientation of I^{th} layer
	These three data values are repeated 2 per card for all the layers in a laminate unless IHALF (from card 5) is nonzero, then values for only one-half of the laminate need to be input.	
7-24	Coefficient to material polynomials. Equations of form	
	$f(\sigma,T) = C_1+C_2\sigma+C_3T+C_4\sigma^2+C_5T^2+C_6\sigma T$	

Card Number	Variable, Format	Description
	$+ C_2\sigma^3+C_8T^3+C_9\sigma^2T+C_{10}\sigma T^2+C_{11}\sigma^4$	
	$+ C_{12}T^4+C_{13}\sigma^3T+C_{14}\sigma^2T^2+C_{15}\sigma T^3$	
	If KEY(11) = 0, the following applies σ = stress/1000	
7-9	$\frac{1}{E1}\frac{1}{1000}$, 5E15	Inverse of ply longitudinal Young's modulus
10-12	$\frac{1}{E2}\frac{1}{1000}$, 5E15	Inverse of ply transverse Young's modulus
13-15	$G_{12}\frac{1}{1000}$, 5E15	Ply shear modulus
16-18	V12,5E15	Ply Poisson's ratio
19-21	AL1,5E15	Ply longitudinal thermal expansion coefficient
22-24	AL2,5E15	Ply transverse thermal expansion coefficient
	Cards 7-24 are repeated for each material.	
	The following applies to Cards 7-24 if KEY(11) = 1,	
	σ = stress	
7-9	E1,5E15	Ply longitudinal Young's modulus
10-12	E2,5E15	Ply transverse Young's modulus
13-15	G_{12},5E15	Ply shear modulus
16-18	V12,5E15	Ply Poisson's ratio
19-21	AL1,5E15	Ply longitudinal thermal expansion coefficient
22-24	AL2,5E15	Ply transverse thermal expansion coefficient
	Cards 7-24 are repeated for each material	
	If KEY(9) equals 0, skip to card 31	

Card Number	Variable, Format	Description
25-30	Coefficient to failure polynomials.	
	The form of the polynomial is	
	$F = C_1+C_2T+C_3T^2+C_4T^3+C_5T^4+C_6T^5+C_7T^6$	
25-26	F1,5E15	Ply longitudinal ultimate stress
27-28	F2,5E15	Ply transverse ultimate stress
29-30	F12,5E15	Ply shear ultimate stress
31	IPROB,I5	Problem number printed with output
	NTEMP,I5	Number of temperature increments
	BTEMP,F10	Beginning temperature
	ETEMP,F10	End temperature
	NLOAD,I5	Number of load increments for nonlinear stress-strain solution
32-37	BLOAD(I),E15.5	Beginning I^{th} component of {N} and {M} loads
	ELOAD(I),E15.5	Ending I^{th} component of {N} or {M} loads
	where I=1, N_x; I=2, N_y; I=3, N_{xy}; I=4, M_x; I=5, M_y; I=6, M_{xy} as defined in Section 5.1.1	
38	More, I10	= 0 To end execution
		= 1 To start another problem with the same material. Restart at Card 2 and skip cards 7-30.
		= 2 To do another temperature/load sequence starting at card 31.

NOTE: The intermittent stress values printed during a temperature

change are not the correct values of stress at that intermittent temperature. The only purpose of incrementing temperature change is to allow for the nonlinearity of the material properties with respect to stress, not temperature.

DISTRIBUTION LIST

Prof. Donald F. Adams
Dept. Of Mechanical Engineering
University Of Wyoming
Larmie, WY 82070

Dr. N. R. Adsit
General Dynanics Convair
P.O. Box 80637
San Diego, CA. 92138

Dr. J. A. Bailie
D81-12 Bldg. 154
Lockheed Missiles & Space Co,Inc
1111 Lockheed Way
Sunnyvale, CA. 94088

Mr. Henry W. Bergner, Jr.
The Boeing Company
Mail Stop 3707
Seattle, WA. 98124

Dr. Charles W. Bert, Director
School Of Aerospace, Mechanical
& Nuclear Engineering
The University Of Oklahoma
Norman, Oklahoma 73069

Mr. Richard Boitnott
Mail Stop 190
Nasa-Langley Research Center
Hampton, VA. 23665

Mr. David Bowles
Mail Stop 188B
NASA-Langley Research Center
Hampton, Va. 23665

Dr. H. F. Brinson
ESM Dept.
VPI&SU
Blacksburg, VA. 24061

Dr. Michael F. Card
Mail Stop 190
NASA-Langley Research Center
Hampton, VA 23665

Dr. C. Chamis
NASA-Lewis Research Center
2100 Brook Park Rd.
Cleveland, Ohio 44135

Dr. Paul A. Cooper
Mail Stop 190
NASA-Langley Research Center
Hampton, Va. 23665

Dr. Frank Crossman
Lockheed Research Lab
Org. 52-41, Bldg. 204
3251 Hanover Street
Palo Alto, CA. 94304

Dr. I. M. Daniel, Manager
IIT Research Institute
10 West 35 Street
Chicago, IL. 60616

Dr. John R. Davidson
Mail Code 188E
MD-Structural Integrity Branch
Langley Research Center
Hampton, VA. 23665

Dr. John G. Davis, Jr.
Mail Stop 188A
Langley Research Center
Hampton, VA. 23665

Mr. Jerry W. Deaton
Mail Stop 188A
NASA-Langley Research Center
Hampton, VA. 23665

Mr. H. Benson Dexter
Mail Stop 188A
NASA-Langley Research Center
Hampton, VA. 23665

Mr. O. Earl Dhonau
Section 2-53400
Vought Corp.
P.O. Box 5907
Dallas, TX. 75222

Dr. S. C. Dixon
Mail Stop 395
NASA-Langley Research Center
Hampton, VA. 23665

Dr. J. E. Duberg
Mail Stop 103
NASA-Langley Research Center
Hampton, Va. 23665

Dr. M. F. Duggan
52-33/205/2
Lockheed Palo Alto Lab.
3251 Hanover St.
Palo Alto, Ca. 94304

Dr. Wolf Elber
Mail Stop 188E
NASA-Langley Research Center
Hampton, VA. 23665

Mr. Gary L. Farley
Mail Stop 188A
NASA-Langley Research Center
Hampton, VA. 23665

Mr. Larry Fogg
Lockheed-California
Dept. 7572, Bldg. 63, Plant A1
P.O. Box 551
Burbank, CA. 91520

Dr. R. L. Foye
USAMRDL
SAUDLAS (207-5)
Moffet Field, CA. 94035

Dr. D. Frederick
ESM Dept.
VPI&SU
Blacksburg, VA. 24061

Mr. Samuel P. Garbo
McDonnell Aircraft Co.
Bldg. 34, Post 350
St. Louis, MO. 63166

Mr. Ramon Garica
Mail Stop 190
NASA-Langley Research Center
Hampton, VA. 23665

Dr. Login B. Greszczuk
McDonnell Douglas Astr. Co.
5301 Bolas Avenue
Huntington Beach, CA. 92647

Mr. Glen C. Grimes, Engr. Spec.
Structures R & T, Dept 3780/62
Northrop Corp., Aircraft Div.
3901 W. Broadway
Hawthorne, CA. 90250

Dr. H. T. Hahn
Washington University
St. Louis, MO. 63130

Dr. J. C. Halpin
Flight Dynamics Lab
Wright-Patterson AFB
Ohio 45433

Professor Z. Hashin
School of Engineering
Dept. of Solid Mech. Materials
and Structures
Tel Aviv University
Tel Aviv, Israel

Dr. R. A. Heller
ESM Dept.
VPI&SU
Blacksburg, VA. 24061

Dr. E. G. Henneke
ESM Dept.
VPI&SU
Blacksburg, VA. 24061

Professor Phil Hodge
107 Aeronautical Engr. Bldg.
University of Minnesota
Minneapolis, MN 55455

Dr. K. E. Hofer
IIT Research Institute
10 West 35 Street
Chicago, Illinois 60616

Mr. Edward L. Hoffman
Mail Stop 188A
NASA-Langley Research Center
Hampton, VA. 23665

Dr. Peter W. Hsu
Mail Stop 1-1-12
Hamilton Standard Division
Windsor Locks, CT. 06096

Mr. Edward A. Humphreys
Materials Science Corporation
Blue Bell Office Campus
Blue Bell, PA. 19422

Dr. Michael W. Hyer
ESM Dept.
VPI&SU
Blacksburg, VA. 24061

AVCO, Systems Division
Subsystems & Meth. Structures
201 Lowell Street
Wilmington, MA. 01887

Dr. Eric R. Johnson
ESM Dept.
VPI&SU
Blacksburg, VA. 24061

Dr. N. J. Johnson
Mail Stop 226
NASA-Langley Research Center
Hampton, VA. 23665

Dr. M. P. Kamat
ESM Dept.
VPI&SU
Blacksburg, VA. 24061

Dr. Keith T. Kedward
1768 Granite Hills Dr.
El Cajon, CA. 92021

Mr. John M. Kennedy
Mail Stop 188E
NASA-Langley Research Center
Hampton, VA. 23665

Mr. James F. Knauss
Section 2-30400
Vought Corp.
P.O. Box 225907
Dallas, TX. 75265

Dr. Ronald D. Kriz
Dept. Com. NBS Bldg. 2
Boulder, CO. 80302

Dr. S. V. Kulkarni
L342 Lawrence Livermore Lab
P. O. Box 808
Livermore, Ca. 94550

Dr. M. R. Louthan
Materials Engineering
VPI&SU
Blacksburg, VA. 24061

Mr. Vic Mazzio
General Electric Co.
P.O. Box 8555
Bldg. 100, Rm. M4018
Philadelphia, PA. 19101

Mr. Robert R. McWithey
Mail Stop 190
NASA-Langley Research Center
Hampton, VA. 23665

Dr. Martin M. Mikulas
Mail Stop 190
NASA-Langley Research Center
Hampton, VA. 23665

Mr. J. Steve Mills
6100 Edinger Ave., Apt. 525
Huntington Beach
CA 92647

Dr. D. H. Morris
ESM Dept.
VPI&SU
Blacksburg, VA. 24061

Mr. Anya Nagarkar
Material Sciences Corp.
Blue Bell Office Campus
Blue Bell, PA. 19422

NASA Scientific & Technical
Information Facility
P.O. Box 8757
Baltimore/Washington Inter. Air.
Baltimore, MD. 21240

Newman Library - VPI&SU

Mr. David A. O'Brien
5902 Kingsford Pl.
Bethesda, MD 20034

Dr. Donald W. Oplinger
Army Materials & Mechanics
Research Center
Department of the Army
Watertown, MA. 02171

Dr. Nicholas J. Pagano
WPAFB/MBM
Wright Patterson AFB
Ohio 45433

Dr. Nicholas Perrone, Director
Structural Mechanics Program
Department of the Navy
Office of Naval Research
Arlington, VA. 22217

Prof. T. H. H. Pian
Mass. Inst. of Tech.
Dept. of Aero. & Astr.
Cambridge, MA. 02139

Mr. Marek-Jerzy Pindera
Mail Stop 188A
NASA-Langley Research Center
Hampton, VA. 23665

Dr. R. Byron Pipes
Dept. of Mech. & Aero. Engr.
107 Evans Hall
University of Delaware
Newark, DE. 19711

Dr. K. L. Reifsnider
ESM Dept.
VPI&SU
Blacksburg, VA. 24061

Dr. Gary D. Renieri
McDonnell Douglas Astro. Co-East
P.O. Box 516
Bldg. 106, Level 4, Post C-5
St. Louis, MO. 63166

Dr. Michael W. Renieri
McDonnell Aircraft Co.
Bldg. 34, Post 350
St. Louis, MO. 63166

Dr. Larry Roderick
Mail Stop 188E
NASA-Langley Research Center
Hampton, VA. 23665

Dr. B. W. Rosen
Materials Science Corporation
Blue Bell Office Campus
Blue Bell, PA. 19422

Dr. R. E. Rowlands
Dept. of Engineering Mechanics
University of Wisconsin
Madison, WI. 53706

Dr. Edmund F. Rybicki
Battelle
Columbus Laboratories
505 King Avenue
Columbus, OH. 43201

Mr. Harminder Saluja
Boeing Vertol Company
Structural Technology
P.O. Box 16858
Philadelphia, PA. 19142

Dr. J. Wayne Sawyer
Mail Stop 190
NASA-Langley Research Center
Hampton, VA. 23665

Dr. George P. Sendeckyj
Structures Division
Air Force Flight Dynamics Lab.
Wright-Patterson AFB
Onio 45433

Mr. Steven M. Serabian
28 Berkeley Drive
Chelmsford, MA. 01824

Mr. Mark J. Shuart
Mail Stop 188
NASA-Langley Research Center
Hampton, VA. 23665

Dr. James H. Starnes, Jr.
Mail Stop 190
NASA-Langley Research Center
Hampton, VA. 23665

Prof. Yehuda Stavsky
Gerard Swope Prof. of Mech.
Technion-Israel Inst. of Tech.
Technion City, Haifa, Israel

Dr. W. W. Stinchcomb
ESM Dept.
VPI&SU
Blacksburg, VA. 24061

Dr. Darrel R. Tenney
Mail Code 188B
MD-Materials Research Branch
Langley Research Center
Hampton, VA. 23665

Dr. S. W. Tsai
Nonmetallic Materials Division
Air Force Materials Laboratory
Wright-Patterson AFB
Ohio 45433

Dr. J. R. Vinson
6242 Urey Hall
Applied Mechanics & Science Dept
Univ. of California-San Diego
La Jolla, CA. 92037

Mr. M. E. Waddoups
General Dynamic Corp.
Fort Worth, TX 76101

Dr. T. A. Weisshaar
Aero & Ocean Engr. Dept.
VPI&SU
Blacksburg, VA. 24061

Dr. J. M. Whitney
Nonmetallic Materials Division
Air Force Materials Laboratory
Wright-Patterson AFB
Ohio 45433

Mr. Thomas A. Zeiler
Aerospace Engr.
VPI&SU
Blacksburg, VA. 24061

Dr. Carl H. Zweben
General Electric Co.
Space Division
P.O. Box 8555
Philadelphia, PA. 19101